1-27-2009

Utility of Cationic and Anionic Chiral Surfactants in Capillary Electrophoresis (CE) and CE Coupled to Mass Spectrometry (CE-MS)

Bin Wang

UTILITY OF CATIONIC AND ANIONIC CHIRAL SURFACTANTS IN CAPILLARY ELECTROPHORESIS (CE) AND CE COUPLED TO MASS SPECTROMETRY (CE-MS)

by

BIN WANG

Under the Direction of Dr. Shahab A. Shamsi

ABSTRACT

The research presented in this thesis involves the application of chiral cationic and anionic surfactants for simultaneous enantioseparation of structurally similar compounds in capillary electrophoresis (CE) and CE coupled to mass spectrometry (CE-MS). The first chapter briefly introduces the fundamentals of CE and CE-MS, emphasizing the micellar electrokinetic chromatography (MEKC) and MEKC-MS techniques, as well as ionic liquids (ILs) and affinity CE (ACE).

In chapter 2, a mixture of five racemic profen (PROF) drugs are simultaneously separated with the combined use of 2,3,6-tri-O-methyl-β-cyclodextrin (TM-β-CD) and IL-type surfactant, *N*-undecenoxycarbonyl-L-leucinol bromide (L-UCLB). Enantioseparations of these

PROFs are optimized using a standard recipe containing 35.00 mM TM-β-CD, 5.00 mM sodium acetate at pH 5.0, and varying the concentration as well as chain length of the IL surfactants. The batch-to-batch reproducibility of L-UCLB is found to be acceptable in terms of enantiomeric resolution, and migration time. A competitive inhibition mechanism is proposed to investigate the ternary interactions among TM-β-CD, ILs, and PROFs. The apparent binding constant of TM-β-CD to L-UCLB is estimated by nonlinear and linear plotting methods. The binding constants of one representative PROF (e.g., fenoprofen) to TM-β-CD and to L-UCLB are estimated by a secondary plotting approach. The *R*- and *S*-fenoprofen having different binding constant values, resulting in the enantioseparation due to the synergistic effect of TM-β-CD and L-UCLB.

The *R*- and *S*-configurations of barbiturates display differences in potency and biological activity. In Chapter 3, a multivariate MEKC-ESI-MS approach for the simultaneous analysis of the racemic mixture of three barbiturates is presented. The chiral selector employed is the polymeric surfactant polysodium *N*-undecenoxycarbonyl-L-isoleucinate. The central composite design is used to optimize the chiral resolution, decrease the total analysis time, and improve the ESI-MS signal-to-noise ratio for these barbiturates. In preliminary experiments, the ranges of the factors investigated in the multivariate approaches are determined. Then the multivariate optimizations are conducted to determine the best overall chiral resolution with shortest possible run times for barbiturates. The limit of detection of ESI-MS is several folds higher compared to the UV detection. The predicted optimum results are in good agreement with the experimental data.

INDEX WORDS: Capillary electrophoresis, Micellar electrokinetic chromatography, Simultaneous enantioseparation, Binding constant, Mass spectrometry , Electrospray ionization

UTILITY OF CATIONIC AND ANIONIC CHIRAL SURFACTANTS IN CAPILLARY ELECTROPHORESIS (CE) AND CE COUPLED TO MASS SPECTROMETRY (CE-MS)

by

BIN WANG

A Thesis Submitted in Partial Fulfillment of the Requirements for the Degree of

Master of Science

in the College of Arts and Sciences

Georgia State University

2009

UTILITY OF CATIONIC AND ANIONIC CHIRAL SURFACTANTS IN CAPILLARY ELECTROPHORESIS (CE) AND CE COUPLED TO MASS SPECTROMETRY (CE-MS)

by

BIN WANG

Committee Chair: Dr. Shahab A. Shamsi

Committee: Dr. Gangli Wang
Dr. Yujun G. Zheng

Electronic Version Approved:

Office of Graduate Studies
College of Arts and Sciences
Georgia State University
May 2009

DEDICATION

To my parents

ACKNOWLEDGEMENTS

This thesis shows my most important research work at the Department of Chemistry, Georgia State University, which would not be accomplished without the help people offered me here.

First of all, I would like to full-heartedly thank my research advisor, Professor Shahab A. Shamsi, for his generous support. His professional advices inspired my study and research, his strict requirements for the research work trained me as a serious scientist, and his kindness helped me a lot for my study and life here in Atlanta.

In addition, I want to express my gratitude to Jun He and William Bragg, who are not only my colleagues but also my friends. They show their talent in their study and work. I am very glad to work with them. I would also like to thank all of the people who ever work with me, Dr. Syed Asa Ali Rizvi, Dr. Jack Zheng, Dr. Congyin Gu, Victoria Bianchi, and Manan Patel.

Finally, I would like to thank the committee members (Dr. Gangli Wang and Dr. Yujun G. Zheng) for their suggestions. Moreover, I would like to thank the Department of Chemistry, Georgia State University for the financial support.

TABLE OF CONTENTS

LIST OF TABLES

LIST OF FIGURES

CHAPTER 1. INTRODUCTION

1.1 Capillary electrophoresis

Capillary electrophoresis (CE) is a family of separation techniques with different separation mechanisms. The most simplified version is capillary zone electrophoresis (CZE), in which separation is based on the differences of ion linear velocity in an electric field [1]. The ion linear velocity of a species is determined by the intrinsic ion mobility of this species and the voltage applied through the capillary, as shown by the following equation [1]:

$$v = \mu \cdot E = \mu \cdot V/L \qquad \text{(Equation 1.1)}$$

where v represents the ion linear velocity, μ represents the mobility, E represents the electric field, V represents the applied voltage, and L represents the total length of the capillary [1]. Usually, background electrolyte is used to maintain a constant electric field along the capillary [1]. The injected sample (analyte) incorporated in the background electrolyte will migrate with the linear velocity proportional to its mobility [1]. Therefore, the separation of analytes in CZE is caused by the different mobilities for different ionic species. The ion mobility is related to the charge and size of the ions, as well as the viscosity of the solution, as can be seen in Equation 1.2 [2]:

$$\mu = q/(6 \cdot \pi \cdot r \cdot \eta) \qquad \text{(Equation 1.2)}$$

where the μ represents the mobility, q represents the charge of the ion, r represents the hydrodynamic radius, η represents the viscosity of the solution [2]. The Equation 1.2 suggests that the smaller size and more charged molecules will have higher mobilities than larger and less charged ones. The size of an ion in the solution is determined by the hydrodynamic radius of the ion, which refers to the radius of an equivalent sphere dependent on the structure of the ion [2]. Moreover, the electrophoretic mobility decreases as the viscosity of the solution is

increased. The schematic of the movement of ions with one charge in the CE capillary is shown in Figure 1.1. When positive polarity is used in CZE mode, the small positive species migrate fastest to the cathode since they have high charge-to-size ratio. The large positive species migrate slower than the small one because of the lower charge-to-size ratio. The neutral species migrate with the bulk solution at the same mobility as the electroosmotic flow (EOF), which will be described in section 2. On the other hand, the negative species tend to migrate to the anode, and the small negative species migrate faster to the anode than the large negative species due to higher charge-to-size ratio. However, the EOF of bulk solution drags all of the negative species moving to the cathode, resulting in the migration order of small positive ion, large positive ion, neutral species, large negative ion, and small negative ion, as shown in Figure 1.1.

The application of Equation 2 shows limitations for the irregularly shaped ions and can not explain the influence of counterion atmosphere in the medium [1]. Therefore, it is more accurate to describe the ion mobility as follows:

$$\mu = \frac{\varepsilon \cdot \zeta}{6 \cdot \pi \cdot \eta} = \frac{2 \cdot \varepsilon_0 \cdot \varepsilon_r \cdot \zeta}{3 \cdot \eta} \qquad \text{(Equation 1.3)}$$

where ε_0 represents the permittivity of vacuum, ε_r represents the relative permittivity of the buffer, ε represents the permittivity of the buffer ($\varepsilon = 4 \cdot \pi \cdot \varepsilon_0 \cdot \varepsilon_r$), ζ represents the zeta potential [1]. Although the zeta potential is not an easily accessible quantity to predict ion mobility, the physical meaning of zeta potential provides qualitative evaluation of the influence of important parameters on ion mobility [1].

The zeta potential is derived from the double layer theory, which describes the interface between a single ion and its counter ions and the surrounding solution [1]. The mostly accepted model of the double layer structure is the Gouy-Chapman-Stern (GCS) model. As can be seen

in Figure 1.2, some of the counter ions are assumed to be associated with the central ions and form compact layer, while other freely moving counter ions form a diffuse layer around the central ions, resulting in an exponentially decaying potential [1]. Under the influence of an electric field, the associated ions and molecules will move along with the central ion, forming a shear plane (at the distance x=a in Figure 1.2) with the surrounding medium [1]. The zeta potential is the electric potential at the shear plane [1]. The relationship between zeta potential and the ion size, ion charge, and the buffer concentration (ionic strength) can be seen in Figure 1.3. According to GCS model, increasing the size of the ion pushes the shear plane outward, thereby reduces the zeta potential and the mobility consequently [1]. Increasing the charge of the ion increases the zeta potential, thereby increases the mobility of the ion [1]. When the ionic strength of the buffer is increased, the potential of the counter ions will decay faster, resulting in the decrease of zeta potential and ion mobility [1].

1.2 Electroosmotic flow

The electroosmotic flow (EOF) refers to the bulk flow of the liquid in the capillary caused by the effect of the electric field applied on counterions adjacent to the negatively charged capillary wall [3]. When a buffer at pH > 3 is flushed through a fused silica capillary, the inner surface of the capillary generates negative charges due to the ionization of silanol (Si-OH) groups [2], and positive counterions in the bulk solution are concentrated to the capillary wall [3]. Consequently, an electric double layer structure forms on the interface between the capillary and the solution, as shown in Figure 1.4 [4]. According to GCS model, the double layer structure includes Helmholtz (compact) layer and diffused layer. The electric potential at the shear plane ($x=x_2$) is the zeta potential, as same as the one shown in Figure 1.2.[1] The

layer of positive ions is dragged to the negative electrode (cathode) by an electric field applied through the capillary, resulting in the bulk flow of liquid toward the cathode, known as EOF [3]. The relation between zeta potential and electroosmotic mobility shown below is similar to the one for ions, except for the proportionality factor that transfers the geometry from curve to flat [1].

$$\mu_{eo} = \frac{\varepsilon \cdot \zeta}{4 \cdot \pi \cdot \eta} = \frac{\varepsilon_0 \cdot \varepsilon_r \cdot \zeta}{\eta} \qquad \text{(Equation 1.4)}$$

The observed electroosmotic velocity is proportional to the applied electric field [1]:

$$v_{eo} = \mu_{eo} \cdot E \qquad \text{(Equation 1.5)}$$

The direction of EOF is determined by how the inner surface of the capillary is treated. When the acidic silanol groups on the fused silica surface are deprotonated, the excess charge in the solution are cations. The EOF will move to the direction of the cathode (Figure 1.5A) [2]. The zero EOF (Figure 1.5B) and reverse of EOF (Figure 1.5C) can be accomplished by the static or dynamic wall coating [2]. The static coating is usually the chemical modification of the capillary wall by polymers such as polyacrylamide, polyvinylalcohol, or polyvinylpyrrolidone [2]. The dynamic coating involved the addition of cationic surfactants or amphiphilic polymers [2]. When positively charged surfactants are adsorbed to the negatively charged surface, the surface of the capillary will be neutralized, resulting in reduced EOF (Figure 1.5B) [2]. Furthermore, the bilayer structure of the cationic surfactants will reverse the charges on the surface to positive if the concentration of surfactant is increased in the solution. The positive charges on the surface of the bilayer associate with the counterions (anions) in the solution and form a double layer structure of anions. This process is similar to the one generated by deprotonated silanol groups on the surface of bare fused silica capillary expect that the EOF is

caused by the anions in the bulk solution. Therefore, the EOF is reversed and move to the anode (Figure 1.5C) [2].

Other factors to influence the magnitude of EOF include the pH and concentration of the buffer used in CE [1]. The pH value of the buffer influences the deprotonation of the silanol groups, thereby determines the surface charge density of the fused silica capillary [1]. The EOF is very slow at pH lower than 3 since the surface is barely deprotonated [1]. The increase of pH causes the increased charge density on the surface and increased EOF. The pH higher than 8 still increases EOF but more modestly [1]. The concentration of buffer influences the ionic strength, which relates to the zeta potential and mobility [1]. When the buffer concentration or ionic strength increases, the zeta potential decreases and the electric double layer becomes thinner. Consequently, the electroosmotic flow is decreased, which is similar to the electrophoretic mobility of ions [1].

The voltage driven flow profile of EOF in CE is shown in Figure 1.6 and compared with the pressure driven flow profile of mobile phase in gas chromatography (GC) or high performance liquid chromatography (HPLC) [2]. Research has proved that the velocity of the fluid in CE capillary is not a function of radial position when the inner diameter of the capillary is in the magnitude of μm [3]. Therefore, the flow profile of EOF is generally flat through the intersect surface of the capillary. For the pressure driven flow, the velocity profile is a parabolic shaped laminar flow, which causes the broadening of the solute zone [3]. The flat profile is one of the major reasons for the high efficiency in CE separation than other techniques such as GC and HPLC [3].

The mobility or velocity experimentally measured in CE is called apparent mobility (μ_a), which is the vectorial sum of electrophoretic mobility (μ_{ep}) and electroosmotic mobility [1]. The

apparent velocity (v_{app}) is the sum of electrophoretic velocity (v_{ep}) and electroosmotic velocity (v_{eo}). They are defined by Equation 1.6 and Equation 1.7.

$$\mu_{app} = \mu_{ep} + \mu_{eo} \quad \text{(Equation 1.6)}$$

$$v_{app} = \mu_{app} \cdot E = (\mu_{ep} + \mu_{eo}) \cdot E = v_{ep} + v_{eo} \quad \text{(Equation 1.7)}$$

In a fused silica capillary with positively charged inner surface, the cationic species will migrate to the cathode with their μ_{app} greater than the μ_{ep} and μ_{eo}. Neutral species will migrate together with EOF. The anionic species will migrate to the cathode in the same direction as EOF if their μ_{ep} is smaller than the μ_{eo}, or in the opposite direction to the anode if their μ_{ep} is greater than the μ_{eo}.

The various modes and techniques of CE include capillary zone electrophoresis (CZE), capillary gel electrophoresis (CGE), micellar electrokinetic chromatography (MEKC), capillary isoelectric focusing (CIEF), capillary isotachophoresis (CITP), and capillary electro-chromatography (CEC) [2]. MEKC is the CE technique using micelles in the CE buffers to separate both charged and neutral compounds. CEC is the CE technique that combines liquid chromatography (LC) and CE by using packing material as stationary phase in the capillary. Among these modes, CZE, MEKC, and CEC are three mostly used modes in the field of CE. This thesis focuses on the theory related to MEKC modes and its application in analytical chemistry.

1.3 Instrumentation of CE

The instrument of CE generally includes an electric power supply, a fused silica capillary with the inner diameter ranging from 20 to 200 μm, two buffer reservoirs holding the inlet and outlet of capillary, two electrodes connecting the power supply to the buffer reservoirs, and on-line spectroscopic detector, as shown in Figure 1.7 [2]. The power supply provides high voltage through 0 to 30 kV [2]. The capillary is coated with polyimide on its outside wall to prevent breaking in the instrument [2]. The buffer reservoirs and electrodes connect the capillary to the electronic circuit. The detector mostly used is an ultraviolet-visible (UV-Vis) detector measuring the UV-Vis absorption of the sample. Before the voltage is applied, the capillary is first filled with background electrolyte (BGE) or buffer [2]. Next, the sample is injected hydrodynamically or electrokinetically into the inlet end of the capillary. Then, the inlet and outlet ends are put into the buffer reservoirs with the electrodes. The separation will start after the voltage is applied. The UV-Vis absorption is monitored at an interface close to the outlet end of the capillary.

1.4 Micellar Electrokinetic Chromatography

The micellar electrokinetic chromatography (MEKC) was first introduced by Terabe in 1984 for the purpose of separating neutral compounds in CE [2]. As mentioned earlier, in the CZE mode, the separation is simply based on the difference in electrophoretic mobilities of analytes [1]. The neutral compounds will migrate together with EOF and cannot be distinguished. However, the use of micelles in the BGE can achieve separations of both charged and neutral compounds.

The micelles are the aggregates of surfactants, which are amphiphilic molecules with nonpolar, hydrophobic long chain and polar, hydrophilic head group [2]. These surfactant molecules spontaneously assemble to form micelles in solutions when the concentration is above a certain value named critical micelle concentration (CMC, Figure 1.8) [2]. In aqueous solution, the nonpolar long chains of the surfactant molecules form the hydrophobic core due to hydrophobic interaction, while the polar or ionic head groups orient towards the surface of the micelle and contact with the aqueous environment. The analyte molecules can partition between the polar, hydrophilic aqueous solutions and nonpolar, hydrophobic micelle phase. Therefore, the separation of neutral compounds is achieved by the partitioning between aqueous phase and micelle phase. The separation principle of MEKC is shown in Figure 1.8 [2]. The anionic surfactant molecules form micelles carrying negative charges. The electrophoretic mobility of these micelles is toward the anode while the direction of EOF is toward the cathode. If the electroosmotic mobility is greater than the electrophoretic mobility of the micelles, the micelles will migrate to cathode after the EOF. The analytes injected in the capillary partition between the micelle phase and aqueous phase due to the hydrophobicity of the analytes. Therefore, the neutral species have different mobilities with EOF and will elute between EOF and the micelles. Different species have different hydrophobicity so that they have different degree of partitioning with the micelles. The more percentage of an analyte partitions into the micelle, the slower this analyte migrates [2].

MEKC shows some obvious advantages over other techniques. The neutral and charged species can be separated simultaneously [1, 3]. High efficiency is achieved with minute consumption of samples [1, 3]. The micellar phase, known as pseudostationary phase (PSP), is not chemically bonded to the capillary so that it can be refreshed and changed [3].

The surfactants used in MEKC can be anionic, cationic, zwitterionic, nonionic, or the mixture of different types of surfactants that form mixed micelles [3]. In enantioselective MEKC, the surfactants with chiral structures are used to separate the enantiomers [3].

1.5 Ionic liquid modified MEKC

Ionic liquids (ILs) are a class of compounds that are organic salts consisting ionic components with melting points at or close to room temperature (below 100°C) [5]. Due to the combined structures of bulk organic groups and ions, ILs show wide range of solubility in both polar and nonpolar solvents, and negligible vapor pressures than conventional solvents [5].

ILs have shown increasing applications in various research areas, including the organic synthesis, electrochemistry, material science, and environmental science. Analytical chemists, especially those in the field of separation science, have paid more attention to ILs as stationary phase and mobile phase modifiers in GC and LC. In the field of CE, ILs have been used as PSP in MEKC, support coatings on the capillary wall, BGE in nonaqueous CE, and additives in CE buffer with cyclodextrin (CD) for achiral and chiral separation.[5] The ILs with surfactant properties can form micelles and be used in MEKC. Especially, the chiral ILs have been reported as micelles forming surfactants for chiral separation.[6] This thesis involves the application of several surfactants including the amino acid derived cationic chiral ILs used in MEKC, and polymeric anionic surfactants in MECK coupled to mass spectrometry (MEKC-MS).

1.6 The theory for the affinity CE (ACE) and the estimation of binding constants

1.6.1 ACE as a methodology to measure the binding constants

The study of the association equilibrium of a dynamic chemical system requires the measurement of the equilibrium constant (or binding constant) [7]. Various techniques and experimental approaches have been used to estimate binding constants. These techniques include spectroscopy, chromatography, calorimetry, and potentiometry etc [7]. In biochemistry, the enzyme-catalyzed reactions are investigated by measuring the substrate affinity to the enzyme [8]. The theory and experimental approaches have been well developed to deal with enzymatic reactions under various circumstances such as the inhibition of the enzyme-substrate reaction with different mechanisms and the enzyme reactions with multiple substrates [8-9]. In chemistry, the study of binding constants is usually limited to simple ligand-receptor reactions. However, some reactions and systems studied in the conventional fields of chemistry encounter mechanisms more complicated than the ones used for reactions between only two reactants. Obviously, some of the approaches used in biochemistry can be applied in other disciplines such as analytical chemistry. One of the CE techniques, which measure the specific interactions of ligands with receptors or antigens with antibodies, is referred to as affinity capillary electrophoresis (ACE) [10]. When using ACE, the migration patterns of interacting molecules are used to identify and quantify specific binding and to estimate binding constants in two steps: (1) the solutes are first separated by CZE, (2) the CE run buffer is doped with a complexing agent, which is specific for the solute. The change in t_R of the solute is recorded before and after the addition of complexing agent [10]. Strictly speaking, MEKC can also be considered as an ACE method since the partitioning and the electrostatic interactions between the solute and the micelles are the affinity interactions between these two species [10].

However, most of the reactions studied by ACE are noncovalent molecular interactions confined to ligand-receptor or ligand-substrate mode [10].

A molecular association between an analyte and a ligand can be described by the general rectangular hyperbolic form of a binding isotherm equation shown below [11]:

$$y = \frac{ax}{b + cx} \qquad \text{(Equation 1.8)}$$

where y is the experimentally measured response of the ligand-substrate system [11]. The free variable x is the concentration of free ligand. The a, b, and c are constants determined by the properties of the substrate, ligand, and complex, and they also include the information of the binding constants and stoichiometry [11]. This binding isotherm equation is used in many fields of chemistry and biochemistry to estimate the binding constant. To generate the signal response y, various spectroscopic methods have been used, such as UV-Vis absorption, IR absorption, and NMR [10]. Other techniques such as electrochemical methods, chromatography, and calorimetry have also been applied to provide different signals between the bound and free substrate [10]. All these methods utilize different physical properties inherent to the complex and free form of analytes, such as extinction coefficients in spectroscopy, chemical shifts in NMR, and electrophoretic mobility in electrophoresis [7].

1.6.2 The derivation of the isotherm equation in CE

In a 1:1 ligand-substrate reaction, the equilibrium constant of the affinity of the ligand molecule to the substrate is governed by the law of mass action [10].

$$S + L \rightleftharpoons SL$$

$$K_{eq} = \frac{[SL]}{[S] \bullet [L]} \qquad \text{(Equation 1.9)}$$

where [S] represents the substrate concentration, [L] represents the ligand concentration, and [SL] represents the concentration of the complex formed by substrate and ligand (assuming the activity coefficients is neglected and set to unity) [10]. In equation 1.9, K_{eq} is the equilibrium constant of the reaction (also known as association constant). Because the association constant provides the measurement of the ligand affinity to a substrate, it can also provide the energetics of ligand/substrate binding by the following thermodynamic relationship:

$$\Delta G = - RT \bullet \ln K_{eq} \qquad \text{(Equation 1.10)}$$

In equation 10, ΔG is the Gibbs free energy change of the binding reaction, R is the gas constant, and T is the absolute temperature [10].

In ACE approach, a low concentration of substrate is injected into a capillary filled with the ligand at a concentration [L] [10]. Once the dynamic equilibrium is established, the effective net mobility of the substrate (μ) is the combination of the mobility of free and bound substrate weighted by their molar fractions [10]:

$$\mu = x_S \bullet \mu_S + x_{SL} \bullet \mu_{SL} \qquad \text{(Equation 1.11)}$$

where μ_S is the effective mobility of the free substrate, μ_{SL} is the effective mobility of the bound substrate, x_S and x_{SL} are the molar fraction of the free and bound substrate, respectively [10]. The molar fractions are expressed as

$$x_S = \frac{[S]}{[S]+[SL]} \quad \text{and} \quad x_{SL} = \frac{[SL]}{[S]+[SL]} \qquad \text{(Equation 1.12)}$$

Similar to chromatography, the ratio of bound to free substrate molecules is defined as capacity factor k' [10]:

$$k' = \frac{n_{SL}}{n_S} = \frac{[SL]}{[S]} = K_{eq} \bullet [L] \qquad \text{(Equation 1.13)}$$

Combining Equation 1.13 and Equation 1.12 gives

$$x_S = \frac{1}{1 + \frac{[SL]}{[S]}} = \frac{1}{1 + k'} \quad \text{and} \quad x_{SL} = \frac{\frac{[SL]}{[S]}}{1 + \frac{[SL]}{[S]}} = \frac{k'}{1 + k'} \qquad \text{(Equation 1.14)}$$

In the absence of the interactions to capillary wall, and without other species of substrate, Equation 1.11 is simplified to:

$$\mu = x_S \bullet \mu_S + \left(1 - x_S\right) \bullet \mu_{SL} = \frac{1}{1 + k'} \bullet \mu_S + \frac{k'}{1 + k'} \bullet \mu_{SL} \qquad \text{(Equation 1.15)}$$

Replacing k' with Equation 1.13 gives

$$\mu = \frac{1}{1 + K_{eq} \bullet [L]} \bullet \mu_S + \frac{K_{eq} \bullet [L]}{1 + K_{eq} \bullet [L]} \bullet \mu_{SL} = \frac{\mu_S + K_{eq} \bullet [L] \bullet \mu_{SL}}{1 + K_{eq} \bullet [L]} \qquad \text{(Equation 1.16)}$$

To fit with the form of Equation 1.8, Equation 1.16 is transferred to an isotherm equation:

$$\mu - \mu_S = K_{eq} \bullet [L]\left(\mu_{SL} - \mu\right) = \frac{\left(\mu_{SL} - \mu_S\right) \bullet K_{eq} \bullet [L]}{1 + K_{eq} \bullet [L]} \qquad \text{(Equation 1.17)}$$

In Equation 1.17, the dependent variable, which is the y in equation 1.8, is the value of μ-μ_S, which is the change of the effective mobility of the analyte under the presence and absence of ligand in the buffer, the a term (in Equation 1.8) is $(\mu_{SL}$-$\mu_S)\bullet K_{eq}$, the b term is 1, and the c term is K_{eq}. The y is decreasing with the increasing [L] (the x in Equation 1.8), which shifts the binding reaction to form more bound substrate SL, and increase the weight of μ_{SL} in the net mobility μ, as shown in Equation 1.15 [10]. The values of [L] are set for a serious of CE buffers, the values of μ are obtained from the electropherograms, and then the K_{eq} can be obtained from the isotherm plot [10].

The isotherm equation used in enzyme kinetics is called Henri-Michaelis-Menten equation [8]. However, the enzymatic reaction is the rapid equilibrium between the free enzyme and substrate to form the enzyme-substrate complex (ES), followed by another step to

release the product [8]. The application of Henri-Michaelis-Menten equation is limited to the condition when the concentration of ES reaches a steady state [8]. In the field of enzyme kinetics, the steady state is defined as a time period of the enzymatic reaction during which the rate of ES formation is exactly matched by its rate of decay to free enzyme and products [8]. Therefore, the experimental measurement of signal response should be conducted when ES is present at the steady state [8].

The data treatment of isotherm plot is difficult without the help of computers. However, evaluation of experimental data is possible by converting Equation 1.17 to a linear form. The three linearized equations used for plotting methods are shown below [10]:

X-reciprocal equation (Eadie-Scatchard equation in biochemistry):

$$\frac{\mu - \mu_S}{[L]} = -K_{eq}(\mu - \mu_S) + K_{eq}(\mu_{SL} - \mu_S) \qquad \text{(Equation 1.18)}$$

Y-reciprocal equation:

$$\frac{[L]}{\mu - \mu_S} = \frac{1}{\mu_{SL} - \mu_S}[L] + \frac{1}{K_{eq}(\mu_{SL} - \mu_S)} \qquad \text{(Equation 1.19)}$$

Double reciprocal equation (Lineweaver-Burk equation in biochemistry):

$$\frac{1}{\mu - \mu_S} = \frac{1}{K_{eq}(\mu_{SL} - \mu_S)}\frac{1}{[L]} + \frac{1}{(\mu_{SL} - \mu_S)} \qquad \text{(Equation 1.20)}$$

To draw the plots for Equation 1.18, 1.19, and 1.20, the y axis is the term at the left side of each equation, the x axis is (μ-μ_S), [L], and 1/[L], respectively. Linear regression equations can be obtained from these plots. The values of K_{eq} can be obtained from the intercepts and slopes of these linear plots without difficulty. For X-reciprocal plotting method, the slope of the linear regression line is $-K_{eq}$, and the value of K_{eq} is calculated from the negative value of the slope. For Y-reciprocal plotting method, the slope is $1/(\mu_{SL}-\mu_S)$, the intercept is $1/(K_{eq}\cdot(\mu_{SL}-\mu_S))$, the

value of K_{eq} is calculated from slope/intercept. For double reciprocal plotting method, the slope is $1/(K_{eq}\cdot(\mu_{SL}-\mu_S))$, the intercept is $1/(\mu_{SL}-\mu_S)$, the value of K_{eq} is calculated from intercept/slope.

These transformations change the statistical weights of the data points and thereby show different uncertainties for the value of K_{eq} [10]. For example, in the double reciprocal plot, there is more emphasis on the data points corresponding to the lowest values of the ligand concentration. As a result, the estimated mobility of the complex, μ_{SL}, shows more uncertainties at the point of intersection [10]. There are various reasons that can cause deviations from linearity. For instance, slow equilibration, adsorption at the capillary wall, and the presence of higher order equilibriums often cause lower correlation coefficients, which in turn cause incorrect value of equilibration constants.

1.7 CE-mass spectrometry (CE-MS) and MEKC-MS

Mass spectrometer is the device that ionizes molecules (charged molecules or ionized fragments) in the gas phase using an ionization source, then separates the ions according to their mass to charge ratio by the mass analyzer, and finally detects the gas phase ions by the electron multiplier [3]. Mass spectrometry is considered as an important technique to extract the ion from a mixture and provide the structural information of the analyte molecules [3]. The use of MS as a detector for CE can easily identify the analyte and significantly improve the limit of detection [3].

The most widely used ionization technique of MS coupled to CE is the electrospray ionization (ESI), which uses an electrospray interface to connect the capillary outlet from CE instrument to the electrically induced nebulization process in the MS instrument [3]. A flow of

dry nitrogen helps the evaporation of the highly charged droplets until these droplets break up to gaseous ions flying into the highly vacuumed MS detector [3]. The MS can be coupled to CZE, MEKC or CEC in a commercial CE-MS instrument to combine the advantages of both CE and MS. Especially, the high efficiency of separation and high sensitivity of detection are achieved for the simultaneous separation. This thesis also focuses on the MEKC-MS and its application for the simultaneous enantioseparation of barbiturates [7, 12-15].

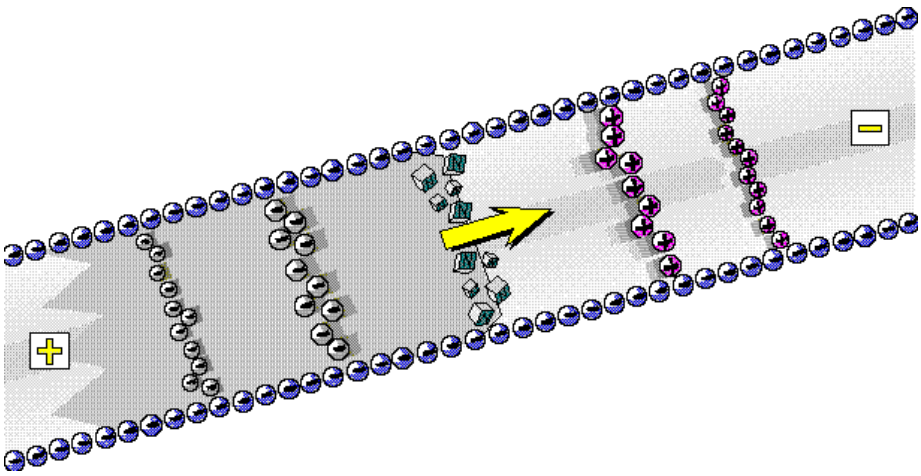

Figure 1.1 The electrophoretic mobilities of negatively charged, positively charged, and neutral species in CE. (Taken from 3D-CE/MSD ChemStation software, Agilent Technologies, Inc.)

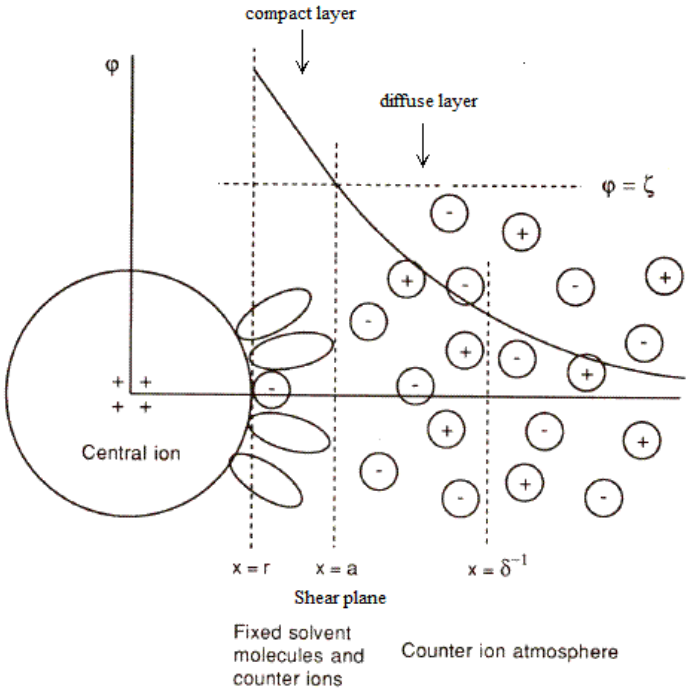

Figure 1.2 The Gouy-Chapman-Stern model of the electric double layer structure surrounding a cation [1]. r = geometric ion radius, a = shear plane, δ^{-1} = Debye length (used in physical chemistry) [1].

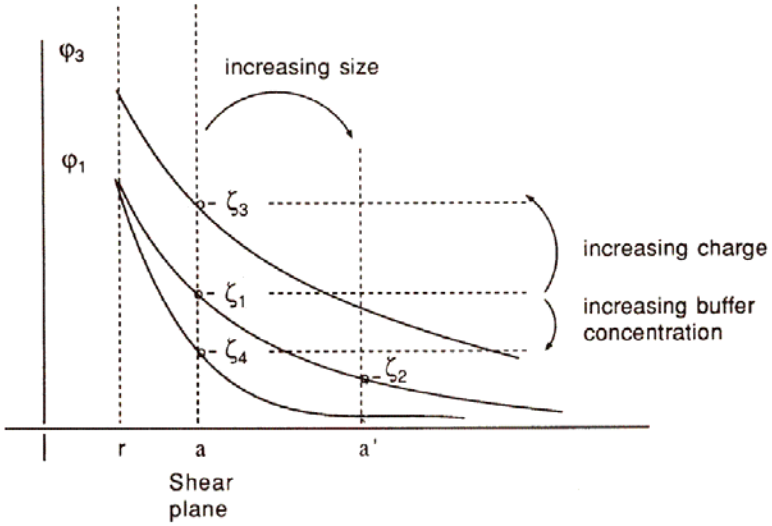

Figure 1.3 The effects of size, charge, and buffer concentration on the zeta potential [1].

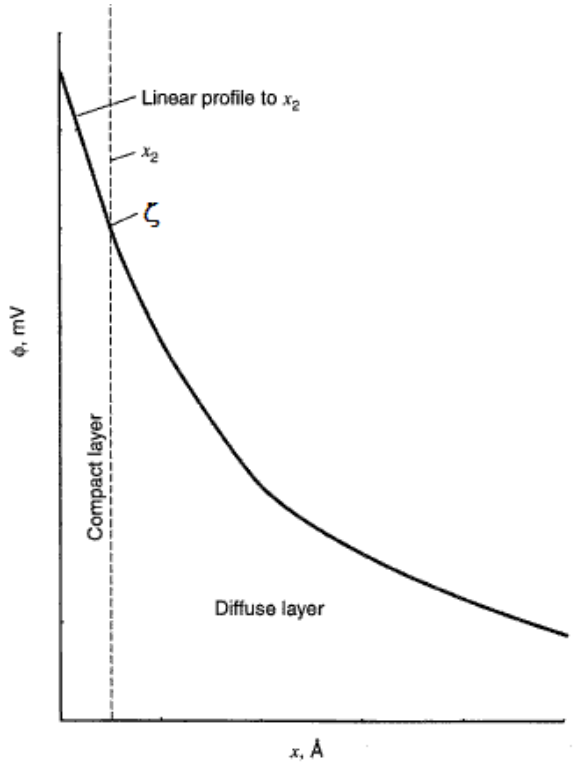

Figure 1.4 The Gouy-Chapman-Stern model of the electric double layer structure formed between capillary wall and the solution. x_2 = shear plane. The curve shows the potential profile through the solution side of the double layer [4].

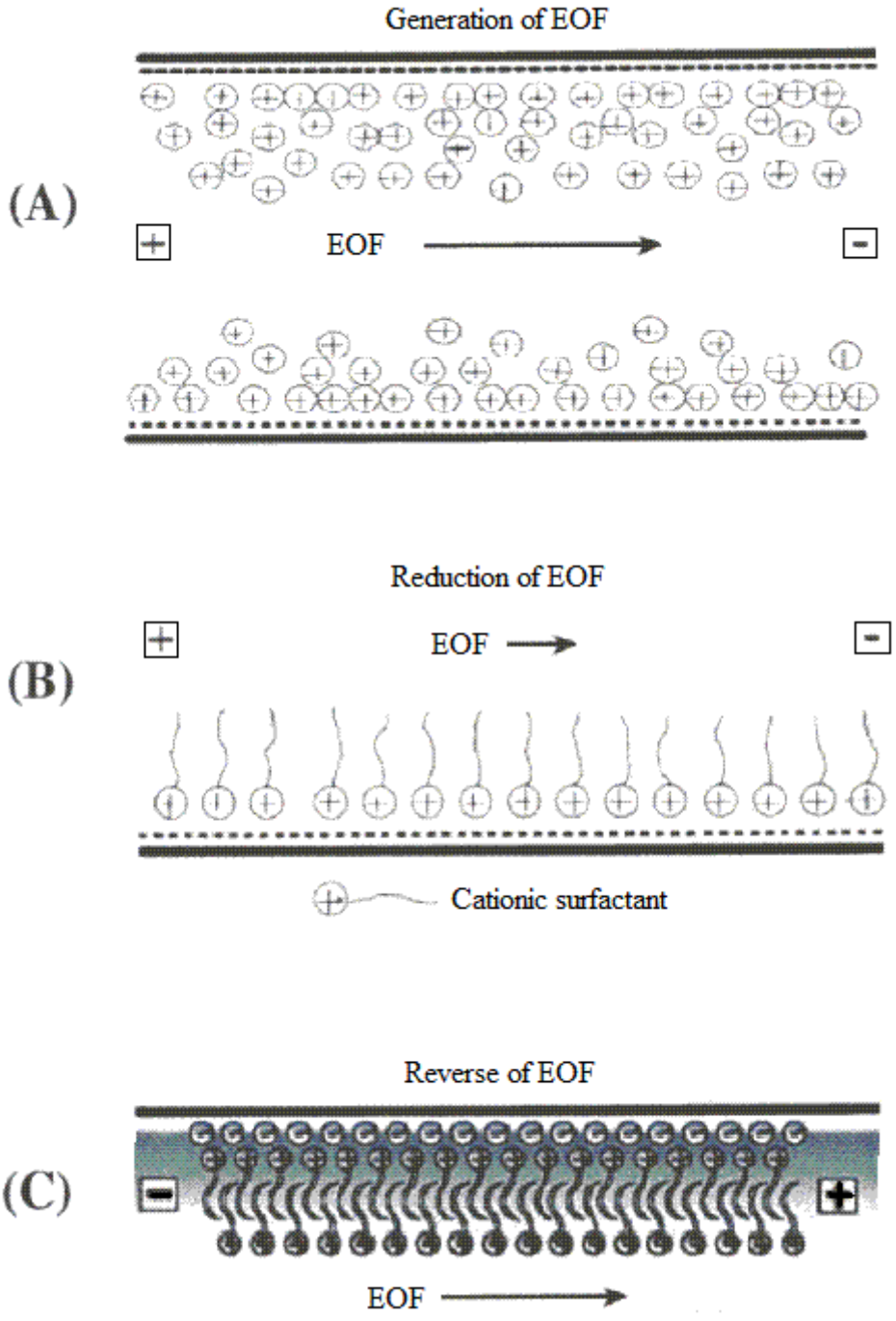

Figure 1.5 The schematic of EOF in the capillary. (A) The generation of EOF, (B) the reduction of EOF, (C) the reversal of EOF [2].

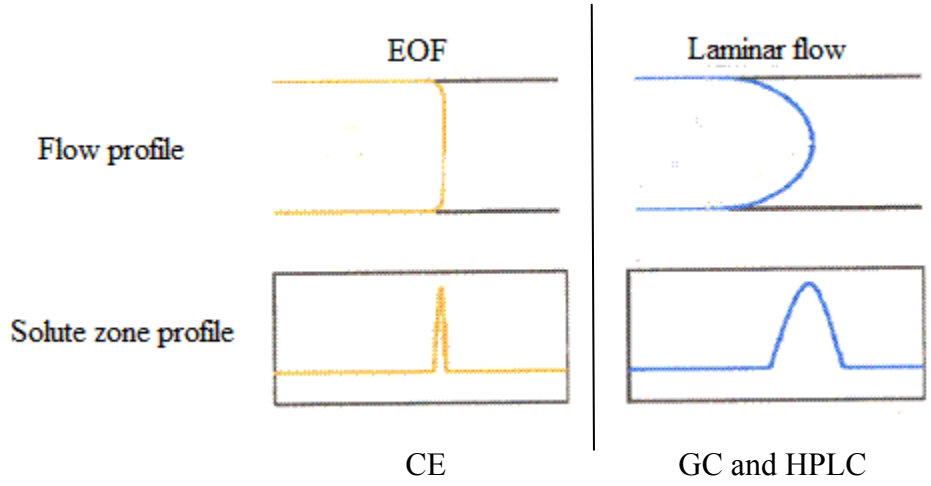

Figure 1.6 The flow profiles and corresponding solute zones of voltage driven system (CE) and pressure driven system (GC, HPLC) [2].

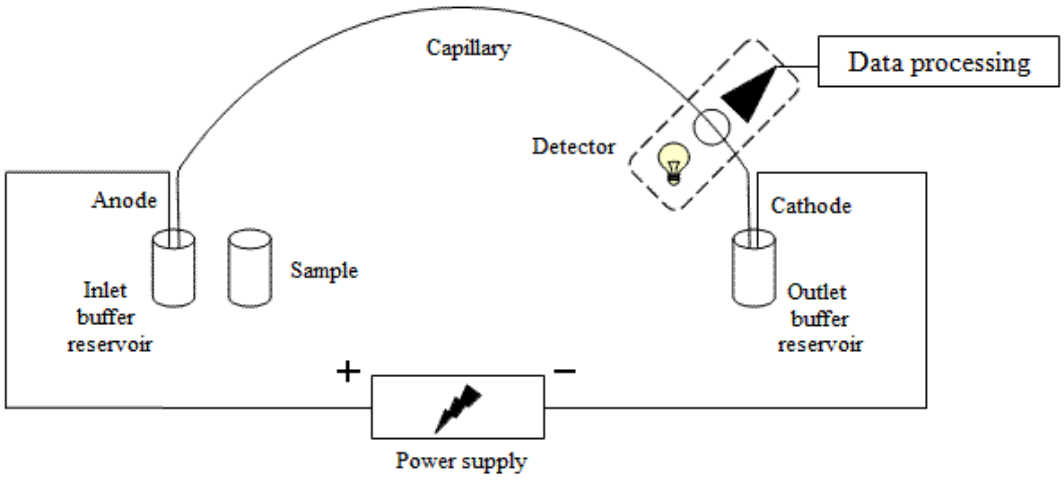

Figure 1.7 The schematic of CE instrument [2].

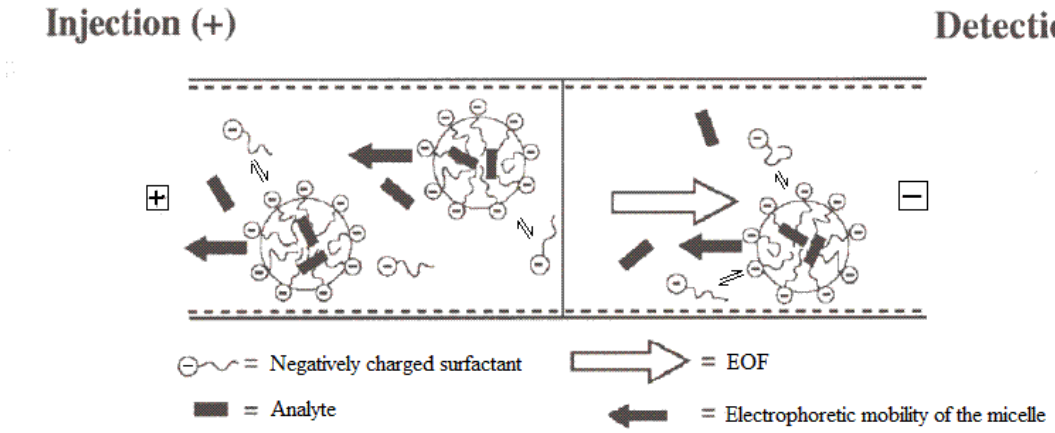

Figure 1.8 The illustration of the separation principle of MEKC (using negatively charged surfactants in aqueous solutions) [2].

CHAPTER 2. COMBINED USE OF IONIC LIQUIDS AND CYCLODEXTRIN FOR SIMULTANEOUS ENANTIOSEPARATION OF ANIONIC PROFENS

2.1 Introduction

Separations of chiral compounds on analytical-scale are subject to immense interest. This is mainly because currently there are strict regulatory issues for the preparation of enantiomerically pure compounds. Therefore, dedicated analytical assay for enantiomeric purity are essential for drug screening in the pharmaceutical industry. In addition, chiral discrimination has also been shown to be increasingly important in agricultural, environmental and biological sciences [1]. Capillary electrophoresis (CE) has proved to be an effective tool for chiral discrimination, studying chiral interactions and measurement of binding constants of enantiomers. This is due to high efficiency, short analysis time and requirement of only a small quantity of exotic chiral selector. Among the various chiral reagents, native cyclodextrins (CDs) and their derivatives [2] macrocyclic antibiotics [3] as well as polymeric surfactants [4] have proven to be very successful for CE. However, the utility of the aforementioned reagents as a single chiral selector to resolve enantiomers is not always satisfactory. Hence, the utility of more than one chiral reagent in CE to improve the enantioseparation has drawn increase attention in recent years [5-7].

Ionic liquids (ILs) are organic salts consisting ionic components with low melting points (i.e., at or close to room temperature) [8-9]. Very recently, our group reported the first use of two new cationic ILs type surfactants as a single chiral selector in micellar electrokinetic chromatography (MEKC) [10]. Subsequently the cationic IL, *N*-undecenoxyl-carbonyl-L-leucinol bromide (L-UCLB) and *N*-undecenoxyl-carbonyl-L-pyrrolidinol bromide (L-UCPB) and their polymers were synthesized, characterized and compared for the enantioseparation of

two negatively charged enantiomers (α-bromo-phenyl acetic acid, and phenoxy propionic acid). The primary interaction of afore-mentioned ILs is thought to involve electrostatic attractive interactions. Proposed secondary interactions include steric, hydrophobic and hydrogen-bonding interactions. Very recently, the combined use of various CD derivatives and two chiral ILs (ethyl- and phenyl-choline of bis (trifluoromethylsulfonyl) imide) was evaluated for enantiomeric separations by CE. Although no clear trend was observed, enhancement in chiral selectivity and resolution of two profens (e.g., carprofen and suprofen) were achieved, which suggests synergistic effect [11]. A similar report on the use of chiral IL, S-[3-(chloro-2-hydroxypropyl)trimethylammonium][bis(trifluoromethyl)sulfonyl]amide has been reported in combination with 1-*S*-octyl-β-D-thiogluco-pyranoside (OTG) and/or sodium cholate for the enantioseparation of ibuprofen and flurbiprofen, respectively [12].

This work is focused on the combined use of cationic IL-type surfactants (L-UCLB) and heptakis 2,3,6-tri-O-methyl-β-CD (TM-β-CD) as a dual chiral selector for MEKC. Because L-UCLB did not provide any enantioselectivity with regard to model class of analytes (PROFs) under the reversed electroosmotic flow (EOF) MEKC, the influence of L-UCLB was studied in combination to TM-β-CD under the normal EOF MEKC. As demonstrated in this paper, the presence of L-UCLB would widen the scope of application of TM-β-CD. For example, the widening of the chiral window was obtained upon addition of L-UCLB. This implies that simultaneous enantioseparation of the five structurally similar aryl-propionic acids (PROFs) would be achieved in a high throughput fashion. The enantiomeric resolution, selectivity and the total analysis time were compared using concentration and chain length of ILs. In addition, batch-to-batch reproducibility of IL surfactants for the simultaneous enantioseparation was also compared. Finally, an approach originated from enzyme kinetics was used to study the binding

constants of L-UCLB to TM-β-CD, PROFs to TM-β-CD, and of PROFs to L-UCLB. This approach is applicable based on the assumption that two or more additives have significant interactions with each other. We hypothesize that the IL, L-UCLB act as an *"inhibitor",* reducing the interaction between TM-β-CD and the PROFs. To test the aforementioned hypothesis, we proposed a general model for the ternary interactions among profens, TM-β-CD and L-UCLB. To the best of our knowledge, this is the first study in which the simultaneous enantioseparation of PROF drug is achieved using a mixture of IL and TM-β-CD as a dual chiral selector.

2.2 Materials and methods

2.2.1 Reagents and chemicals

The five PROF compounds (ibuprofen, fenoprofen, indoprofen, suprofen, and ketoprofen), dimethyl sulfoxide (DMSO, anhydrous, 99.9+%), and TM-β-CD were purchased from Sigma-Aldrich (St. Louis, MO, USA). Sodium acetate was purchased from Fisher Scientific (Chemical Manufacturing Division, Fair Lawn, NJ, USA). Acetic acid, dichloromethane, ethyl acetate, and acetone were purchased from Caledon Laboratories (Georgetown, ON, Canada). Deionized water was prepared with a Barnstead "NANOpure" ultrapure water system (Dubuque, Iowa, USA).

The reagents ω-undecylenyl alcohol, 2-bromoethylamine hydrobromide, pyridine anhydrous, *S*-(+)-leucinol, formic acid (≥95), and formaldehyde (37 wt. % solution in water) used for the synthesis of ILs were purchased from Sigma-Aldrich (St. Louis, MO, USA). 7-Octen-1-ol and triphosgene were obtained from TCI (Tokyo Kasei Kogyo Co. LTD, Tokyo, Japan). Hydrochloric acid and sodium sulfate anhydrous were purchased from EMD Chemicals

(Gibbstown, NJ, USA). Sodium bicarbonate was purchased from Mallinckrodt Baker (Phillipsburg, NJ, USA). Sodium hydroxide (50% w/w) was purchased from Fisher Scientific (Pittsburgh, PA, USA). Two ILs, L-UCLB and *N*-octenoxycarbonyl-L-leucinol (L-OCLB, Figure 2.1) were synthesized following a previously optimized procedure [10].

2.2.2 CE instrumentation

All CE experiments were performed on an Agilent CE system (Agilent Technologies, Santa Clara, CA, USA) equipped with an on-line diode array detector (DAD) for the absorbance measurements at 214 nm. The temperature control of the sample carousel at 16 °C was maintained by Fisher ISOTEMP 3016S refrigerating circulator (Fisher Scientific, Pittsburgh, PA, USA). The 3D-CE Chemstation software was used for the instrumental control, data acquisition, and data analysis. The fused silica capillaries (Polymicro Technologies, Phoenix, AZ, USA) with dimensions of 64.5 cm total length, 56.0 cm effective length, 50 μm i.d., and 365 μm o.d. were used throughout the study. The exact values of the total length and effective length of the capillaries were measured and used for the calculation of binding constants.

2.2.3 CE conditions and methods

2.2.3.1 Simultaneous enantioseparation of profen drugs using L-UCLB and L-OCLB

The concentration of each PROF stock solution prepared in pure MeOH was 2.0 mg/mL. A fixed aliquot of ibuprofen, fenoprofen, indoprofen, suprofen, and ketoprofen racemates were respectively dissolved in a binary solvent mixed with MeOH and H_2O in the ratio of 70:30 (v:v). The 5 mM NaOAc solution was prepared by dissolving $NaOAc{\cdot}3H_2O$ in triply DI water. The pH of this solution was adjusted to 5.0 using 15.1 μL of 17.4 M HOAc solution. A bare fused

silica capillary was first preconditioned for 60 minutes with 1 M NaOH at 50 °C, and then flushed for 30 min with triply DI water at 16 °C. Before each injection, the capillary was flushed with the separation buffer for 5 min. After each run, the capillary was postconditioned with DI water for 5 min, 0.1 M aqueous NaOH solution for 10 min, and DI water for 5 min. The sample was hydrodynamically injected at 3 mbar, 8 seconds. The separations were carried out under an applied voltage of +30 kV and a temperature of 16 °C. The absorbance of PROF drugs in the CE buffer was monitored at 214 nm.

2.2.3.2 Estimation of the binding constant between TM-β-CD and L-UCLB (K_1)

The stock solution of L-UCLB was prepared by dissolving in 5 mM NaOAc aqueous buffer (pH 5.0) at the concentration of 4.0 mM. The DMSO was dissolved in 5 mM NaOAc buffer (pH 5.0) at the concentration of 0.1 mg/mL. Consequently, 100 μL of L-UCLB and DMSO solutions were added to a vial and vortexed to make a mixture solution to be injected into the capillary with an injection size of 50 mbar, 20 sec. The CE buffers used in this study were 5 mM NaOAc aqueous buffer (pH 5.0) without TM-β-CD, and the same buffer with TM-β-CD at concentrations ranging from 2.5 mM to 10.0 mM. The capillary rinsing procedure before the first run, the precondition before each run, and the postcondition after each run were generally the same as described in section 2.3.1 except that the postcondition of 0.1 mM NaOH was 5 min instead of 10 min. The separations were carried out with an applied voltage of +20 kV and a temperature of 16 °C. The direct UV detection of L-UCLB was achieved at 200 nm.

The addition of TM-β-CD in the CE buffer will change the viscosity of the buffer, and thereby affect the mobility of the L-UCLB in the buffer with different concentration of TM-β-CD [13-14]. To study this effect, the relative viscosities of the TM-β-CD buffer were measured

by hydrodynamic injection of the sample containing 2.0 mM L-UCLB and 0.05 mg/mL DMSO in 5 mM NaOAc buffer (pH 5.0) with the injection size of 50 mbar, 20 sec. The sample was pushed through the detector with a constant pressure of 50 mbar [13-14]. The viscosity correction factor was estimated using the following equation:

$$\nu = \frac{\eta}{\eta_0} = \frac{t}{t_0}, \qquad \text{(Equation 2.1)}$$

where η_0 is the viscosity of the CE buffer without TM-β-CD, and η is the viscosity of the CE buffer with a certain concentration of TM-β-CD [13-14]. The time t_0 and t represent the time required for the sample plug to move through the injection end of the capillary to the detector in a CE buffer without and with a certain concentration of TM-β-CD, respectively. The sample plugs used to estimate the relative viscosity were monitored at 200 nm.

Affinity capillary electrophoresis (ACE) is widely used to measure the binding constant [15]. This method is based on the changes of effective mobilities of the free and bound forms of analytes due to the association-dissociation kinetics between the analyte and ligand [15]. The shift of the position of the L-UCLB peak relative to the position of the TM-β-CD peak was measured with the increasing concentration of TM-β-CD. The neutral marker, DMSO, was used to indicate the position of TM-β-CD peak and calculate the effective mobilities of free and bound L-UCLB. The binding constant between L-UCLB and TM-β-CD (K_1) was estimated by the linear plotting methods using Microsoft Excel software (version 2007), as listed in Table 2.1. The plots used were X-reciprocal, Y-reciprocal, and double-reciprocal methods [15]. In the equations shown in Table 2.1, μ_f is the effective mobility of the free form of L-UCLB in the absence of TM-β-CD, μ_i is the effective mobility of the L-UCLB in equilibrium with TM-β-CD in serial CE buffers containing increasing concentrations of TM-β-CD. The μ_c is the effective mobility of the TM-β-CD/L-UCLB complex form at saturating conditions, which is difficult to

measure experimentally but can be easily obtained from any standard nonlinear regression software [14, 16]. The ν is the viscosity correction factor, as we described before. The values of binding constant K_1 were calculated from the slopes and intercepts of the linear plots, as shown in Table 2.1 [14, 16]. The nonlinear isotherm plot was obtained by a nonlinear regression fitting equation shown in Table 2.1 [14, 16]. The Origin (version 7.5) software was used for the data treatment of nonlinear plotting method [14].

2.2.3.3 Estimation of the binding constants of fenoprofen to TM-β-CD and fenoprofen to L-UCLB (K_2 and K_i)

The stock solutions of fenoprofen (0.20 mg/mL) and DMSO (0.50 mg/mL) were prepared in 5 mM aqueous buffer of NaOAc at pH 5.0. The mixture solution to be injected into the capillary was made by adding 100 μL of each stock solution of fenoprofen and DMSO in a sample vial. The mixture was then injected with the injection size of 5 mbar, 10 sec. The concentrations of TM-β-CD ranged from 1.0 to 50 mM. The viscosity correction factors for these buffers were obtained by the same method described in section 2.3.2. The binding experiment for measurement of K_2 was performed under a voltage of +10 kV, temperature of 16 °C with UV detection at 200 nm. The migration time of *R* and *S* enantiomers of fenoprofen was used to estimate the binding constants.

The K_2 value between TM-β-CD and fenoprofen enantiomers were obtained from the same double-reciprocal plotting method described in section 2.3.2. The values of K_2 were different in the absence and presence of L-UCLB. The inhibition constant K_i was estimated from a secondary plot obtained by the method originated from enzyme kinetics [17, 18]. The details of inhibition study are explained in section 3.2.

2.3 Results and discussion

2.3.1 Studies on simultaneous enantioseparation of profens

2.3.1.1 Evaluation of synergistic effect between L-UCLB and TM-β-CD

With a goal to extend the enantioselective capability of L-ULCB, a series of structurally similar anionic drugs (e.g., PROFs, shown in Figure 2.1) was investigated. No enantioselectivity was observed for any PROF drug when using L-UCLB as a single chiral selector. It is well-documented that among the several native and derivatized CDs, the TM-β-CD is the best chiral selector for the separation of PROFs [19]. Next, we investigated the association between L-UCLB and TM-β-CD to search for possible synergistic effects. As shown in Figure 2.2A, TM-β-CD exhibits reasonable enantioselectivity for individual anionic PROFs, but it was less successful in completely resolving the PROF enantiomers in complex mixtures of structurally similar PROFs. For example, only slight resolution was observed for ibuprofen enantiomers (1,1'). In addition, the later eluting enantiomers of indoprofen (3') co-eluted with the first eluting enantiomer of suprofen (4). Hence, TM-β-CD only partially separated the enantiomeric mixture of PROFs with a narrow chiral window. However, upon addition of 1.5 mM L-UCLB to the CE buffer containing TM-β-CD, all enantiomers of PROFs were baseline resolved (except for ibuprofen, which provided *Rs* value of 1.32) with a significant widening of the chiral window (Figure 2.2B). Furthermore, the peak efficiency improved by 3-10 times (data not shown). We hypothesize that these improvements in simultaneous enantioseparation of PROFs are due in large part to the interaction between TM-β-CD and L-UCLB, which in turn reduces the interaction of the L-UCLB with the capillary wall.

2.3.1.2 Evaluation of the profen/TM-β-CD/IL interaction system

The five PROF enantiomers (Figure 2.1) studied in this work have *pKa* values less than 5.0, and the background electrolyte, sodium acetate used in this work, has a pH value of 5.0. Therefore, all of the PROFs were partially anionic in the CE buffer. During the MEKC separation, the capillary is filled with the CE buffer contained three major species: the neutral chiral selector TM-β-CD, the positively charged chiral selector L-UCLB, and negatively charged analytes PROFs. As can be seen in Figure 2.3, the interactions among these species could be divided into three parts: (a) the interactions (K_1) between the TM-β-CD and the IL monomers or micelles, (b) the interactions (K_i) between the PORFs and IL monomer or micelles, and (c) the interactions (K_2) between PROFs and TM-β-CD. The monomer of IL might form inclusion complex with TM-β-CD. It should be noted that he IL monomers or micelles are cationic while the PROFs are anionic. Hence, the interactions between these two species might include electrostatic attraction (ion-pair), hydrogen bonding, and hydrophobic interactions. In addition, the PROFs might also form inclusion complex with TM-β-CD. When a positive polarity was used in CE separation, the L-UCLB monomer or micelles migrated before EOF, TM-β-CD migrated with EOF, and PROFs migrated after EOF. It cannot be ascertained from the schematic (shown in Figure 2.3) whether the anionic PROFs partition exclusively to the TM-β-CD cavity or whether the PROF-(L-UCLB) complex is included in the TM-β-CD cavity. Nevertheless, the interactions among these species caused the differential binding forces between the racemic pairs of the PROFs and the two chiral selectors TM-β-CD and L-UCLB; thereby the enantioseparation could be achieved.

2.3.1.3 Influence of ionic liquid concentration on resolution and migration time

Figure 2.4 shows the electropherograms illustrating the effect of low mM concentrations of L-UCLB as an additive to the TM-β-CD buffer. The increasing concentrations of L-UCLB from 1.0 to 3.0 mM had a significant influence on the resolution and migration time of anionic PROFs. As can be seen in Figure 2.4A-C, the chiral and achiral resolutions of all PROFs increased, comparing to the ones in Figure 2.4A. In addition, the electroosmotic mobility decreased dramatically over the same concentration range from 1.998×10^{-4} $cm^2\cdot V^{-1}\cdot s^{-1}$ to 8.964×10^{-5} $cm^2\cdot V^{-1}\cdot s^{-1}$ due to adsorption of L-UCLB to the capillary wall. The inset plot in Figure 2.4 shows that the increasing concentration of L-UCLB caused the highest change in resolutions of fenoprofen racemate (from 2.6 to 5.0) and the smallest change in the resolution of ibuprofen racemate (from 1.1 to 1.7). Furthermore, the achiral resolution between critical pair of indoprofen and suprofen (3'/4) also increased from 1.7 (1.0 mM L-UCLB) to 1.9 (3.0 mM L-UCLB). However, the continuous increase in migration times made the buffer with concentration higher than 3.0 mM L-UCLB not applicable. The optimum concentration of L-UCLB for simultaneous enantioseparation seems to be 2.0 mM, which provides a good compromise between analysis time and resolution values.

2.3.1.4 Batch-to-batch reproducibility

We also investigated the batch to batch reproducibility of the L-UCLB synthesis. Figure 2.5 is a representative series of electropherograms for the simultaneous enantioseparation of profens using three batches of L-UCLB. All three electropherograms were generated under same buffer conditions using the same capillary. The %RSD of electroosmotic mobility was 0.84%. The %RSD for the average efficiency of each batch is 7.53%, whereas the %RSD for

the migration time of the profens range from 1.06% to 2.56%. The %RSD of the resolution between two consecutive profen peaks in Figure 2.5 (i.e., from peak 1 to 5') were 8.47%, 8.68%, 6.76%, 3.66%, 3.27%, 5.00%, 3.09%, 3.20%, 4.79%, and 7.76%. Therefore, it can be concluded that the procedure for synthesis of L-UCLB is sufficiently reproducible.

2.3.1.5 Influence of chain length

Previously, the polymeric anionic surfactants with leucinate head group and C_8-C_{11} chain length were evaluated for the simultaneous enantioseparation of eight β-blockers [20]. The eight carbon chain chiral surfactant provided the overall best enantioselectivity. However, the anionic chiral polymeric surfactants are not very suitable for anionic chiral analytes. To study the effect of the chain length, we synthesized another cationic IL such as L-OCLB with eight carbon chain. A generalized structure of optically pure cationic surfactant can be seen in Figure 2.1. The only difference between these two chiral surfactant-type IL L-UCLB and L-OCLB is the length of the hydrocarbon chain attached to the leucinol head group via carbamate linkage. Figure 2.6 compares the simultaneous enantioseparation of five profen drugs using the same concentration of L-UCLB (Figure 2.6A) and L-OCLB (Figure 2.6B). As expected, the migration times of all profens and EOF in Figure 2.6A are all longer with the use of eleven carbon chain IL micelles than the use of eight carbon chain IL micelle (Figure 2.6B). For example, the migration time of the latest peak (*S*-ketoprofen) eluted at 52.3 min when using L-UCLB, while it eluted at 44.8 min when using L-OCLB. However, unexpectedly, the chiral resolutions and selectivities of the racemic profen pairs did not change very much. This study suggests that L-UCLB and L-OCLB performed similar binding interactions with TM-β-CD.

2.3.2 Theory of the binding constants and mechanism of separation

As discussed above, the ILs are the micelle of a cationic surfactant, while the PROFs are partially anionic in the MEKC buffer. If the interactions between these two species are strong, the PROFs should migrate with ILs and before EOF. However, the PROFs eluted after the EOF, and the migration time of PROF increased with the increasing concentration of ILs. This phenomenon indicates that both TM-β-CD and the ILs played an important role for the enantioseparation. In this section, we propose an inhibition mechanism for the interactions of PROF with L-UCLB and TM-β-CD. The concept of inhibition originated from enzyme kinetics. It is well-known that the enzyme and substrate have specific interaction between each other, and an inhibitor may also bind to the same enzyme [17]. For the competitive inhibition, the inhibitors can exclusively interact with the free enzyme. In other words, the enzyme binds either the substrate or the inhibitor, but not both simultaneously. For noncompetitive inhibition, the inhibitor binds with free enzyme and with enzyme-substrate complex simultaneously. In case of uncompetitive inhibition, the inhibitor binds exclusively with enzyme-substrate complex [17].

In our system, we hypothesize that the L-UCLB and TM-β-CD are competing with each other for the binding sites on the PROF. The addition of L-UCLB to the TM-β-CD could decrease the interaction between the PROF and TM-β-CD, thereby inhibiting the formation of PROF-(TM-β-CD) complexes. Moreover, the interaction between the two chiral selectors (i.e., L-UCLB and TM-β-CD) also decreases the binding of the PROF to each of them. During the separation, the PROFs had weaker interactions with both TM-β-CD and ILs due to this inhibition mechanism, which probably resulted in the enantioseparation. The reactions for the competitive inhibition mechanism are shown as follows:

Scheme 1. competitive inhibition:

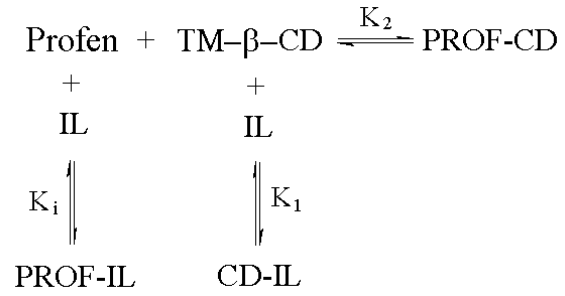

where PROF-CD represents the complex formed between profens and TM-β-CD, PROF-IL represents the complex formed between profens and ILs, CD-IL represents the complex formed between TM-β-CD and ILs. Note that the inhibitor L-UCLB has interactions with both PROFs and the TM-β-CD, so it inhibited the chiral interaction between TM-β-CD and PROFs. In addition to competitive inhibition, noncompetitive and uncompetitive inhibitions are also possible.

Scheme 2 represents a noncompetitive inhibition in which the L-UCLB binds with the free PROF and with PROF-CD complex.

Scheme 2. noncompetitive inhibition:

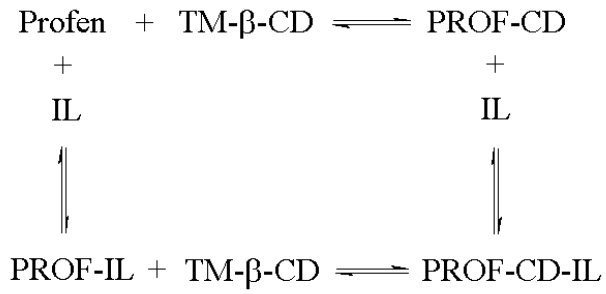

where PROF-IL and PROF-CD represent the same complexes as mentioned above. However, the PROF-CD-IL represents the ternary complex eventually formed by the three species profen,

TM-β-CD, and L-UCLB. The binding of L-UCLB can also occur exclusively with PROF-CD complex, which can mimic uncompetitive inhibition model as shown below in Scheme 3.

Scheme 3. uncompetitive inhibition:

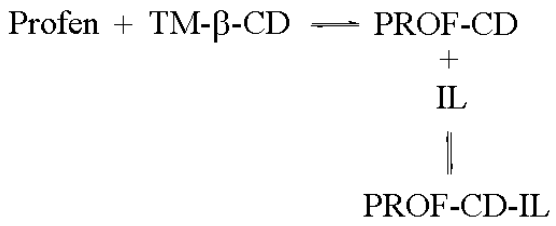

In the above Scheme 3, the profen firstly binds to TM-β-CD, and then to L-UCLB. The final product is the PROF-CD-IL, which is essentially the same ternary product as the one shown in Scheme 2.

The double-reciprocal plot (or Lineweaver-Burk plot in biochemistry) can be used to determine the mode of inhibition [17, 18]. The double-reciprocal plots for the binding of TM-β-CD and the PROF sample were obtained under several fixed concentrations of the inhibitor L-UCLB, respectively (see section 2.3.3). Overlaying these straight lines will show a pattern that can determine the type of inhibition. For example, the linear plots obtained for competitive inhibition will show same y intercept values but increasing slope values with the increase of inhibitor concentration. On the other hand, the overlaid plots for uncompetitive inhibition should appear as a series of parallel lines that intersect the y axis at different y values. For the noncompetitive inhibition, both the slope and the y intercept of the double-reciprocal plot will increase with increasing concentration of the inhibitor.

2.3.2.1 Determination of TM-β-CD/L-UCLB binding constant (K_1)

To investigate the mechanism of inhibition, the binding constant between TM-β-CD and L-UCLB was first measured by the conventional linear plotting methods used in most of the published work related to ACE [21-25]. As mentioned earlier, Figure 2.4 suggests that the migration time of the EOF shifted with increasing concentration of L-UCLB, which is due to the increase in viscosity of the MEKC buffer. Therefore, we had to allow for viscosity correction when calculating the L-UCLB effective mobilities (see section 2.3.2). Table 2.1 shows the four equations used to estimate the binding constant K_1 between TM-β-CD and L-UCLB after multiplying the mobilities with the viscosity correction factor (ν). The effective mobilities of L-UCLB (μ_f and μ_i) were calculated at different concentrations of TM-β-CD.

The four equations shown in Table 2.1 are equivalent in their algebraic forms. However, the experimental precision on the dependent and independent variables will affect the correlation differently [15]. This difference will be dependent on whether the variables are placed in the numerator or denominator of the equation. For instance, the effect of the precision on variable [TM-β-CD] will alter when the data are transferred to 1/[TM-β-CD] for plotting in the X-reciprocal and double-reciprocal methods. Moreover, it is worth mentioning that X-reciprocal, Y-reciprocal, and double-reciprocal methods can not measure the actual mobilities of the complexed L-UCLB cation (μ_c) whereas the nonlinearized regression of isotherm equation can provide the value of μ_c using any standard software [14-16]. In general, a good estimation of μ_c can be obtained by measuring the limited effective mobility of the L-UCLB cation at very high TM-β-CD concentration [14-16].

The data treatment of the free and complex mobility as well as the viscosity correction is tabulated in Table 2.2. Figure 2.7 shows the electropherograms obtained with a bare silica

capillary filled with various concentration of TM-β-CD. Upon increasing the concentration of TM-β-CD, an increase in migration time of L-UCLB cation was observed. This relationship indicates a decrease in charge-to-mass ratio of L-UCLB once complexed with TM-β-CD. The time difference between the peaks of L-UCLB and TM-β-CD (the same peak as neutral marker) decreased gradually with the increasing concentration of TM-β-CD, and the binding constant was estimated from this time difference.

Figure 2.8A-C shows the linearized representations (X-reciprocal, Y-reciprocal, double-reciprocal plots, see Table 2.1 for equations of the 1:1 binding isotherm for (L-UCLB)-(TM-β-CD) complex). Note that the negative deviation in linearity on the y-axis at the x-axis maxima (low TM-β-CD concentration) of the double-reciprocal plot (Figure 2.8C) represents the concentration of TM-β-CD at which sample overloading is present. Although the correlation using X-reciprocal method (Figure 2.8A) was only moderate, the high degree of correlation obtained by Y-reciprocal and double-reciprocal plots (Figure 2.8B and 2.8C, respectively) suggests that 1:1 complexation model is acceptable [15].

The binding constants (i.e., K_1) values between TM-β-CD and L-UCLB are listed in Table 2.3. The deviations of K_1 values were from the errors of different plotting methods [15]. The non-linear isotherm plot of L-UCLB mobility is shown in Figure 2.8D. As shown in Figure 2.8D, the corrected effective mobility of L-UCLB reached a plateau when the CE buffer contained more than 10 mM of TM-β-CD. The value of K_1 calculated was 1093 M^{-1} ± 123, which is consistent with the values obtained from the linear plotting methods. In general, the value of K_1 obtained in Table 2.3 was around 1000 M^{-1}, which is comparable with the binding constants between TM-β-CD and imidazole based ILs [7]. These reported K_1 values implied that TM-β-CD and L-UCLB have relatively high interaction with each other.

2.3.2.2 Determination of profen/TM-B-CD binding constant K_2

The second step was to measure the binding constants of one representative PROF (fenoprofen) to TM-β-CD. This experiment was conducted together with the experiments to measure the binding constant of fenoprofen to L-UCLB. In other words, the measurements of K_2 and K_i were achieved in one series of experiments by double-reciprocal plotting method. The TM-β-CD concentration in the CE buffers ranged from 1.0 mM to 50.0 mM. Note that in Figure 2.9A and 2.9B, the linear plot in the absence of L-UCLB (i.e., 0.0 mM L-UCLB) has the smallest slope compared to the other linear plots in the presence of various concentration of L-UCLB. In other words, the slopes of the linear plots in Figure 2.9 increased as the concentration of L-UCLB increased. Because K_2 is obtained from the ratio of slope/intercept, therefore, the values of K_2 decreased with the increasing concentration of L-UCLB in the CE buffer. The values of K_2 were calculated from these linear regression plots and are shown in Table 2.4. For the *R*-fenoprofen, the K_2 decreased from 598±26 M^{-1} to 198±22 M^{-1} upon increasing the concentration of L-UCLB up to 0.8 mM, and then slightly increased to 215±19 M^{-1} when the concentration of L-UCLB is further increased 1.0 mM. For the *S*-fenoprofen, the K_2 decreased from 625±22 M^{-1} to 207±24 M^{-1} and then increased slightly to 226±21 M^{-1}. The abnormal increase of K_2 upon increasing L-UCLB from 0.8 mM to 1.0 mM is probably caused by the experimental errors that will be explained in the following section (i.e., section 3.2.3). Nevertheless, for both enantiomers, the minimal K_2 values showed at 0.8 mM L-UCLB. This trend implied that the L-UCLB in the buffer interacted with fenoprofen, which in turn reduced the affinity between fenoprofen and TM-β-CD. The increasing amount of L-UCLB in the buffer will cause the decreasing affinity between fenoprofen and TM-β-CD.

2.3.2.3 Determination of profen/L-UCLB binding constant K_i

The third step was to estimate the binding constants of fenoprofen to L-UCLB. We respectively added L-UCLB into the 5.0 mM NaOAc buffer at concentrations of 0.0, 0.2, 0.5, 0.8, and 1.0 mM, which were considered as the concentration of inhibitors, L-UCLB. Next, the double-reciprocal plots were generated at each fixed concentration of L-UCLB. Figure 2.9A and 2.9B showed the patterns of double-reciprocal plots for *R*- and *S*-fenoprofen, respectively. The R-squared values of these lines were better than the one for the binding between TM-β-CD and L-UCLB, because 10 kV was applied instead of 20 kV. Table 2.5 listed the values of slopes and intercepts of these linear regression plots. For the *R*-fenoprofen (columns 2 and 3), the slope values changed from 13.4±0.5 to 37.0±1.6, while the y-intercept values range from 7134±696 to 8392±155. The %RSD of the y-intercept values is about 6.0%. In Figure 2.9, the error bars on the data points were removed for clarity of presentation. The 95% confidence interval (95%CI) of the data point in double reciprocal plot at a fixed concentration of 1.0 mM TM-β-CD but variable concentration of L-UCLB (i.e., 0.8 and 1.0 mM), were ±4820 $V \times s \times cm^{-2}$ and ±3961 $V \times s \times cm^{-2}$, respectively. These 95% CI values are much greater than the ones for the other data points of the respective plots. The deviation of the intercept values (especially for the plot at 0.8 mM L-UCLB) were due to the inaccuracy and irreproducibility of the migration times of fenoprofen at low concentrations of TM-β-CD. For example, under the conditions of 0.8 mM or 1.0 mM L-UCLB, and the concentrations of TM-β-CD at 0.0 or 1.0 mM in the CE buffers, it took more than 2 hrs for the fenoprofen peaks to elute out and caused greater error on the migration time than at other concentration of L-UCLB. However, this relatively high deviation is acceptable in the literature of biochemistry when determining the type of

inhibition [26]. The data for *S*-fenoprofen showed the same trends for the slopes and intercepts with the greatest deviation at 0.8 mM L-UCLB. As we discussed in section 3.2 and shown in Figure 2.9 as well as Table 2.5, we believe that the pattern of the double-reciprocal plots with increasing slope values but constant intercept values implies that the inhibition happened between L-UCLB and the (TM-β-CD)-(fenoprofen) complex is similar to the enzyme-substrate-inhibitor systems [26], and mainly it is a type of competitive inhibition.

The data generated in Table 2.5 can be used to obtain the inhibition constant between L-UCLB and fenoprofen (K_i) from a secondary plot of which the x-axis is the concentration of the L-UCLB and y-axis is the slope values of the double-reciprocal plots obtained from Table 2.5 [18, 26]. Here the inhibition constant is the dissociation constant of the (L-UCLB)-(fenoprofen) complex [17, 18]. As can be seen in Figure 2.10, the value of the x-intercept of the linear plot was the negative value of the inhibition constant K_i [18], which was $4.81\pm1.18\times10^{-4}$ M for *R*-fenoprofen, and $4.73\pm1.18\times10^{-4}$ M for *S*-fenoprofen. However, strictly speaking, the inhibition constant we obtained was an apparent inhibition constant.

2.3.3 The binding constant of the enantiomers

In the experiments discussed above to determine the values of K_2 and K_i, the sample used was the racemic mixture of fenoprofen. The separation of the racemic pair was based on the different binding constants between the enantiomers and the two chiral selectors TM-β-CD and L-UCLB. Figure 2.11 showed the double-reciprocal plots for *R*- and *S*-fenoprofen at a fixed concentration of 0.5 mM L-UCLB using various concentrations of TM-β-CD ranging from 0.0 mM to 50.0 mM. It is clear that at low concentration (i.e., below 5 mM TM-β-CD) the regression trendlines for the two enantiomers overlapped, suggesting no chiral resolution.

When the concentration of TM-β-CD is greater than 5 mM, the y axis values of the *R*- and *S*-fenoprofen at the same concentration of TM-β-CD deviated from each other with the increasing concentration of TM-β-CD. Table 2.5 showed the K_2 values for *R*- and *S*-fenoprofen at different concentration of L-UCLB. The K_2 values for *S*-fenoprofen were always greater than *R*-fenoprofen at all concentration of L-UCLB ranging from 0.0 to 1.0 mM. This trend implied that the interaction between *S*-fenoprofen and TM-β-CD was stronger compared to the one between *R*-fenoprofen and TM-β-CD. The addition of L-UCLB did not change this trend, but increase the chiral resolution, which gradually changed from no resolution to partial resolution and then baseline resolution. This trend is consistent with the enantioseparation shown in Figure 2.3.

2.4 Concluding remarks

The simultaneous enantioseparation of five profens was achieved by the addition of L-UCLB in the low concentration range (1.5 to 2.0 mM) in the TM-β-CD buffer. The resolutions (both achiral and chiral resolutions) and migration times of the profens were very sensitive to the concentration of L-UCLB. Unlike the literature report on the effects of the chain length of anionic surfactants, decreasing length of the hydrocarbon chain of the cationic IL surfactants did not show any significant influence on the chiral resolutions. However, the migration times decreased as expected. The final method permits to simultaneously resolve the enantiomers of the PROFs with an analysis time of 44 min. Three batches of L-UCLB made in different months were tested for the simultaneous enantioseparation of PROFs under same conditions. The migration times, efficiencies, and resolutions of the PROFs showed little deviation, which implies that the batch-to-batch reproducibility of L-UCLB synthesis is satisfied for the

enantioseparation. Finally, the concepts of enzymatic reactions were successfully applied to determine the mode of inhibition of L-UCLB. Using fenoprofen as a model compound that strongly interacts with TM-β-CD, a series of double reciprocal plot showed a trend of increasing slope values with almost a constant intercept. This trend is in accordance with the observation described in the literature [26], suggesting that the inhibition observed in chiral separation of PROFs is a competitive inhibition. Future studies will be focused on the combined use of the same dual chiral selector (i.e., TM-β-CD and L-UCLB) for the separation of neutral compounds.

2.5 References

[1] Gal, J., *Chirality in Drug Research Vol 33,* Francotte, E., Lindner, W. (Eds.), Wiley VCH, Weinheim, Germany 2006, pp. 3-24.

[2] Maruszak, W., Schmid, M. G., Gubitz, G., Ekiert, E., Trojanowicz, M., *Methods in Molecular Biology, Vol 243, Chiral Separation Methods and Protocols*, Gubitz, G and Schmid, M. G (Eds), Humana Press Inc., Totowa, N.J 2004, pp.275-289.

[3] Gasper, M. P., Berthod, A., Nair, U. B., Armstrong, D. W., *Anal. Chem.* 1996, *68*, 2501-2514.

[4] Shamsi, S. A., Cedillo, B., Haddadian, F., Warner, I. M., *Anal. Chem.* 2003, *75*, 379-387.

[5] Han, Y., Chen, Yi., *Electrophoresis* 2007, *28*, 2765-2770.

[6] Huang, Lu., Lin, J., Xu, L., Chen, G., *Electrophoresis* 2007, *28*, 2758-2764.

[7] Mwongela, S.M., Numan, A., Gill, N. L., Agbaria, A. R., Warner, I. M., *Anal. Chem.* 2003, *75*, 6089-6096.

[8] Seddon, K. R., *J. Chem. Technol. Biotechnol.* 1997, *68*, 351-356.

[9] Wilkes, J. S., Levisky, J. A., Wilson, R. A., Hussey, C. L., *Inorg. Chem.* 1982, *21*, 1263-1264.

[10] Rizvi, S. A., Shamsi, S. A., *Anal. Chem*. 2006, *78*, 7061-7069.

[11] François, Y., Varenne, A., Juillerat, E., Villemin, D., Gareil, P., *J. Chromatogr. A*. 2007, *1155*, 134-141.

[12] Tran, C. D., Mejac, I., *J. Chromatogr. A*. 2008, *1204*, 204-209.

[13] François, Y., Varenne, A., Sirieix-Plenet, J., Gareil, P., *J. Sep. Sci.* 2007, *30*, 751-760.

[14] Karakasyan, C., Tavern, M., Millot, M., *J. Chromatogr. A* 2004, *1032*, 159-164.

[15] *Affinity capillary electrophoresis in pharmaceutics and biopharmaceutics*, Neubert, R. H. H., Ruttinger, H. (Eds), Marcel Dekker, New York, 2003.

[16] Rundlett, K. L., Armstrong, D. W., *J. Chromatogr. A* 1996, *721*, 173-186.

[17] Copeland, R. A., *Enzymes: a practical introduction to structure, mechanism, and data analysis,* 2nd ed., Wiley-VCH, New York, 2000.

[18] Smith, H. J., Simons, C., *Enzymes and their inhibition: drug development*, CRC press, Boca Raton, 2005.

[19] Martín-Biosca, Y., Garcia-Ruiz, C., Marina, M., *Electrophoresis* 2001, *22*, 3216-3225.

[20] Rizvi, S. A., Shamsi, A. S., *Electrophoresis* 2005, *26*, 4172-4186.

[21] Gomez, F. A., Avlla, L. Z., Chu, Y., Whitesides, G. M., *Anal. Chem.* 1994, *66*, 1785-1791.

[22] Rundlett, K. L., Armstrong, D. W., *Electrophoresis* 1997, *18*, 2194-2202.

[23] Rundlett, K. L., Armstrong, D. W., *Electrophoresis* 2001, *22*, 1419-1427.

[24] Heegaard, N. H. H., Nissen, M. H., Chen, D. D. Y., *Electrophoresis* 2002, *23*, 815-822.

[25] Heegaard, N. H. H., *Electrophoresis* 2003, *24*, 3879-3891.

[26] Barkhimer, T. V., Kirchhoff, J. R., Hudson, R. A., Messer, W. S., *Anal. Biochem.* 2005, *339*, 216-222.

Table 2.1 Equations used to estimate K_1 between TM-β-CD and L-UCLB.

Plotting method	Regression equation	Calculated K_1
Nonlinear isotherm	$\nu\mu_i - \mu_f = K[\text{TM-β-CD}](\mu_c - \nu\mu_i) = \frac{(\mu_c - \mu_f)K[\text{TM-β-CD}]}{1 + K[\text{TM-β-CD}]}$	Nonlinear regression by software
X-reciprocal	$\frac{\nu\mu_i - \mu_f}{[\text{TM-β-CD}]} = -K(\nu\mu_i - \mu_f) + K(\mu_c - \mu_f)$	-slope
Y-reciprocal	$\frac{[\text{TM-β-CD}]}{\nu\mu_i - \mu_f} = \frac{1}{\mu_c - \mu_f}[\text{TM-β-CD}] + \frac{1}{K(\mu_c - \mu_f)}$	slope/intercept
Double reciprocal	$\frac{1}{\nu\mu_i - \mu_f} = \frac{1}{K(\mu_c - \mu_f)}\frac{1}{[\text{TM-β-CD}]} + \frac{1}{\mu_c - \mu_f}$	intercept/slope

Table 2.2 Calculation of the mobility values and viscosity correction factors for K_1.

[TM-β-CD] (Mm)	t(i)[a] (min)	t(m)[b] (min)	$\mu(f)=(1/t(i)-1/t(m))\times L_d\times L_t/V$ ($cm^2\times V^{-1}\times s^{-1}\times 10^{-4}$)	t_0 (min)	$\nu=t/t_0$
0.00	7.60 7.68 7.66	12.22 12.60 12.64	1.524±0.024	15.93	1.000

[TM-β-CD] (Mm)	t(i)[a] (min)	t(m)[b] (min)	$\mu(i)=(1/t(i)-1/t(m))\times L_d\times L_t/V$ ($cm^2\times V^{-1}\times s^{-1}\times 10^{-4}$)	t[c] (min)	$\nu=t/t_0$
2.50	8.16 7.93 7.72	11.46 11.10 10.71	1.078±0.015	16.75	1.051
3.00	7.50 7.60 7.83	10.26 10.50 10.88	1.082±0.009	16.15	1.014
3.50	7.52 8.10 8.13	10.25 11.35 11.48	1.071±0.008	16.08	1.009
4.00	8.04 9.06 9.61	11.30 13.39 14.62	1.075±0.004	15.96	1.002
4.50	9.22 8.71 9.63	13.61 12.61 14.49	1.057±0.012	15.94	1.000
5.00	9.15 9.03 9.09	13.32 12.99 13.33	1.033±0.017	16.04	1.007
5.50	10.00 10.57 9.41	15.17 16.42 14.02	1.030±0.019	16.10	1.011
6.00	8.63 8.18 8.53	12.20 11.41 11.93	1.023±0.017	16.16	1.014
7.00	8.30 8.51 8.59	11.43 11.92 12.05	1.004±0.011	16.57	1.040
8.00	9.04 8.53 9.14	12.86 11.87 13.07	0.991±0.001	16.74	1.050
9.00	9.02 8.92 9.12	12.85 12.62 12.94	0.986±0.011	16.63	1.044
10.00	9.04 9.50 10.05	12.74 13.89 14.94	0.982±0.018	16.40	1.029

a) t(i): the migration time of L-UCLB.

b) t(m): the migration time of neutral marker DMSO.

c) t: the elution time used to calculate the viscosity correction factor.

Table 2.3 Data treatment for the plots used to estimate the binding constant K_1.

Nonlinear isotherm		X reciprocal	
[TM-β-CD] Unit: M	ν×μ(i)-μ(f) Unit: $cm^2 \times V^{-1} \times s^{-1} \times 10^{-3}$	ν×μ(i)-μ(f) Unit: $cm^2 \times V^{-1} \times s^{-1} \times 10^{-3}$	(ν×μ(i)-μ(f))/[TM-β-CD] Unit: $cm^2 \times V^{-1} \times s^{-1} \times M^{-1}$
0.0000	0.0000	N/A	N/A
0.0025	-0.0391	-0.0391	-0.01565
0.0030	-0.0426	-0.0426	-0.01421
0.0035	-0.0443	-0.0443	-0.01266
0.0040	-0.0447	-0.0447	-0.01117
0.0045	-0.0467	-0.0467	-0.01037
0.0050	-0.0484	-0.0484	-0.00968
0.0055	-0.0482	-0.0482	-0.00877
0.0060	-0.0487	-0.0487	-0.00811
0.0070	-0.0480	-0.0480	-0.00685
0.0080	-0.0483	-0.0483	-0.00604
0.0090	-0.0494	-0.0494	-0.00549
0.0100	-0.0513	-0.0513	-0.00513
Y reciprocal		Double reciprocal	
[TM-β-CD] Unit: M	[TM-β-CD]/(ν×μ(i)-μ(f)) Unit: $V \times s \times M \times cm^{-2}$	1/[TM-β-CD] Unit: M^{-1}	1/(ν×μ(i)-μ(f)) Unit: $V \times s \times cm^{-2} \times 10^3$
0.0025	-63.98	400	-2.559
0.0030	-70.37	333	-2.346
0.0035	-79.00	286	-2.257
0.0040	-89.51	250	-2.238
0.0045	-96.49	222	-2.144
0.0050	-103.42	200	-2.068
0.0055	-114.10	182	-2.075
0.0060	-123.37	167	-2.056
0.0070	-145.99	143	-2.086
0.0080	-165.66	125	-2.071
0.0090	-182.13	111	-2.024
0.0100	-195.12	100	-1.951

Table 2.4 The estimated values of K_1 by linear plotting methods.

Plotting method	Regression equation	K_1 value
Nonlinear isotherm	y= -0.05536x/(1+1093x)	$K_1 = 1093\pm123\ M^{-1}$
X-reciprocal	y = -0.9534x-0.054	$K_1 = -(-0.9534\pm0.110\times1000) = 953\pm110\ M^{-1}$
Y-reciprocal	y = -18280x-15.51	$K_1 = (-18280\pm322)/(-15.51\pm1.97) = 1179\pm151\ M^{-1}$
Double reciprocal	y = -17.433x-17902	$K_1 = (-17902\pm351)/(-17.433\pm1.537) = 1027\pm93\ M^{-1}$

The standard deviations for non-linear regression and linear regression data were calculated by Origin 7.5 and MS Office Excel 2007 software, respectively.

Table 2.5 The estimated values of K_2 for *R*- and *S*-fenoprofen from double-reciprocal plots.

[L-UCLB] (mM)	Slope for *R* form ($V\times s\times M\times cm^{-2}$)	Intercept for *R* form ($V\times s\times cm^{-2}$)	K_2 for *R* form (M^{-1})	Slope for *S* form ($V\times s\times M\times cm^{-2}$)	Intercept for *S* form ($V\times s\times cm^{-2}$)	K_2 for *S* form (M^{-1})
0.00	13.4±0.5	8018±173	598±26	13.1±0.4	8205±139	626±22
0.20	17.6±0.4	8392±155	477±14	17.3±0.4	8595±138	497±14
0.50	20.9±0.2	8162±71	391±5	20.6±0.2	8397±67	408±5
0.80	36.0±1.9	7134±696	198±22	35.7±2.0	7394±734	207±24
1.00	37.0±1.6	7966±614	215±19	36.6±1.8	8280±662	226±21

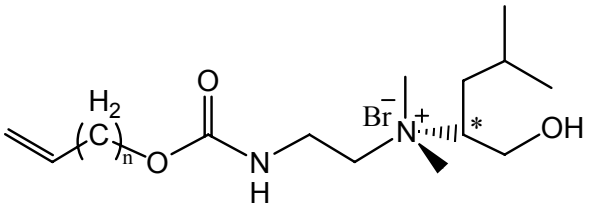

n = 9 = undecenoxycarbonyl-L-leucinol bromide (L-UCLB)

n = 6 = octenoxycarbonyl-L-leucinol bromide (L-OCLB)

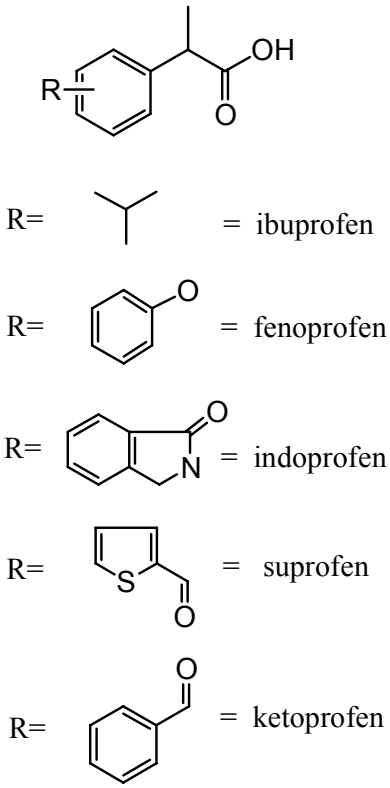

Figure 2.1 Structural formulas of ionic liquids L-UCLB and L-OCLB, and the studied aryl propionic acids (profens).

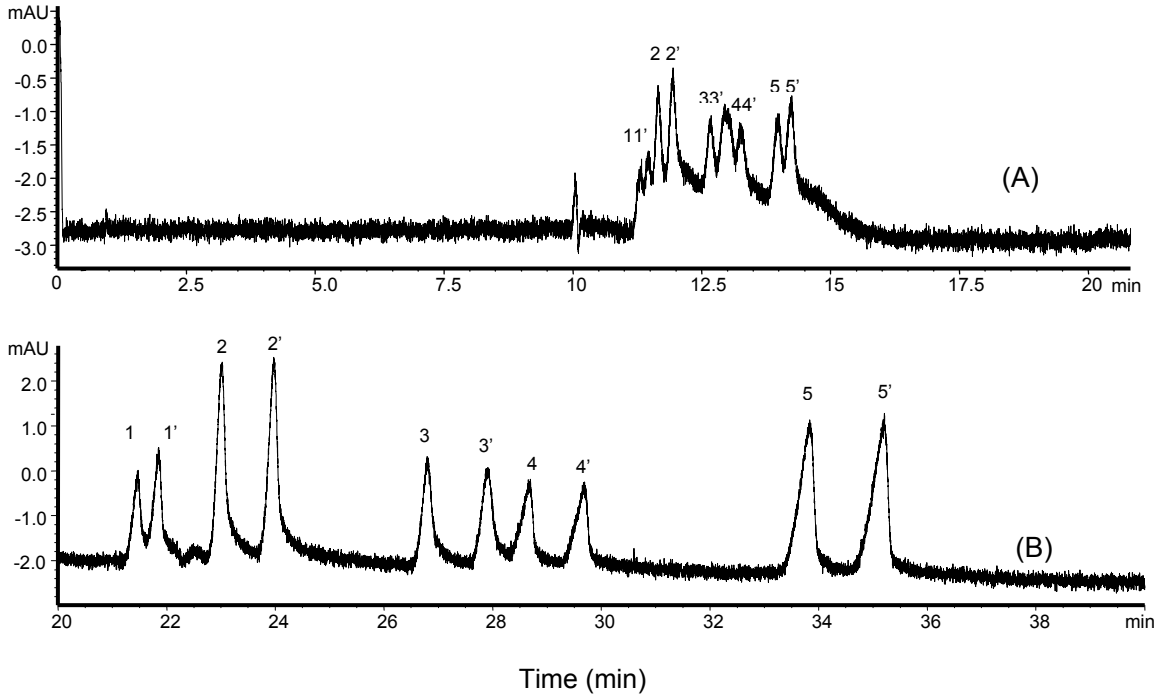

Figure 2.2 Simultaneous enantioseparation of profen (PROF) drugs in the absence (A), and presence (B) of L-UCLB. CE conditions: 5.00 mM NaOAc, 2.63 mM HOAc (pH 5.0) containing 35.0 mM TM-β-CD (A), and 35.0 mM TM-β-CD, 1.5 mM L-UCLB (B). Fused silica capillary, 64.5 cm total length and 50 μm i.d.; separation temperature 16 °C; applied voltage +30 kV; pressure injection: 3mbar, 8 sec. UV detection at 214 nm.

Peaks identification: 11'= R, S–ibuprofen; 22'= R, S–fenoprofen; 33'= R, S–indoprofen; 44'= R, S–suprofen; 55'= R, S–ketoprofen.

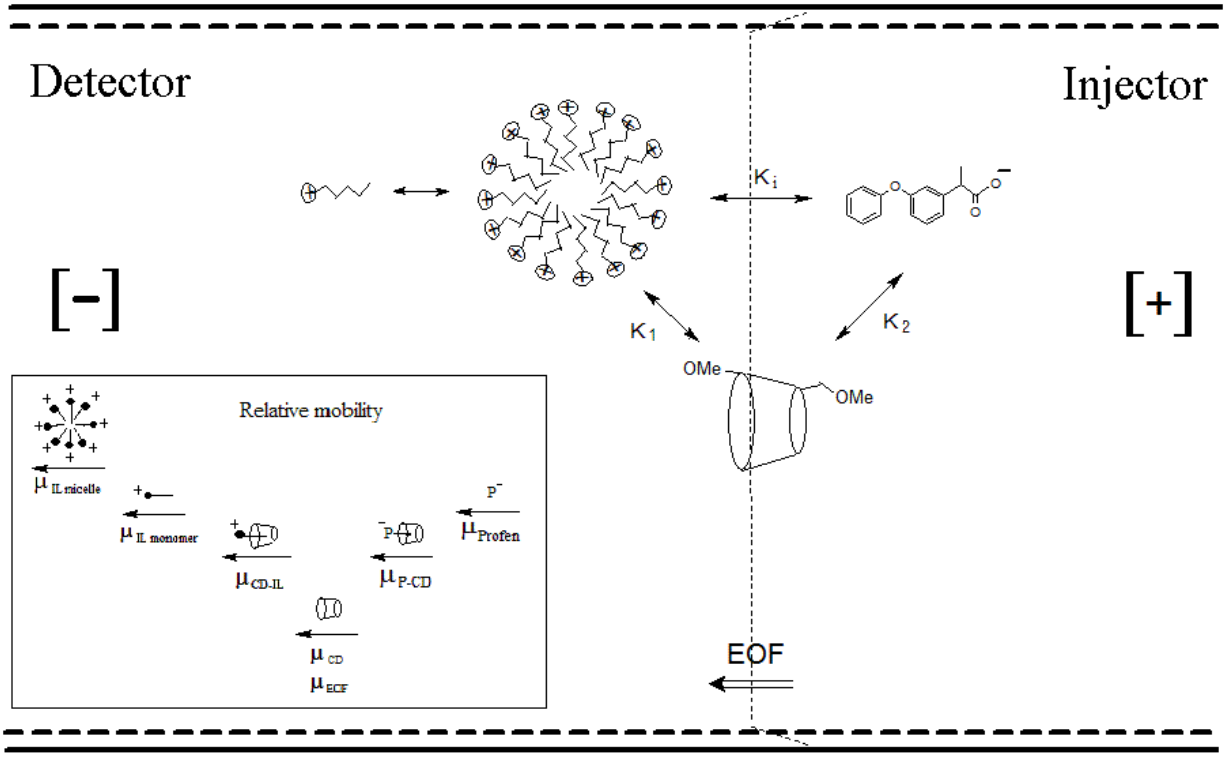

Figure 2.3 Schematic description of the interaction system involving TM-β-CD, anionic PROFs (P^-), and chiral cationic IL-type surfactants.

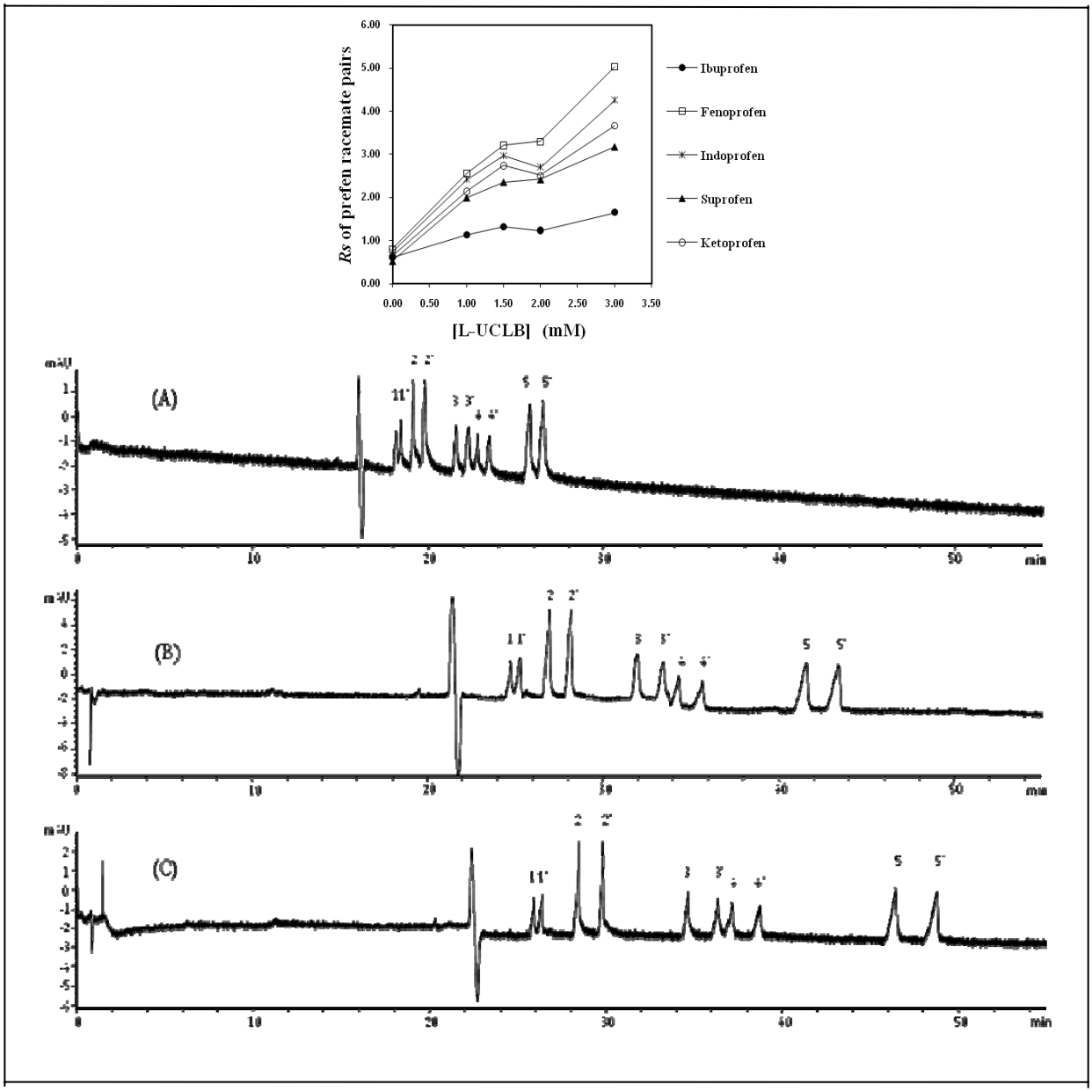

Time (min)

Figure 2.4 Effect of concentration of L-UCLB for the simultaneous enantioseparation of PROF drugs. All other conditions are same as described in Figure 2.2(B) except variable concentration of L-UCLB was used. 1.0 mM L-UCLB (A), 2.0 mM L-UCLB (B), 3.0 mM L-UCLB (C). The inset plot shows the resolutions of profen drugs as a function of L-UCLB concentrations.

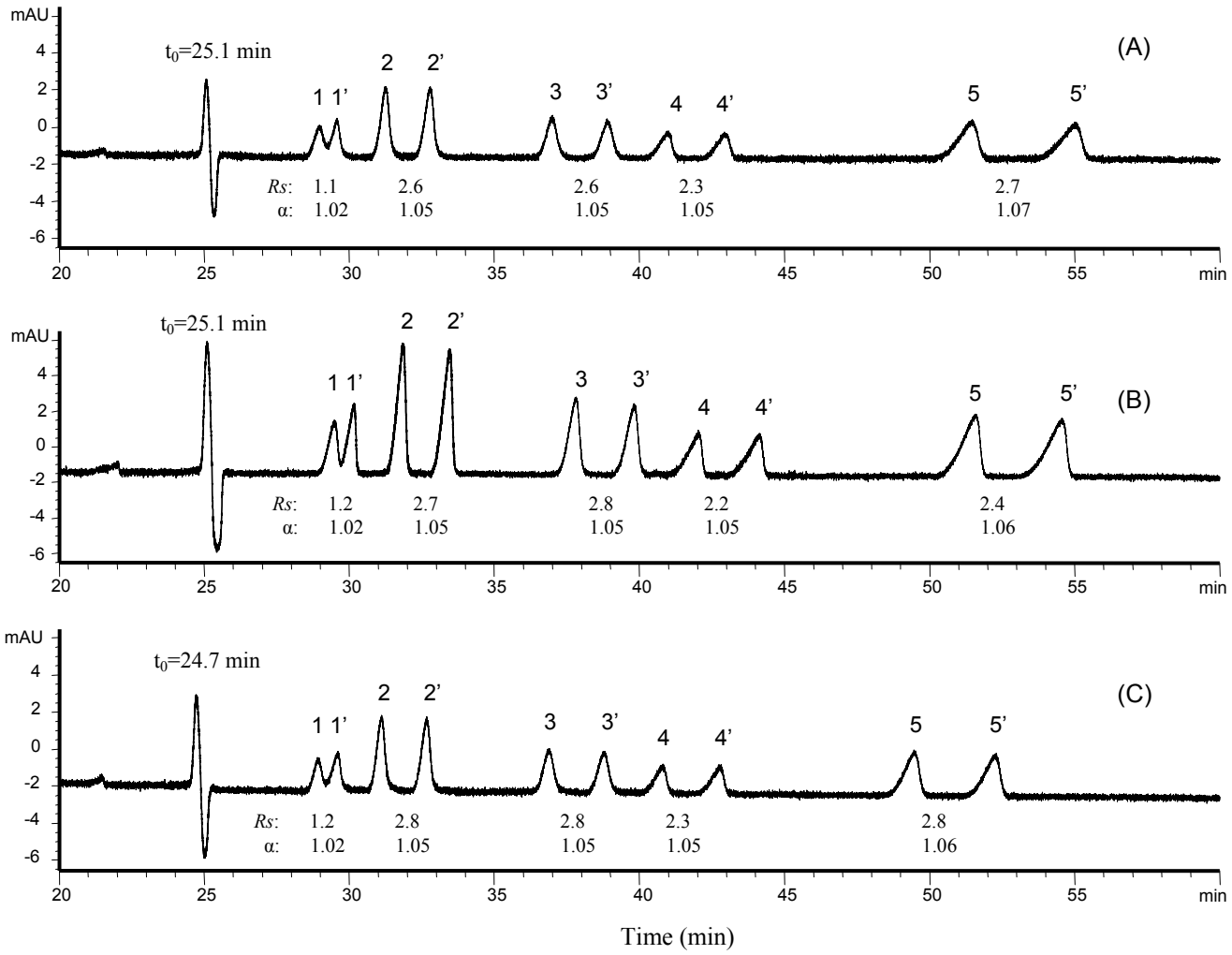

Figure 2.5 Effect of batch-to-batch reproducibility on the simultaneous enantioseparation of profen drugs. 5.00 mM NaOAc, 2.63 Mm HOAc, Ph 5.0; 35.0 Mm TM-β-CD buffer, 3.00 Mm L-UCLB, A: batch091507, B: batch092107, C: batch102207. All other conditions are the same as described in Figure 2.2(B).

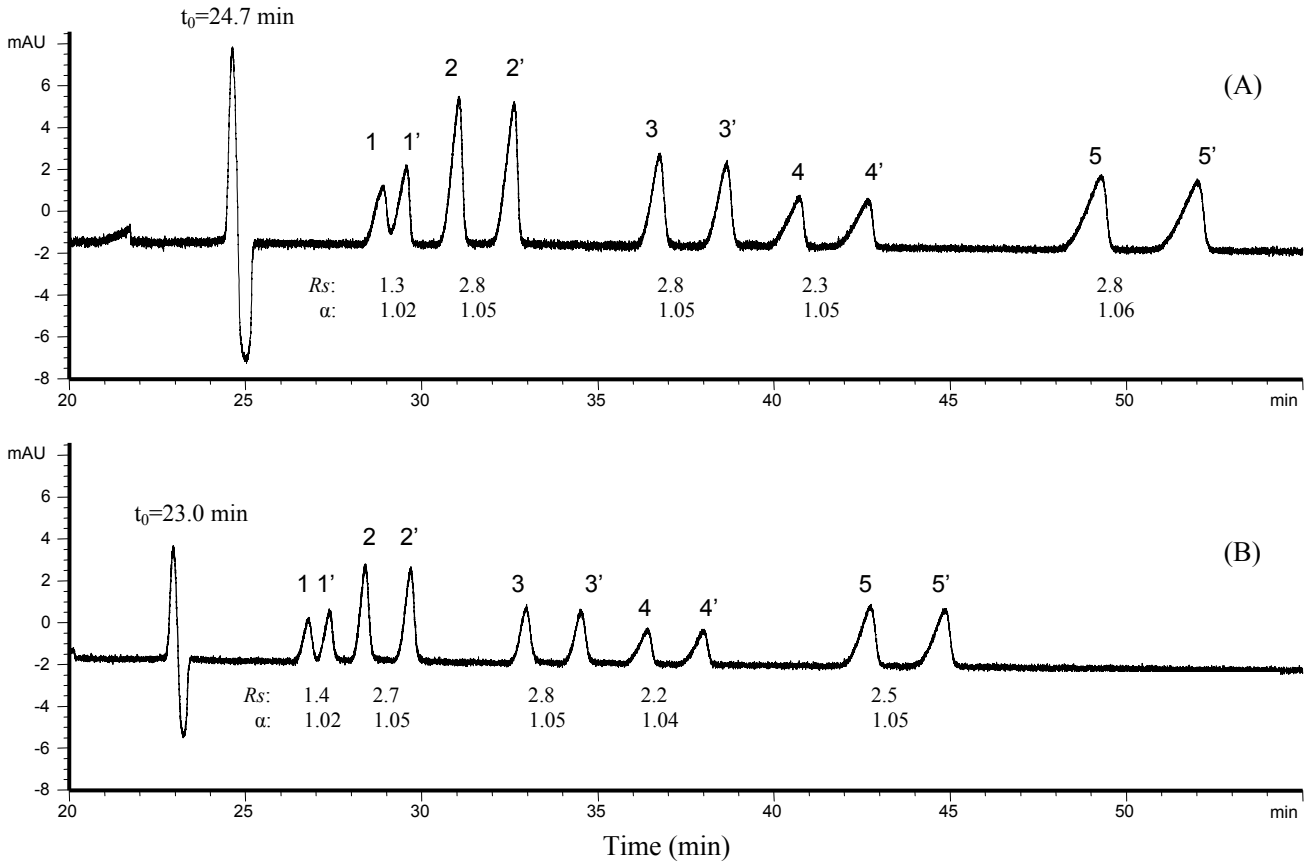

Figure 2.6 Comparison of L-UCLB and L-OCLB ionic liquids for simultaneous enantio-separation of profen drugs. 5.00 mM NaOAc, 2.63 mM HOAc, pH 5.0; 35.0 mM TM-β-CD buffer; 3.0 mM L-UCLB or L-OCLB. All other conditions are the same as described in Figure 2.2(B).

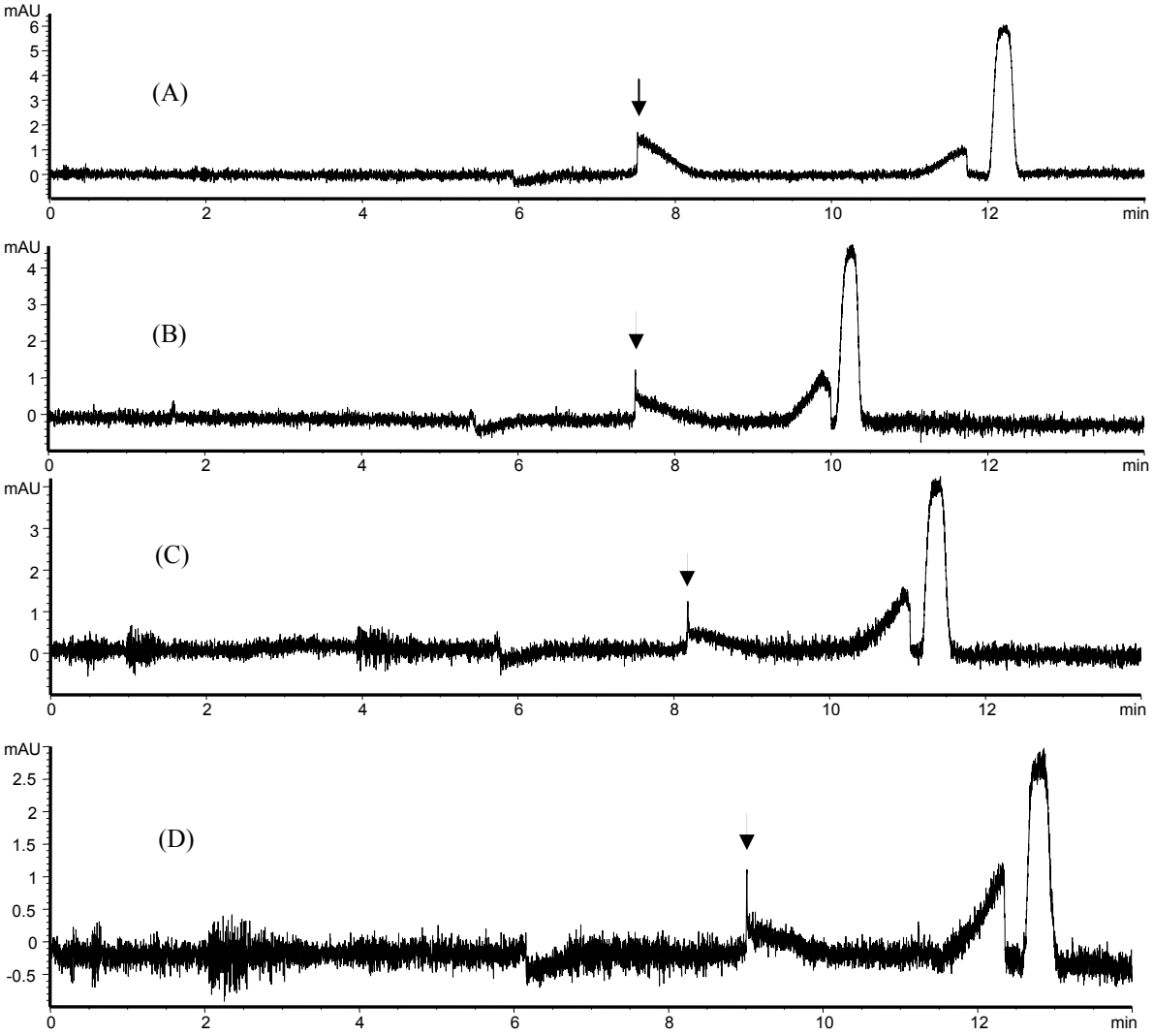

Figure 2.7 The representative electropherograms used to estimate the binding constant of L-UCLB in the sample solution and TM-β-CD in the CE buffer. 5.00 mM NaOAc, pH 5.0 buffer; fused silica capillary, 64.5 cm total length, 56.0 cm from inlet top to detector, and 50 μm i.d.; separation temperature 16 °C; applied voltage +20 kV. Pressure injection: 50 mbar, 20 sec. A: 0.0 mM TM-β-CD; B: 3.0 mM TM-β-CD; C: 6.0 mM TM-β-CD; D: 9.0 mM TM-β-CD. The arrows pointed to the peaks of L-UCLB.

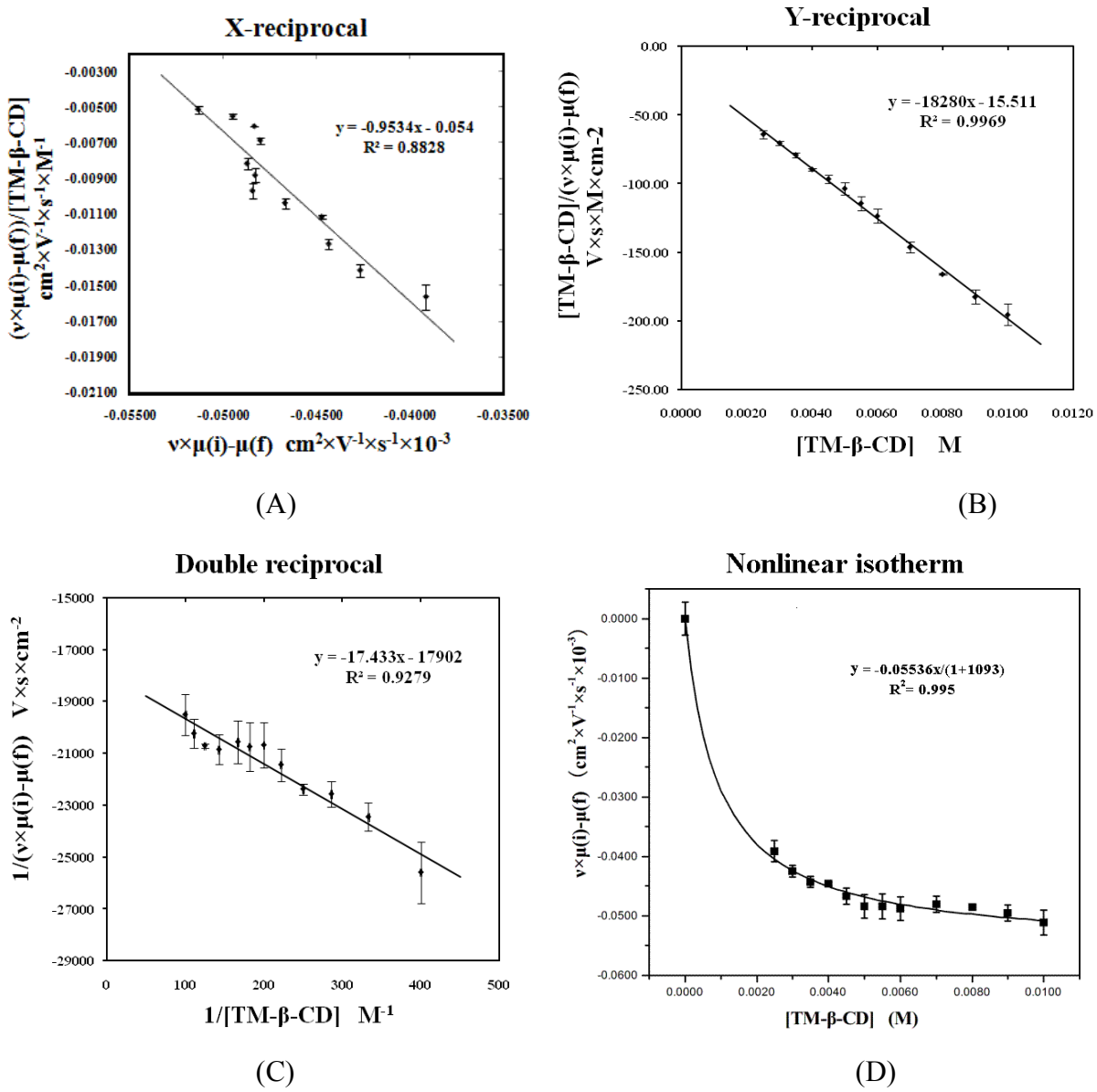

Figure 2.8 The linearized plots (A-C) and non-linearized plot (D) used to estimate the binding constant K_1 between TM-β-CD and L-UCLB. Each data point is the average value of triplicate runs. The error bars represent 95% confidence intervals (95% CI).

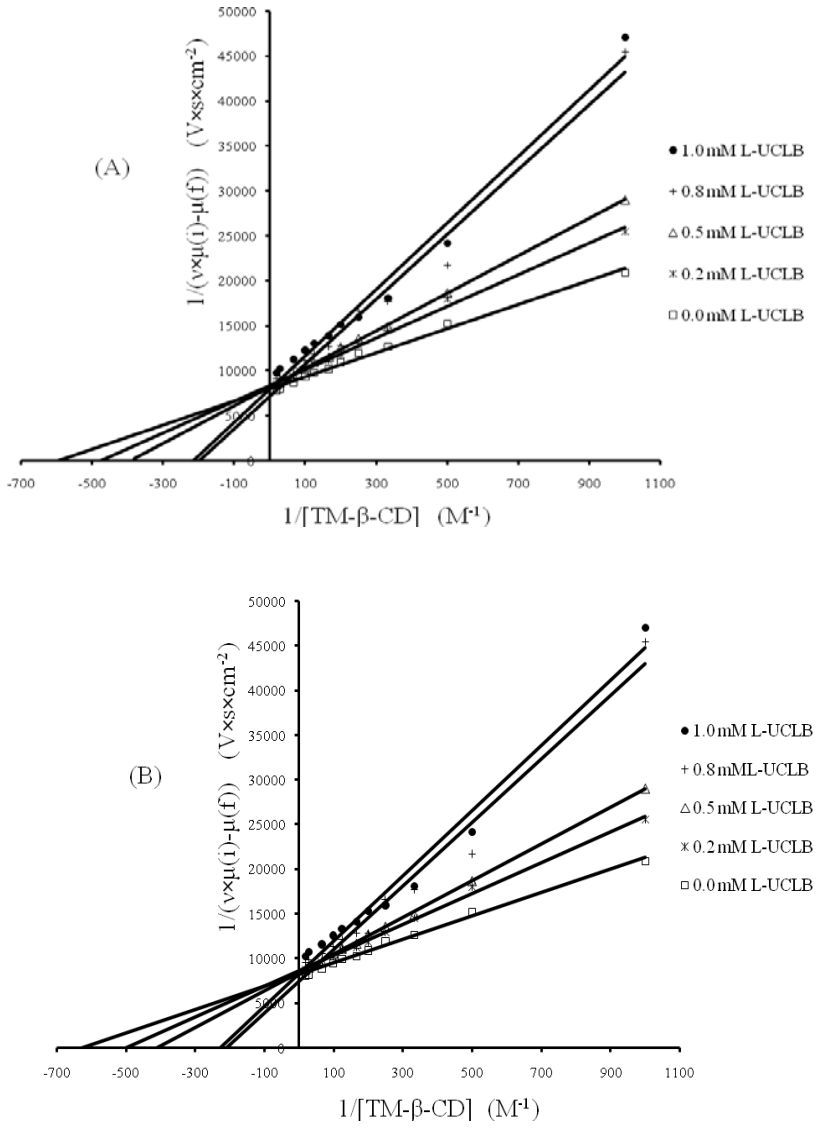

Figure 2.9 The double-reciprocal plots used to study the type of inhibition in TM-β-CD/L-UCLB/profen system. A: *R*-fenoprofen, B: *S*-fenoprofen. CE conditions: 5 mM NaOAc, pH 5.0 buffer; fused silica capillary, 64.5 cm total length, 56.0 cm from inlet top to detector, and 50 μm i.d.; separation temperature 16 °C; applied voltage +10 kV. Pressure injection: 5 mbar, 10 sec. Each data point is the average value of triplicate runs. The error bars were removed for clarity of presentation. The average 95% CI of the data points is ±407 V×s×cm^{-2} for *R*-fenoprofen (A), and ±424 V×s×cm^{-2} for *S*-fenoprofen (B).

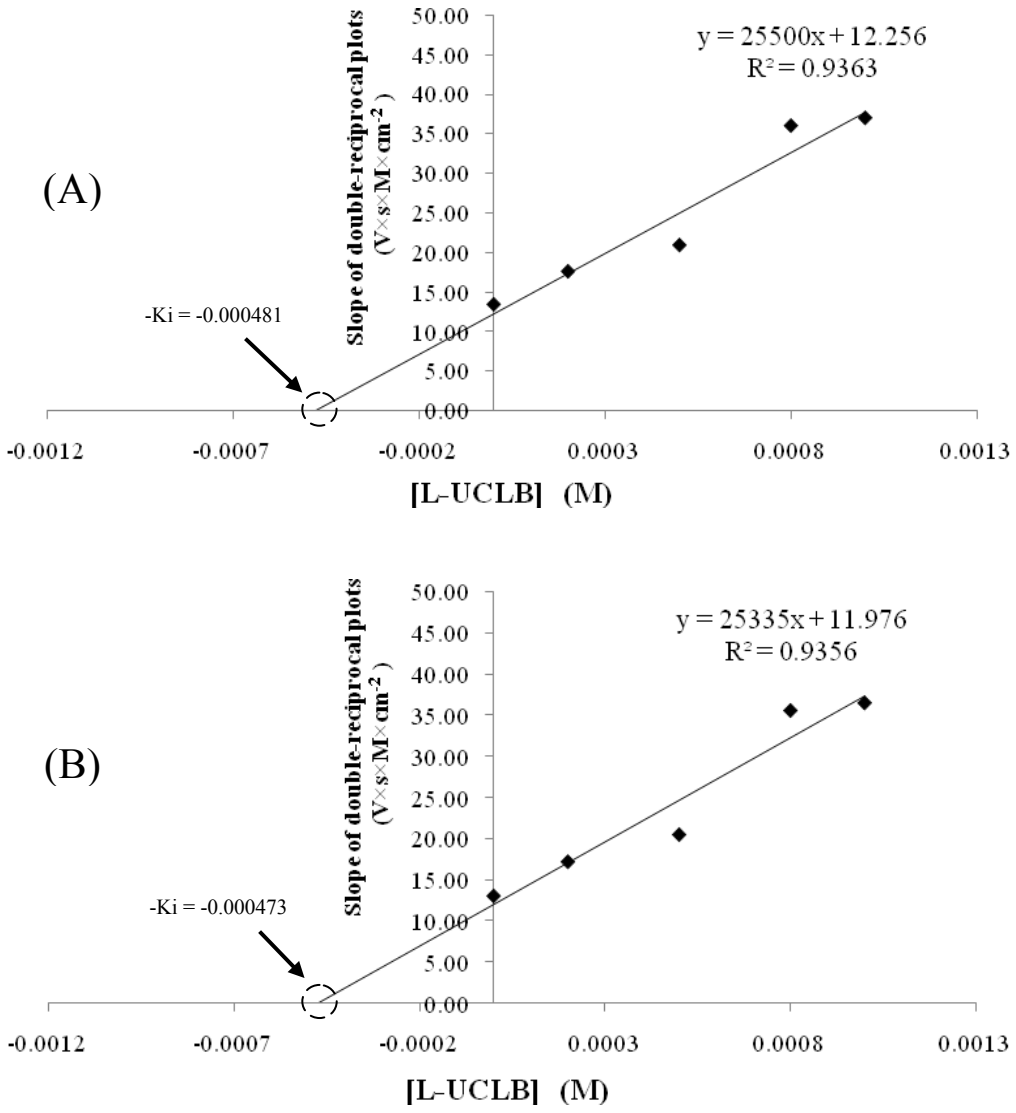

Figure 2.10 The secondary plot used to estimate the apparent inhibition constant K_i. The y-axis was the slope values of the double-reciprocal plots obtained from Figure 2.9. A: *R*-fenoprofen, B: *S*-fenoprofen. The x-intercepts marked with circles represent the negative values of K_i for the two enantiomers.

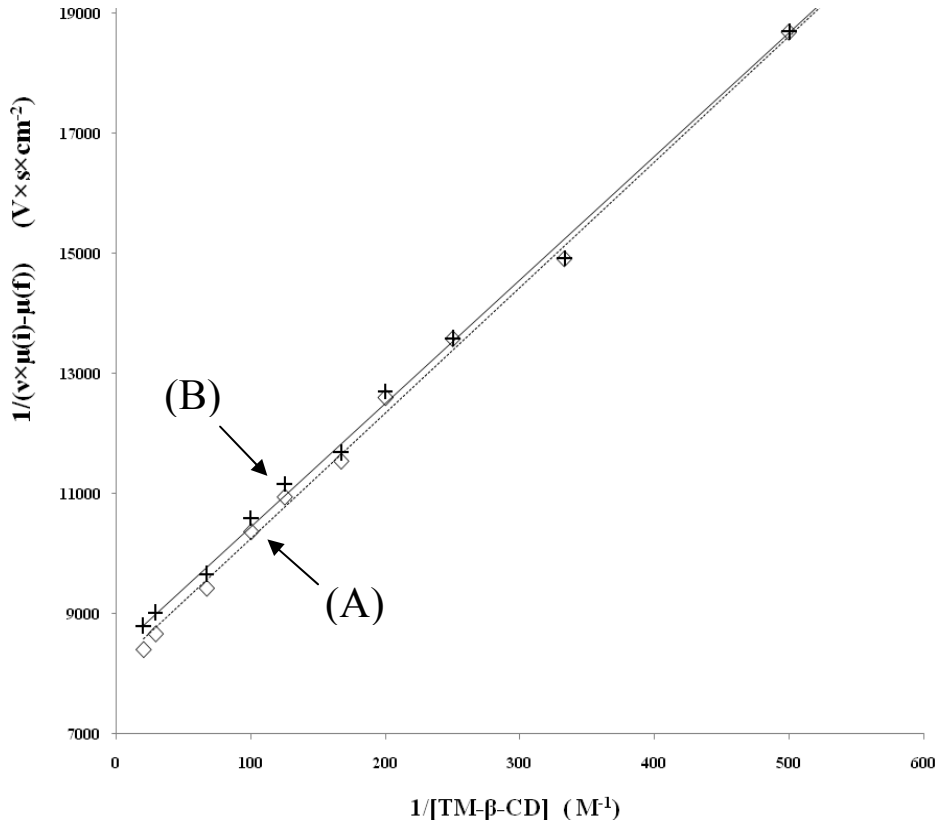

Figure 2.11 The comparison of double-reciprocal plots for the K_2 calculation of *R*- and *S*-fenoprofen in the presence of 0.5 mM L-UCLB. A: *R*-fenoprofen, B: *S*-fenoprofen. Each data point is the average value of triplicate runs. The error bars were removed for clarity of presentation. The average 95% CI of the data points is ±228 V×s×cm^{-2} for *R*-fenoprofen (A), and ±229 V×s×cm^{-2} for *S*-fenoprofen (B).

CHAPTER 3. A HIGH THROUGHPUT MULTIVARIATE OPTIMIZATION FOR THE SIMULTANEOUS ENANTIOSEPARATION AND DETECTION OF BARBITURATES IN MEKC-MS

3.1 Introduction

The chirality of a pharmaceutical drug has gained significant attention in both clinical and pharmaceutical settings due to the different biological activity of the two optical isomers (*R*/*S* or D/L enantiomers). Barbiturates (mephobarbital, pentobarbital, and secobarbital, Figure 3.1) are widely used in pharmaceutical applications as central nervous system (CNS) depressants, and they produce a broad range of effects from mild sedation to anesthesia [1]. They are also effective as hypnotic drugs and as anticonvulsants. Previous studies have shown that stereoselective effects are qualitatively similar for those of racemic barbiturates [1]. In contrast, later research showed that different enantiomers of barbiturates have different biological effects [2-5]. For example, the (*S*)-isomers of pentobarbital and secobarbital are more potent than the (*R*)-isomers [2, 4]. Moreover, in case of mephobarbital, it is reported that the hydroxylation in human liver microsomes is preferential for (*R*)-isomer than (*S*)-isomer [5].

The enantioselective separation of barbiturates has been carried out by various separation techniques. In case of capillary GC, a thermostable chiral polymer, XE-60-L-valine-(*R*)-α-phenylethylamide, was used as stationary phase to separate racemic mephobarbital [6]. A modified β-cyclodextrin (CD) was utilized to coat the capillary GC column for the enantioseparation of *N*-alkylated barbiturates [7]. Enantioseparation have been performed in HPLC incorporating chiral selectors either in the mobile phase or as a stationary phase. The CD and its derivatives were used as additive in the mobile phase for the enantioseparation of mephobarbital and secobarbital [8-10]. In addition, various HPLC chiral stationary phases such

as: 3-(1,8-naphthalimido) propyl-modified silyl silica gel, cellulose tris (4-methylbenzoate), permethylated β-CD bonded to silica, cellulose tris (3,5-dimethylphenylcarabamate) and amylase 3,5-dimethylphenyl-carabamate immobilized on silica have also been used to separate mephobarbital, pentobarbital, secobarbital, and other *N*-alkylated barbiturates [11-15]. However, both GC and HPLC techniques have drawbacks concerning the high cost of the chiral column and the use of large amount of chiral selectors, thereby increasing the expense of analysis. In addition, the efficiencies of the enantioseparation are often low, requiring the use of longer columns.

Enantioseparation by CE has emerged as a powerful analytical-scale technique over the past decade. Some of the key advantages of CE include high efficiency, short analysis time as well minimal consumption of exotic and expensive chiral selectors, therefore reducing the operation cost. Another advantage of using CE for chiral separation is the ability to use multitude of selectors, which not only provides variable selectivities but often reverse enantiomeric elution order. Thus, the latter advantage of CE provides an automated approach with great ease for the development of chiral assays of various classes of pharmaceuticals.

The enantioseparation of barbiturates in CE have been reported using CD and its derivatives as chiral selectors [16-19]. A polymeric chiral surfactant poly sodium *N*-undecenoxyl-D-valinate (poly-D-SUV) has been utilized in MEKC and MEEKC to separate pentobarbital and secobarbital [20]. However, the low sensitivity and poor selectivity of the UV detection in CE have prompted the development of MS as end-capillary detection method. Recently, packed column capillary electrochromatography (CEC) using a permethyl-β-CD-silica as the stationary phase has been coupled to coordination ion spray-mass spectrometry (CIS-MS) for the on-line enantioseparation and detection of mephobarbital [21]. In a different study, the

noncovalent interactions between CD derivatives and barbiturates have been investigated by CE (as solution phase complexes) and by ESI-MS (as gas phase complexes) but not for on-line CE-MS [22].

The development of CE-MS for chiral analysis has enormous potential but the poor volatility and background noise generated by the low molecular weight chiral selectors (e. g., CD and its derivatives, macrocyclic antibiotics, and unpolymerized chiral micelles) are the main limitations. To overcome these limitations, one possible alternative proposed by our research group involves the use of high molecular weight chiral selectors (i. e., the molecular micelles or polymeric surfactant) [23]. Several of our recent publications have shown that the use of chiral molecular micelles in MEKC-MS appears as one of the most promising approaches for simultaneous chiral analysis [24-25]. Notably, the addition of chiral molecular micelle in the MEKC buffer confers high resolving power and a wide chiral window for the simultaneous enantioseparation of structurally similar drugs, thereby increases the throughput. Moreover, by operating the instrument in selective ion monitoring (SIM) or group SIM mode, MS provides a significant improvement in signal-to-noise (*S/N*) ratio. These features of MS improve the limit of detection (LOD) for the barbiturates, thereby providing a potential approach for the analysis of barbiturates in biological samples (e. g., in human blood and urine).

In this work, simultaneous enantioseparation and detection of three barbiturates (mephobarbital, pentobarbital, and secobarbital) is discussed using MEKC-ESI-MS enabling the development of a high-throughput method with high efficiency and sensitivity. The key to achieve a successful simultaneous enantioseparation of these three barbiturates was to carefully screen various polymeric chiral surfactants. Hence, after screening a multitude of molecular micelles, the use of polysodium *N*-undecenoxy-L-isoleucinate (poly-L-SUCIL) as chiral selector

and response surface methodology is proposed. The RSM is a multivariate approach often used to optimize the multiple parameters in CE [26-28]. A three-factor (pH, poly-L-SUCIL concentration, NH_4OAc concentration) full factorial central composite design (CCD) experiment was carried out to obtain the MEKC response for chiral resolution and migration time. Next, a two factors (%methanol and NH_4OH concentration) CCD experiment was conducted for the sheath liquid condition optimization to predict the best *S/N* ratio for the ESI-MS detection. The drying gas temperature (DGT) and drying gas flowrate (DGF) were studied using the same multivariate approach to highlight the significance of these two spray chamber parameters on MS response. Finally, the adequacy of the developed MEKC-MS method was validated by experimental runs at the predicted optimized conditions. Significantly improve *S/N* ratio by MEKC-MS and consequently better LOD were achieved compared to MEKC-UV under identical conditions, demonstrating the potential for the application of this powerful technique in the fields of pharmaceutical and biomedical analysis.

3.2 Experimental

3.2.1 MEKC-ESI-MS instrumentation

All MEKC-ESI-MS experiments were performed on an Agilent Capillary Electrophoresis system (Agilent Technologies, Palo Alto, CA, USA) interfaced to a single quadrupole mass spectrometer, Agilent 1100 series MSD. A G1603A CE-MS adapter kit and a G1607 CE-ESI-MS sprayer kit (all provided from Agilent Technologies) were used to couple the CE instrument to MS. The sheath liquid used in ESI spray chamber was delivered by an Agilent 1100 series HPLC pump equipped with a 1:100 splitter. The temperature control of the sample carousel at 20 °C was maintained by Fisher ISOTEMP 3016S refrigerating circulator (Fisher Scientific,

Pittsburgh, PA, USA). The instrumental control, data acquisition, and data analysis were carried out by Agilent Chemstation and CE-MS add-on software. The fused silica capillaries (Polymicro Technologies, Phoenix, AZ, USA) with dimensions of 125.0 cm total length (60.0 cm length from inlet to UV-detection interface) 50 μm i.d., and 365 μm o.d. were used throughout the study.

3.2.2 Reagents and Chemicals

Mephobarbital, pentobarbital, secobarbital, and ammonium acetate (as 7.5 M aqueous solution) were purchased from Sigma-Aldrich (St. Louis, MO, USA). Ammonium hydroxide was purchased from EM science (Gibbstown, NJ, USA). Acetonitrile (ACN), methanol (MeOH), dichloromethane, ethyl acetate, 2-propanol, and acetone were purchased from Caledon Laboratories (Georgetown, ON, Canada). Deionized water was prepared with a Barnstead "NANOpure" ultrapure water system (Dubuque, Iowa, USA).

The reagents ω-undecylenyl alcohol, pyridine anhydrous, L-isoleucine, and other amino acids used for the synthesis of polymeric surfactants were purchased from Sigma-Aldrich (St. Louis, MO, USA). Triphosgene was obtained from TCI (Tokyo Kasei Kogyo Co. LTD, Tokyo, Japan). Hydrochloric acid and sodium sulfate anhydrous were purchased from EMD Chemicals (Gibbstown, NJ, USA). Sodium hydroxide (50% w/w) was purchased from Fisher Scientific (Pittsburgh, PA, USA). Sodium carbonate was purchased from Acros Organics (Geel, Belgium). The polymeric surfactant, poly-L-SUCIL was synthesized following a previously optimized procedure [29-30].

3.2.3 MEKC-ESI-MS conditions

The concentration of each barbiturate stock solution prepared in pure ACN was 0.5 mg/mL. To prepare a mixture sample of three barbiturates, a fixed aliquot of mephobarbital, pentobarbital, and secobarbital were dissolved in the binary solvent of ACN and H_2O in a ratio of 80:20 (v:v). The final concentration of each barbiturate in the mixture was 125 µg/mL. The ammonium acetate solution was prepared by diluting 7.5 M NH_4OAc aqueous solution in triply deionized water. The pH of the buffer was adjusted to a required value using 1.0 M ammonium hydroxide. The polymeric surfactants were individually dissolved in the ammonium acetate buffer.

A bare fused silica capillary was first preconditioned for 60 minutes with 1 M NH_4OH at 50 °C, and then flushed for 30 min with triply deionized water at 20 °C. Before each injection, the capillary was flushed with the separation buffer for 5 min. After each run, the capillary was postconditioned with deionized water for 5 min, 0.1 M aqueous NH_4OH solution for 5 min, and deionized water for 5 min. The sample was hydrodynamically injected at 3 mbar for 8 seconds. The separations were carried out under an applied voltage of +25 kV and a temperature of 20 °C. The absorbance of barbiturates in the MEKC buffer was simultaneously monitored by UV detection at 214 nm. The MS detection was set to negative ion in the group-SIM mode at m/z 225, 237, and 245 to monitor the $[M-H]^-$ ions of pentobarbital, secobarbital and mephobarbital, respectively. The MEKC-ESI-MS conditions, which include MEKC conditions (pH, poly-L-SUCIL concentration, and NH_4OAc concentration), the sheath liquids composition ($MeOH/H_2O$ ratio, concentration of NH_4OAc or NH_4OH), and spray chamber parameters (i. e., DGF and DGT) were optimized using multivariate CCD discussed in section 2.5.

3.2.4 Preliminary experiments

The preliminary experiments were first conducted to screen the significant factors that influence the enantioseparation and *S/N*. For the MEKC conditions, these factors include the concentration of BGE (ammonium acetate), different types of surfactants used to form micelles, ratio of surfactants in the mixed micelles, and ratio of organic solvent (ACN) in the aqueous buffer. For the ESI-MS sheath liquid conditions, the composition of MeOH/H_2O in mM concentration of NH_4OAc vs. NH_4OH were compared as additive to the sheath liquid. For ESI spray chamber conditions, these factors include the DGF, DGT, and nebulizer pressure (NP). The use of mixed micelles and organic modifiers in the CE buffer were also studied, although their effects were not very significant. These preliminary experiments were conducted before the multivariate approaches so that the factors explored in multivariate approaches can be narrowed to the effective ranges.

3.2.5 The multivariate optimization approach

The response surface method used in this work is a CCD experimental design, which was accomplished by the Design-Expert (version 7.0, Stat-Ease, MN, USA) software. In response surface methodology, CCD is a second-order design used to fit a second-order model, which can be described by the equation below [31]:

$$Y_{\mathbf{x},t} = \beta_0 + \sum_{i=1}^{p} \beta_i x_i + \sum_{i=1}^{p} \beta_{ii} x_i^2 + \sum_{i<j} \beta_{ij} x_i x_j + \epsilon_{\mathbf{x},t} \qquad \text{(Equation 3.1)}$$

In the Design-Expert software, $Y_{x,t}$ is called the response, x is called the factor, β_0, β_i, β_{ii}, and β_{ij} are called coefficients for the intercept, the factors, and the interaction between two factors, the $\varepsilon_{x,t}$ is called residual. In this quadratic model, the zero order term is the intercept, the first order terms are the $\beta_i x_i$ terms, and the second order terms are $\beta_{ii} x_i^2$ and $\beta_{ij} x_i x_j$ terms. When the x^2

terms are absent, the model is called a 2-factor interactions (2FI) model. When all of the second order terms are absent, the model is regressed to a linear model. The CCD model design can be described as follow [31]:

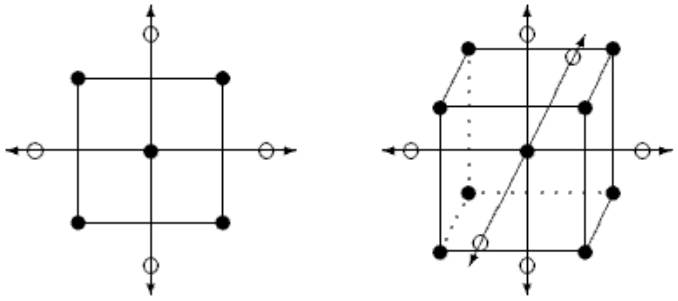

p = 2 *p* = 3

The filled circles represent the center point and factorial points, while the empty circles represent the axial points. The *p* here represents the number of factors investigated in the experimental design. If there are *p* factors, there are 2*p* distinct axial points, one center point, and 2^p factorial points [31]. For example, if there are two factors, then the CCD design need at least four factorial points, four axial points, and one center point. Similarly, if there are three factors, then the CCD design need at least eight factorial points, six axial points, and one center point. However, when the model is designed, replicates of some points are usually required to improve the result of lack of Fit test, which is the variation of the data around the fitted model. After the experimental responses are obtained, the fitness of a model was determined by the F-test and Lack of Fit test based on the experimental data. For example, when the value of Prob>F for the F-test is less than 0.05, the model has a significant effect on the response. On the other hand, for the Lack of Fit test, a value of Prob>F less than 0.05 means that the model does not fit the data well. Other criteria to show the fitness of the model are the R^2, adjusted R^2, and predicted R^2. The R^2 is the correlation coefficient that measures the amount of variation around the mean explained by the model. The adjusted R^2 is the R^2 adjusted for the number of terms in the

model relative to the number of points in the design. The predicted R^2 is a measure of how good the model predicts a response value, based on the amount of variation in new data explained by the model. The adjusted R^2 and predicted R^2 should be within approximately 0.20 of each other. Otherwise, there may be a problem with either data or the model. However, a low R^2 only does not always mean an unfitted model because the F-test is more important in the experimental design.

3.3 Results and discussions

The general structure of barbiturates (Figure 3.1) shows that the molecule contains a balance of hydrophilic and lipophilic functionality. The hydrophilicity (polarity) is contributed by 2, 4, 6-pyrimidine trione ring structure, which is a function of number of *N*-substitutes and the p*Ka* of the acidic proton(s). On the other hand, the overall size and structure of the two alkyl substitutes at the 5-position exhibit non-polar characteristic. In addition, due to the presence of one or more acidic protons, barbiturates can be easily converted to water soluble salts. Furthermore, note that the chiral center of mephobarbital is located at the 5-position of the 2, 4, 6-pyrimidine trione ring, while the chiral centers of pentobarbital and secobarbital are located in a side chain outside the ring at the methylbutyl substitution.

As barbiturates are acidic in nature, a sheath liquid of 80% MeOH and 20% H_2O containing 5 mM NH_4OAc was used and the direct infusion experiments were performed in negative ion mode of ESI-MS. In the ESI-MS of each barbiturate (Figure 3.2), the highest intensity masses correspond to the deprotonated molecular ion $[M-H]^-$ at m/z ratios of 225, 237, and 245 for pentobarbital, secobarbital, and mephobarbital, respectively. Therefore, under on-

line MEKC-MS conditions, a group SIM was set-up to simultaneously monitor all the aforementioned barbiturates as $[M-H]^-$ ion in the negative ion mode.

3.3.1 Preliminary experiments

A series of polymeric surfactants were first screened by varying the type and ratio of the surfactants used to form molecular micelles and mixed micelles, respectively. The polymeric surfactants with different head groups including poly-L-SUCIL, polysodium *N*-undecenoxycarbonyl-L-leucinate (poly-L-SUCL), polysodium *N*-undecenoxyl carbonyl-L-valinate (poly-L-SUCV), polysodium *N*-undecenoxycarbonyl-L-leucine sulfate (poly-L-SUCLS), polysodium *N*-undecenoxycarbonyl-L-valine sulfate (poly-L-SUCVS), polysodium *N*-undecenoxycarbonyl-L-leucyl valinate (poly-L-SULV), and polysodium *N*-undecenoxycarbonyl-L-penicillamine (poly-L-SUPA) were compared. In addition, one eight carbon chain polymeric surfactant, polysodium *N*-octenoxycarbonyl-L-leucinate (poly-L-SO_cCL) and several mixed micelles in 1:1 ratio of poly-L-SUCL/poly-L-SUCIL, poly-L-SUVL/poly-L-SUCIL, and poly-L-SUPA/poly-L-SUCIL were also compared. All of these polymeric surfactants were dissolved in the CE buffer at the same equivalent molar concentration (EMC), which is the concentration of the polymeric surfactant that is equivalent to the equal weight of the same monomeric surfactant. As seen in Figure 3.3 A and C, under the same experimental conditions, poly-L-SUCL and poly-L-SUCV partially resolved three barbiturates, Furthermore, two additional polymeric surfactants poly-L-SULV (Figure 3.3G) and poly-L-SUPA (Figure 3.3H) provided partially resolution of only two of the three racemic barbiturates. However, other polymeric surfactants (Figure 3.3D-F) did not resolve any of the barbiturates. While the mixed micelles of poly-L-SUCL/poly-L-SUCIL, poly-L-SUVL/poly-L-SUCIL, and poly-L-SUPA/poly-L-SUCIL

(Figure 3.3I-K) did improve the chiral resolutions of these three barbiturates but again partially resolution was observed. Nevertheless, poly-L-SUCIL was the only polymeric chiral surfactant, which provided baseline resolutions for all of the three barbiturates with highest resolution and shortest analysis time (Figure 3.3B).

The effect of organic additive (ACN) in the buffer was also investigated by changing the ACN/H_2O ratio in the buffer solution from 10% to 50% (v:v). However, the addition of ACN in the buffer did not shorten the migration time or improve the chiral resolution of the three barbiturates (data not shown). Therefore, the use of poly-L-SUCIL without any organic modifier was utilized for further optimization of MEKC parameters.

Before using the multivariate CCD experiment for the optimization of MEKC conditions, the sequential preliminary experiments were carried out to determine which factors are important for the enantioseparation and what ranges of these factors needs to be further investigated in the CCD. Hence, a fairly wide range was explored for the following factors: the buffer pH, EMC of polymeric surfactants, and concentration of BGE (NH_4OAc). The effect of buffer pH from 7.0 to 8.0 was investigated. The pH lower than 7.0 was not studied because these three barbiturates will be all neutralized at the pH lower than their p*Ka*. On the other hand, pH higher than 8.0 was found not good for the enantioselectivity. The concentration range of poly-L-SUCIL determined by the preliminary experiments suggests that concentration lower than 20 mM EMC usually does not provide enough enantioresolution, while higher concentration (>50 mM EMC) causes significant suppression of ESI-MS signal. The concentration of NH_4OAc used as BGE ranged from 25 mM to 40 mM. When NH_4OAc concentration was too low, the buffer pH was not well maintained, resulting in irreproducible retention times, whereas too high of NH_4OAc concentration (>40 mM) causes suppression of MS signal. The optimum

conditions determined by univariate approach for enantioseparation of these three barbiturates were as follows: pH 7.2, 50.0 mM poly-L-SUCIL, and 35.0 mM NH_4OAC.

The second step was to determine a suitable range for the sheath liquid composition to improve the MS sensitivity. The sheath liquid used in MEKC optimization was a binary solvent of MeOH and H_2O in a ratio of 80:20 (v:v) containing NH_4OAc or NH_4OH. The *S/N* ratios were compared at the same concentrations of NH_4OAc and NH_4OH (Figure 3.4). Two important trends are worth mentioning. First, the average *S/N* ratios $(S/N)_{avg}$ were always the greatest at 5.00 mM using both NH_4OAc and NH_4OH. Second, the NH_4OH achieved better $(S/N)_{avg}$ than NH_4OAc in the low concentration range of 5 to 20 mM. This second trend shows that the use of basic sheath liquid can improve the ionization of barbiturates when ESI negative mode is used. However, at higher concentration (e. g., 50 mM NH_4OAc or 50 mM NH_4OH), $(S/N)_{avg}$ decreased significantly, mainly because of an increase in peak-to-peak noise and unstable baseline (the suppression effect of sheath liquid additives). The ratio of MeOH and H_2O in the sheath liquid was also investigated in the range from 20% to 80% MeOH containing 5.00 mM NH_4OH. When a 20% MeOH sheath liquid was used, the on-line MS signals of the barbiturates were very weak, whereas greater than 80% MeOH caused unstable current (lack of conductivity). Therefore, for multivariate optimization the concentration of NH_4OH from 5.00 mM to 20.00 mM and %MeOH from 50% to 80% were chosen.

The third step was to determine the range of spray chamber parameters, which include NP, DGF and DGT. As shown in Figure 3.5A, initially increasing the NP from 2 to 3 psi provided somewhat similar $(Rs)_{avg}$ (calculated as average resolution value for the enantiomers). However, as expected, the increasing NP above 3 psi caused a suction effect, showing a gradual decrease in $(Rs)_{avg}$ (Figure 3.5A) but increase in $(S/N)_{avg}$ (Figure 3.5B). Therefore, a NP of 5

psi was chosen as a compromise between $(Rs)_{avg}$ and $(S/N)_{avg}$. The ranges for DGF and DGT were set from 4.0 to 7.0 mL/min and from 190 to 310 °C, respectively. These ranges were determined based on our previous work in which good ESI-MS stability was obtained [32].

3.3.2 The multivariate optimization of MEKC conditions and ESI-MS conditions

3.3.2.1 CCD design

As mentioned earlier in section 3.1, the values of factorial points used in the CCD design were determined by the preliminary experiments. The software then generated the center points and axial points according to the CCD discussed in section 2.4; the values for high and low levels (level +1 and -1) were obtained from preliminary experiments as the factorial points. However, the center points (level 0) and axial points were calculated by software. In this work, the MEKC conditions were investigated by three factors (concentration of NH_4OAc, EMC of poly-L-SUCIL, and pH values) at three levels (Table 3.1, rows 1- 5) to obtain responses for chiral *Rs* and migration time of barbiturates. The MeOH/H_2O ratio and the concentration of NH_4OH in the sheath liquid were used to optimize sheath liquids conditions at three levels (Table 3.1, rows 6-10, columns 1-3) so that highest *S/N* ratio can be obtained. The flowrate and temperature of the drying gas were also evaluated at three levels (Table 3.1, rows 6-10, columns 4-6).

3.3.2.2 Evaluation and optimization of MEKC conditions on chiral resolution and migration time

The experimental sequence and responses for MEKC optimization are shown in Table 3.2. The responses *Rs*11', *Rs*22', *Rs*33', and MigTime represent the chiral resolution of mephobarbital, pentobarbital, secobarbital, and the migration time of the last eluted enantiomer. To improve the model Lack of Fit, the center point was replicated six times and factorial points were repeated twice. Therefore, this CCD design has a total number of twenty eight runs, including six runs for the center point, sixteen runs for factorial points, and six runs for axial points. The six replicated runs at center point were run# 2, 3, 9, 16, 18, and 23. For this 6 replicated runs, the %RSD of the experimental responses, resolution values of the three pairs of enantiomers (*Rs*11', *Rs*22', *Rs*33') and the migration time of the last eluted enantiomer (MigTime), were 6.6%, 11%, 11%, 5.4%, respectively, which seem reasonable. As shown in Table 3.2, enantiomeric resolution varies from 0.47-1.93, 0.82-1.91, and 1.20-2.26 for mephobarbital, pentobarbital, and secobarbital, respectively. In addition, the analysis (i. e., migration time of the last eluted enantiomer) ranged from 26.5 to 49.6 min. Figure 3.6A and 3.6B shows two of the representative electropherograms obtained from CCD experiments (i. e., run 7 and 13 in Table 3.2). The run# 7 represents one of the worst results among all the runs since it showed only partial chiral *Rs* values for all of the three barbiturates but shortest migration time. This trend is observed probably because of the lowest EMC of poly-L-SUCIL (5.00 mM) used in this run. On the other hand, run# 13 demonstrates one of the best overall separations of these enantiomers. This experimental point was repeated at run 4, which showed comparable chiral *Rs* values and migration time (Table 3.2).

The regression coefficient of the coded factors obtained for the response surface models are shown in Table 3.3. A positive coefficient implies a positive effect of the corresponding

factor to the response, and vice versa. The term with greater coefficient has more effect on the response. For example, the EMC of poly-L-SUCIL (factor B in Table 3.3) has a coefficient of 0.37 for *Rs*11', the greatest among all of the coefficients (in column 2, Table 3.3), which implies that the EMC of poly-L-SUCIL has the most effect on the chiral *Rs* of mephobarbital, and the value of chiral *Rs* will increase with the increase of the EMC of poly-L-SUCIL. On the other hand, the pH (factor A in Table 3.3) has the greatest negative coefficient of -0.15 for *Rs*11', which suggests that the pH value has the greatest negative effect on the chiral *Rs* of mephobarbital. The value of chiral *Rs* will decrease with the increase of pH in the buffer. Note that the model for *Rs*11', *Rs*22', and *Rs*33' are quadratic models, which have first and second order terms; while the model for migration time is a linear model, which has only first order terms.

The probabilities of each term having an effect on the response (i. e., Prob>F) are summarized in Table 3.3. A coefficient is not considered significantly different from zero if Prob>F is larger than 0.05. Under such conditions, the corresponding factor is regarded as non-critical. A careful evaluation reveals that four terms, pH (A), [poly-SUCIL] (B), [NH_4OAc] (C), and [poly-SUCIL]^2 (B^2), are significant to the resolution of mephobarbital (11') and secobarbital (33'). In addition, three terms A, B, and B^2 are significant to the resolution of pentobarbital (22'), whereas the terms A, B, and C are significant to the migration times of the three pairs of enantiomers. The R^2, adjusted R^2, and predicted R^2 for chiral *Rs* of each barbiturate are also compared in Table 3.3. The R^2 for mephobarbital is better compared to that of pentobarbital and secobarbital. One possible explanation is the shorter migration time of the mephobarbital enantiomers compared to other two barbiturates. The difference between adjusted R^2 and

predicted R^2 of *Rs*33' is greater than 0.20, which is also caused by the longer migration time of secobarbital.

Figure 3.7 A-C shows the response surface plots of the chiral resolutions of mephobarbital, pentobarbital, and secobarbital as a function of [poly-L-SUCIL] versus pH, [poly-L-SUCIL] versus [NH_4OAc], and [NH_4OAc] versus pH. The values of responses on the designed points (factorial points, center points, and axial points) were obtained from experimental data, and other response values were calculated from Equation 1 (see section 2.4) with the certain values of the factors and their coefficients, resulting in the 3D graphs of response surfaces. In general, for all of the three pairs of enantiomers the highest chiral resolutions were obtained at the highest [poly-L-SUCIL], the highest [NH_4OAc], and the lowest pH values. These trend and the high resolution values are mainly due to the high chiral selectivity of poly-L-SUCIL. On the other hand, high BGE concentration and low pH will decrease the EOF, thereby increasing the interaction between poly-L-SUCIL and barbiturates; consequently, the chiral *Rs* will improve. A close view of Figure 3.7 reveals that the combination of poly-L-SUCIL and NH_4OAc concentrations (i. e., the middle 3D plot in each Figure 3.7 A, B, and C) influenced the chiral *Rs* most for all three barbiturates compared to the other two combinations (i. e., poly-L-SUCIL vs pH, or NH_4OAc vs pH). Moreover, in most instances enantioresolution is least sensitive to the change in pH because the 3D plots are fairly flat along the pH axis. This is not too surprising as the absolute value of coefficient for pH is smallest than that of poly-L-SUCIL and NH_4OAc (Table 3.3, row 5).

In addition to chiral *Rs*, analysis time (i. e., migration time) of the last eluting enantiomer was also studied as a response (Figure 3.8). As shown in Figure 3.8, the shortest migration time was always obtained at the lowest concentration of poly-L-SUCIL and NH_4OAc, and at the

highest pH values. The main reason of increasing migration time with poly-L-SUCIL concentration is that the negatively charged micelles formed by poly-L-SUCIL migrate in the opposite direction to cathodic EOF when using positive polarity CE. The adsorption of surfactant on the capillary wall decreases the EOF and thereby also increase the migration time of barbiturates. Therefore, the EMC of poly-L-SUCIL has a greatest effect on the total analysis time. Similarly, NH_4OAc concentration is directly related to the migration time. The reason is that the high concentrations of NH_4OAc as BGE cause lower EOF and longer total analysis time. As mentioned earlier, increase in the pH value is inversely related to the migration time because the increase of pH value will increase EOF and consequently decrease the total analysis time. Note that the decrease on migration time is relatively more pronounced when poly-L-SUCIL is combined with NH_4OAc (Figure 3.8B), compared to the interactive effect of pH with poly-L-SUCIL (Figure 3.8A) or NH4OAc (Figure 3.8C).

3.3.2.3 Optimizations of ESI-MS conditions

The information gathered in Table 3.4 shows the experimental factors and the responses $(S/N)_{avg}$ for the optimization of sheath liquid conditions. The center point runs were repeated 5 times and each axial point were repeated twice. The center point was set at run# 6, 9, 12, 16, and 17, among which the response of run# 12 deviated obviously from other data. The Q test showed that $Q_{(run\ 12)}$ is 0.974, which is much greater than the $Q_{99\%}$ (0.821); therefore one could ignore that run. The %RSD of the repeatable four runs at center point was 1.8%. As shown in Figure 3.9(A), the highest $(S/N)_{avg}$ was obtained at lowest [NH_4OH] and highest %MeOH, which is 5.00 mM NH_4OH and 80% MeOH. This trend suggests that the lower molar concentration of NH_4OH and higher volume ratio of MeOH in the sheath liquid favor the electrospray ionization

process, and hence the MS signals of barbiturates. The upper half of Table 3.6 shows the regression coefficients for the coded factors in the models of the sheath liquid optimization. The model for sheath liquid is a 2FI model, which has the first order terms and the interaction terms (AB), but no other second order terms (i. e., A^2 and B^2). The 2FI model shows a much better Lack of Fit value than a quadratic model, so we chose this former model for the sheath liquid optimization. The concentration of NH_4OH (A), volume ratio of MeOH (B), and the interaction between these two factors (AB) are significant to $(S/N)_{avg}$. The interaction between [NH_4OH] and %MeOH is probably caused by the influence of MeOH on the volatility and conductivity of the sheath liquid, which is also affected by the NH_4OH in the sheath liquid. The variance between adjusted R^2 and predicted R^2 were caused by experimental errors.

The data in Table 3.5 shows the experimental response of the CCD design for spray chamber optimization. The center point was repeated five times and each factorial point was repeated twice. The %RSD of the runs for center point at run# 2, 6, 9, 11, and 12 is 13%. As seen in Figure 3.9(B), the maximum $(S/N)_{avg}$ was obtained at lowest DGF and highest DGT, which is the setting of 4.0 mL/min and 310 °C, respectively. As shown in lower half of Table 3.6, the model for spray chamber is a quadratic model. The terms of DGF (C), and C^2 are significant to the response $(S/N)_{avg}$ with the Prob>F values of 0.0002 and 0.0314, respectively. The DGT (D) and D^2 are not significant individually but the interaction between DGT and DGF (CD) is a significant term with Prob>F value of 0.0302 for the *S/N* ratio. Again, the variance between adjusted R^2 and predicted R^2 is most probably caused by the experimental errors.

The ANOVA shown in Table 3.7 implies that the quadratic models generated for the three barbiturate enantiomers (i.e., *Rs*11', *Rs*22', *Rs*33') and migration time are all significant to their responses because the F test of the model are all less than 0.05. The Lack of Fit tests of

the quadratic models for the chiral resolutions are not significant, which indicates that the models fit the experimental data. The Lack of Fit test of the linear model for MigTime is significant, and changing the model to a higher order did not improve the lack of Fit test. However, the R^2 for the model of MigTime is better than the R^2 for *Rs*22' and *Rs*33' (Table 3.3). Therefore, we still use this linear model for the optimization of migration time. The model for sheath liquid optimization and spray chamber optimization are both significant to the response of $(S/N)_{avg}$ since their F tests are both less than 0.05. The Lack of Fit test of the model for $(S/N)_{avg}$ by optimizing the sheath liquid parameters is not significant, although the R^2 is relatively low (Table 3.6). The Lack of Fit test for spray chamber optimization is not significant, and its R^2 is better than the one for sheath liquid optimization (Table 3.6). Therefore, we think that the models designed for both sheath liquid and spray chamber optimization fit the data, and use them to predict the optimum conditions.

As shown in Table 3.7, the value of F-ratio for the model of chiral resolution of mephobarbital (66.5) is much greater than pentobarbital and secobarbital (*Rs*22' and *Rs*33'), and the model for chiral resolution of secobarbital has the smallest F-ratio (3.40) compared to the other two barbiturates. This decrease of F-ratio values causes the increase of F-test values from <0.0001 to 0.0131 for these three models, which implies that the significance of the models generated for the chiral resolution is increasing. We believe that the earliest eluted mephobarbital was measured most accurately and caused the least experimental error. However, the latter two barbiturates eluded longer and caused greater variations on the migration time. It is the same reason that causes lower R^2 of the latter two models. The values of Lack of Fit test for these three models increase from mephobarbital to secobarbital according to their elution order, which implies that the quadratic model for the chiral resolution of secobarbital fits

the experimental data best, and the quadratic model for mephobarbital fits worst. This trend is reversed compared to the F-test values of these three models. The reason is probably that the quadratic model for chiral resolution of secobarbital fit the experimental data better than other type of models (i.e., linear or 2FI model) although the experimental data for this model are more deviated.

3.3.2.4 Final optimum conditions and validation studies

The final overall optimum experimental conditions and three representative electropherograms are shown in Figure 3.10. For the optimization of MEKC conditions, the highest resolution values for the three barbiturates and the shortest total analysis time were set as the criteria for a desirability function shown below, which calculated the geometric mean of all responses obtained in the optimization.

$$D = (d_1 \times d_2 \times \ldots \times d_n)^{\frac{1}{n}} = \left(\prod_{i=1}^{n} d_i \right)^{\frac{1}{n}} \qquad \text{(Equation 3.2)}$$

where D is the desirability ranging from 0 (the least desirable) to 1 (the most desirable), d_i is the response (i. e., three chiral resolution values of the barbiturates and the total migration time), n is the number of responses (three in the MEKC optimization). The calculation procedure was conducted by the DOE software to obtain the highest possible D value. The optimizations of *S/N* ratio for the sheath liquid and the spray chamber conditions were obtained by similar approaches. Consequently, the final overall optimization was the combination of the three optimizations: MEKC conditions, sheath liquid composition, and spray chamber parameters. After setting-up a requirement to achieve good trade-off between the chiral resolution and migration time, the optimum MEKC conditions generated by software were 25.00 mM NH_4OAc, pH 7.00, and 39.7 mM poly-L-SUCIL. The optimum $(S/N)_{avg}$ was obtained at the following ESI-

MS conditions. The sheath liquid composition is 5 mM NH_4OH in the binary solvent of MeOH and H_2O in a ratio of 80:20 (v:v). The spray chamber parameters are a NP value of 5 psi, 4.0 mL/min DGF, and 310 °C DGT.

The generated optimized condition was then validated experimentally by a representative series of replicate (n=3) electropherogram (Figure 3.10) of three barbiturates under these conditions, the experimental resolution values are slightly lower than the predicted ones (Figure 3.10 inset table), with the percent discrepancy of 20%, 13%, and 15% for mephobarbital, pentobarbital, and secobarbital, respectively. However, the percent discrepancy of the total analysis time is slightly shorter (13% difference) and the $(S/N)_{avg}$ slightly higher (3% difference) compared to the predicted values.

3.3.2.5 The determination of LOD

The MS detector provides much better sensitivity than the UV detector. Figure 3.11A and B shows the *S/N* ratio for UV and MS signals from the same experiment (using the same capillary) under the optimum MEKC-ESI-MS conditions. When the concentration of each racemic barbiturate was 125 μg/mL, the *S/N* ratio of the MS detection was three folds higher than UV detection for mephobarbital, and at least five times higher than UV detection for pentobarbital and secobarbital (Figure 3.11A and B). When the ESI-MS detector reached its LOD, the concentration of each barbiturate was 7.8 μg/mL (Figure 3.11C). At high concentration (e. g., 125 μg/mL, Figure 3.11B), the MS *S/N* ratio of mephobarbital enantiomers are higher than pentobarbital and secobarbital. However, *S/N* ratios of three barbiturates are very close at the LOD (Figure 3.11C). The standard plots were made to calibrate the peak area values of these three barbiturates for the MS detection (Figure 3.12A-C). The peak area values

shown in this figure are the average values of the two racemic enantiomers. The concentration of barbiturates was tested from 125 μg/mL to 7.8 μg/mL, in the range of LOD. As shown in Figure 3.12, all three barbiturates can be quantitated even at 7.8 μg/mL, although the linear correlation coefficient for mephobarbital (R^2 in Figure 3.12 A) is slightly lower than the other two barbiturates (R^2 in Figure 3.12 B and C).

3.4 Conclusions

The present studies illustrate the effectiveness of MECK-ESI-MS technique for the optimization of enantioseparation and detection of three barbiturates. The simultaneous enantioseparation of all three barbiturates was achieved in a single run under 32 min using a polymeric surfactant poly-L-SUCIL. A three-factor three-level CCD experimental design was used to optimize the MEKC conditions. The EMC of poly-L-SUCIL and concentration of NH_4OAc are the two most significant factors to the chiral resolution and migration time of mephobarbital and secobarbital. On the other hand, the pH values and EMC of poly-L-SUCIL are significant factors to the chiral resolution of pentobarbital. The optimum separation conditions were determined from the CCD model to obtain the highest overall chiral resolution and shortest analysis time. Similarly, the ESI-MS sheath liquid composition and ESI spray chamber parameters were optimized by two-factor three-level CCD design to obtain highest overall *S/N* ratio. For sheath liquid conditions, the concentration of NH_4OH, the volume ratio of MeOH/H_2O, and the interaction between these two factors are significant to *S/N* ratio. In addition, spray chamber parameters, the DGF and the interaction between DGF and DGT are also significant to *S/N* ratio.

The final optimized MECK-ESI-MS conditions were predicted from the desirability function, which is based on the optimization of MEKC conditions, MS sheath liquid composition, and MS spray chamber parameters. This final optimization was tested by a series of experimental runs and the results were in good agreement with the predicted results. The LOD of these three barbiturates for MS detection was determined to be 7.8 μg/mL and was much more sensitive than UV detection. The CCD experimental design proved to be an effective multivariate approach to optimize separation conditions and improve *S/N* ratio of barbiturate samples in MEKC-MS. We believe that the multivariate approaches for optimization of other classes of chiral compound will continue to increase. In this regard, the wider chiral window of molecular micelles in MEKC-MS will allow new application areas for the simultaneous analysis of multiple chiral drugs and their chiral metabolites.

3.5 References

[1] Cordato, D. J., Herkes, G. K., Mather, L. E., Morgan, M. K., *J. Clin. Neurosci.* 2003, *10*, 283-288.

[2] Andrews, P. R., Mark, L. C., *Anesthesiology* 1982, *57*, 314-320.

[3] Huang, L. Y., Barker, J. L., *Science* 1980, *207*, 195-197.

[4] Wenger, R. G., Donald, J. M., Cunny, H. C., *J. Pharmacol. Exp. Ther.* 1986, *237*, 445-449.

[5] Kobayashi, K., Kogo, M., Tani, M., Shimada, N. *et al*, *Drug Metab. Dispos.* 2001, *29*, 36-40.

[6] Koenig, A. W., Ernst, K., *J. Chromatogr.* 1983, *280*, 135-141.

[7] Koenig, A. W., Lutz, S., Evers, P., Knabe, J., *J. Chromatogr.* 1990, *503*, 256-259.

[8] Yang, Z. Y., Barkan, S, Brunner, C., Weber, J. D. *et al*, *J. Chromatogr.* 1985, *324*, 444-449.

[9] Hinze, W. L., Riehl, T. E., Armstrong, D. W. *et al*, *Anal. Chem.* 1985, *57*, 237-242.

[10] Zukowski, J., Sybilska, D., Bojarski, J., *J. Chromatogr.* 1986, *364*, 225-232.

[11] Kuroda, N., Inoue, K., Mayahara, K., Nakashima, K. *et al*, *J. Liq. Chromatogr. Relat. Technol.* 1996, *19*, 2867-2881.

[12] Aboul-Enein, Y. H., Bakr, A. S., *Enantiomer* 1996, *1*, 223-226

[13] Tomlin, S. L., Jenkins, A., Lieb, W. R; Franks, N. P., *Anesthesiology* 1999, *90*, 1714-1722.

[14] Ghanem, A., *J. Chromatogr. A* 2006, *1132*, 329-332.

[15] Ghanem, A., Al-Humaidi, E., *Chirality* 2007, *19*, 477-484.

[16] Francotte, E., Cherkaoui, S., Faupel, M., *Chirality* 1993, *5*, 516-526.

[17] Weng, J., Qiu, J., Chen, G., *Fenxi Huaxue* 1994, *22*, 1085-1088.

[18] Fillet, M., Fotsing, L., Schomburg, G., Hubert, P. *et al*, *Biomed. Chromatogr.* 1998, *12*, 131-132.

[19] Zaugg, S., Caslavska, J., Theurillat, R., Thormann, W., *J. Chromatogr. A* 1999, *838*, 237-249.

[20] Iqbal, R., Rizvi, A. A. S., Akbay, C., Shamsi, A. S., *J. Chromatogr. A* 2004, *1043*, 291-302.

[21] Von Brocke, A., Wistuba, D., Gfrorer, P., Stahl, M. *et al*, *Electrophoresis* 2002, *23*, 2963-2972.

[22] Srinivasan, K., Bartlett, M. G., *Rapid Commun. Mass. Spectrom.* 2000, *14*, 624-632.

[23] Shamsi, A. S., *Anal. Chem.* 2001, *73*, 5103-5108.

[24] Hou, J., Rizvi, S. A., Zheng, J., Shamsi, S.A. *J. Chromatogr. A* 2007, 1159, 208-216.

[25] Akbay, C., Rizvi, A. A. S., Shamsi, A. S., *Anal. Chem.* 2005, *77*, 1672-1683.

[26] Bragg, W., Norton, D., Shamsi, A. S., *J. Chromatogr. B* 2008, *875*, 304-316

[27] Hernandez-Borges, J., Rodriguez-Delgado, M. A., Garcia-Montelongo, F. J., Cifuentes, A., *Electrophoresis* 2004, *25*, 2065-2076.

[28] Lara, F. J., Garcia-Campana, A. M., Ales-Barrero, F., Bosque-Sendra, J. M. *et al*, *Anal. Chem.* 2006, *78*, 7665-7673.

[29] Syed, A. A. R, Shamsi, A. S., *Electrophoresis* 2005, *26*, 4172-4186.

[30] Syed, A. A. R, Shamsi, A. S., *Electrophoresis* 2007, *28*, 1762-1778.

[31] *Design and ananlysis of experiments*, Dean, A. M., Voss, D. T., Springer-Verlag, New York, 1999, pp 562-563.

[32] Hou, J., Zheng, J., Shamsi, A. S., *J. Chromatogr. A* 2007, *1159*, 208-216.

Table 3.1 Levels of factors in the CCD approaches used for the multivariate optimization of MEKC conditions, sheath liquid conditions, and spray chamber conditions.

MEKC conditions			
Level	A: pH	B: [poly-L-SUCIL] (EMC=mM)	C: [NH_4OAc] (mM)
-1	7.00	20.0	25.0
0	7.50	35.0	32.5
+1	8.00	50.0	40.0

Sheath liquid conditions		
Level	A: [NH_4OH] (mM)	B: %MeOH
-1	5.0	50
0	12.5	65
+1	20.0	80

Spray chamber conditions		
Level	C: DGF (mL/min)	D: DGT (°C)
-1	4.0	190
0	5.5	250
+1	7.0	310

Table 3.2 Resolution and retention time data gathered from the CCD experiment for the optimization of separation parameters.

Experimental factors				Experimental responses			
Run order	A: pH	B: [poly-L-SUCIL] (EMC=mM)	C: [NH_4OAc] (mM)	*Rs*11' [a]	*Rs*22' [b]	*Rs*33' [c]	MigTime [d] (min)
1	8.00	20.00	40.00	0.7	1.1	1.4	31.0
2	7.50	35.00	32.50	1.3	1.3	1.5	34.0
3	7.50	35.00	32.50	1.4	1.6	1.8	34.2
4	7.00	50.00	40.00	1.9	1.7	1.9	40.6
5	7.50	35.00	17.50	1.4	1.5	1.8	32.9
6	8.00	50.00	40.00	1.6	1.4	1.8	41.3
7	7.50	5.00	32.50	0.5	0.8	1.2	26.5
8	8.00	50.00	25.00	1.6	1.7	1.8	36.8
9	7.50	35.00	32.50	1.4	1.8	2.0	35.7
10	7.50	35.00	47.50	1.6	1.9	2.3	49.6
11	7.50	65.00	32.50	1.9	1.6	1.7	44.4
12	7.00	20.00	25.00	1.1	1.4	1.8	28.6
13	7.00	50.00	40.00	1.9	1.9	2.1	42.8
14	7.00	20.00	40.00	1.2	1.5	1.9	34.7
15	7.00	20.00	25.00	1.1	1.4	1.9	29.6
16	7.50	35.00	32.50	1.5	1.7	2.0	36.7
17	6.50	35.00	32.50	1.7	1.8	2.0	43.8
18	7.50	35.00	32.50	1.5	1.6	1.9	38.0
19	7.00	50.00	25.00	1.8	1.6	1.8	43.2
20	8.50	35.00	32.50	0.9	1.5	1.7	34.1
21	8.00	50.00	40.00	1.8	1.7	1.8	44.8
22	8.00	20.00	40.00	1.0	1.5	1.9	37.4
23	7.50	35.00	32.50	1.6	1.8	2.1	38.8
24	7.00	50.00	25.00	1.9	1.7	2.0	41.0
25	8.00	20.00	25.00	0.8	1.3	1.6	28.4
26	8.00	20.00	25.00	0.8	1.3	1.6	28.4
27	7.00	20.00	40.00	1.2	1.6	2.0	34.3
28	8.00	50.00	25.00	1.6	1.7	1.8	37.8

[a]: mephobarbital, [b]: pentobarbital, [c]: secobarbital.

[d]: the migration time of the last eluting enantiomer.

Table 3.3 The regression coefficients of the coded factors and ANOVA of the response surface models for chiral resolution and migration time.

	*Rs*11' [a]		*Rs*22' [b]		*Rs*33' [c]		MigTime [d]	
Model order	Quadratic		Quadratic		Quadratic		Linear	
Term	Coefficient	Prob>F[e]	Coefficient	Prob>F[e]	Coefficient	Prob>F[e]	Coefficient	Prob>F[e]
Intercept (β_0)	1.45		1.64		1.89		36.76	
A: pH	-0.15	<0.0001	-0.067	0.0304	-0.088	0.0193	-1.19	0.0447
B:[poly-L-SUCIL]	0.37	<0.0001	0.16	<0.0001	0.074	0.0429	4.64	<0.0001
C:[NH_4OAc]	0.041	0.0264	0.041	0.1672	0.073	0.0450	2.78	<0.0001
AB	0.031	0.1480	0.019	0.5961	0.029	0.4992		
AC	0.0025	0.9051	-0.044	0.2241	-0.029	0.4992		
BC	-0.0038	0.8581	-0.02	0.5720	-0.014	0.7454		
A^2	-0.031	0.0720	-0.0023	0.9329	-0.00047	0.9888		
B^2	-0.059	0.0021	-0.11	0.0008	-0.11	0.0042		
C^2	0.014	0.4113	0.013	0.6505	0.031	0.3627		
R^2	0.97		0.76		0.63		0.80	
Adjusted R^2 [f]	0.96		0.65		0.44		0.78	
Predicted R^2 [g]	0.92		0.45		0.18		0.71	

[a]: mephobarbital, [b]: pentobarbital, [c]: secobarbital.

[d]: the migration time of the last eluting enantiomer.

[e]: probability of the null hypothesis being true (the factor has no significant effect on the response) based on the F-test of comparing model variance with residual variance. Any term with $P<0.05$ is considered significant, and called for rejection of null hypothesis.

[f]: correlation coefficient adjusted for the number of terms in the model relative to the number of points in the design.

[g]: correlation coefficient based on the amount of variation in new data explained by the model.

Table 3.4 The experimental data gathered for *S/N* ratios from the CCD experiment for the optimization of sheath liquid conditions.

	Experimental parameters		Experimental response
Run order	A: [NH_4OAc] (mM)	B: %MeOH	$(S/N)_{avg}$ [a]
1	3.58	65.00	14.6
2	21.42	65.00	1.0
3	12.50	47.16	5.1
4	12.50	47.16	2.3
5	20.00	50.00	6.8
6	12.50	65.00	8.1
7	20.00	80.00	6.1
8	5.00	50.00	3.9
9	12.50	65.00	7.9
10	5.00	80.00	21.0
11	12.50	82.84	3.9
12	12.50	65.00	19.6
13	12.50	82.84	8.3
14	3.58	65.00	7.3
15	21.42	65.00	1.0
16	12.50	65.00	7.8
17	12.50	65.00	7.8

[a]: $(S/N)_{avg}$ = average *S/N* ratio of all six enantiomeric peaks.

Table 3.5 The experimental data gathered for $(S/N)_{avg}$ from the CCD experiment for the optimization of spray chamber parameters.

Experimental parameters			Experimental response
Run order	A: DGF (mL/min) [a]	B: DGT (°C) [b]	$(S/N)_{avg}$ [c]
1	4.0	190	21.1
2	5.5	250	14.9
3	4.0	310	26.5
4	5.5	350	10.4
5	7.0	310	6.1
6	5.5	250	12.0
7	7.0	190	9.2
8	4.0	190	22.2
9	5.5	250	12.9
10	7.0	190	17.8
11	5.5	250	16.1
12	5.5	250	16.5
13	3.0	250	25.2
14	7.0	310	7.2
15	4.0	310	27.8
16	8.0	250	15.8
17	5.5	150	10.0

[a]: DGF = drying gas flowrate,

[b]: DGT = drying gas temperature,

[c]: $(S/N)_{avg}$ = average *S/N* ratio of all six enantiomeric peaks.

Table 3.6 The regression coefficients of the coded factors used in the response surface models for the optimization of sheath liquid conditions and spray chamber parameters.

Sheath liquid conditions		
	$(S/N)_{avg}$ [a]	
Model order	2FI	
Term	Coefficient	Prob>F
Intercept (β_0)	7.06	
A: [NH_4OH]	-3.69	0.0030
B: %MeOH	2.29	0.0403
AB	-4.45	0.0140
A^2		
B^2		
R^2	0.69	
Adjusted R^2	0.62	
Predicted R^2	0.24	
Spray chamber parameters		
	$(S/N)_{avg}$ [a]	
Model order	Quadratic	
Term	Coefficient	Prob>F
Intercept (β_0)	14.95	
C: DGF	-5.35	0.0002
D: DGT	-0.15	0.8787
CD	-3.09	0.0302
C^2	2.46	0.0314
D^2	-1.18	0.2633
R^2	0.81	
Adjusted R^2	0.73	
Predicted R^2	0.35	

[a]: $(S/N)_{avg}$ = average S/N ratio of all six enantiomeric peaks.

Table 3.7 ANOVA of the CCD approaches used for the optimization of MEKC conditions, sheath liquid conditions and spray chamber parameters.

Responses	Source	Sum of squares	Degree of freedom	Mean square	F-ratio	Porb>F
MEKC factors						
*Rs*11' [a]	Model	4.10	9	0.455	66.5	<0.0001
	Residual	0.12	18	0.00684		
	Corrected total	4.22	27			
	p-Lack of Fit					0.3773
*Rs*22' [b]	Model	1.13	9	0.126	6.53	0.0004
	Residual	0.35	18	0.0193		
	Corrected total	1.48	27			
	p-Lack of Fit					0.6649
*Rs*33' [c]	Model	0.85	9	0.0945	3.40	0.0131
	Residual	0.50	18	0.0278		
	Corrected total	1.35	27			
	p-Lack of Fit					0.8344
MigTime [d]	Model	737.08	3	245.69	32.4	<0.0001
	Residual	181.98	24	7.58		
	Corrected total	919.06	27			
	p-Lack of Fit					0.0314
Sheath liquid parameters						
$(S/N)_{avg}$ [e]	Model	261.54	3	87.18	9.10	0.0020
	Residual	115.01	12	9.58		
	Corrected total	376.56	15			
	p-Lack of Fit					0.1230
Spray chamber parameters						
$(S/N)_{avg}$ [e]	Model	582.33	5	116.47	9.45	0.0011
	Residual	135.65	11	12.33		
	Corrected total	717.98	16			
	p-Lack of Fit					0.0530

[a]: mephobarbital, [b]: pentobarbital, [c]: secobarbital.

[d]: the migration time of the last eluting enantiomer.

[e]: $(S/N)_{avg}$ = average *S/N* ratio of all six enantiomeric peaks.

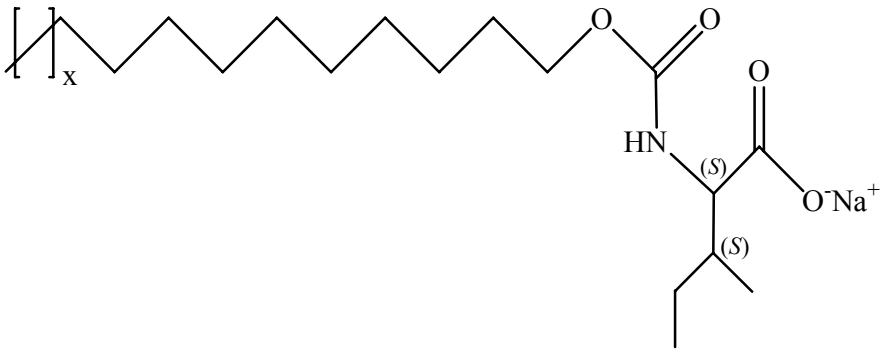

Polysodium *N*-undecenoxy carbonyl-L-isoleucinate (poly-L-SUCIL)

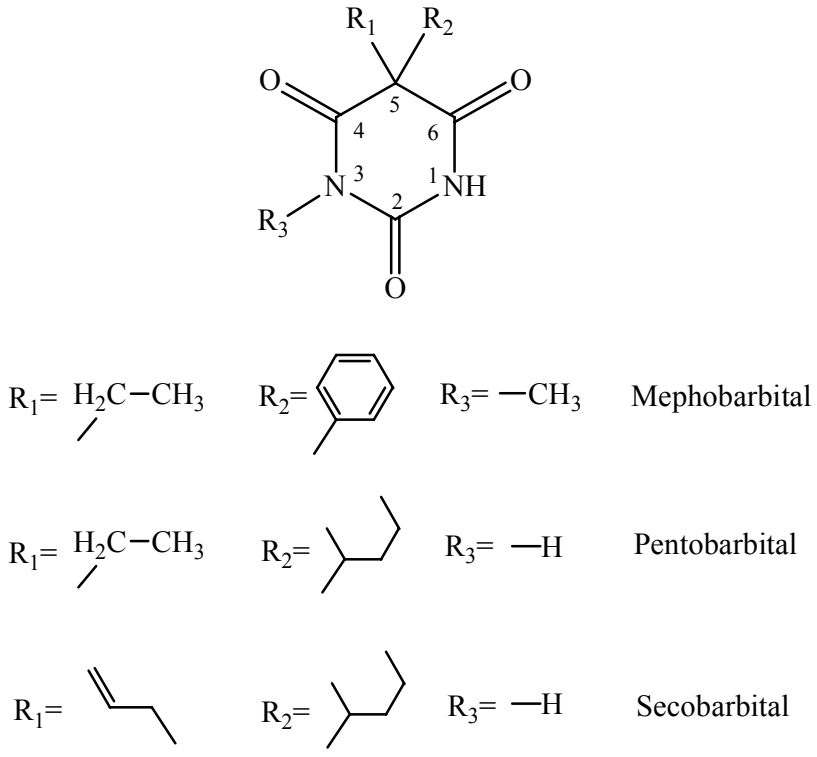

Figure 3.1 Structure of chiral polymeric surfactant, poly-L-SUCIL, and the barbiturates.

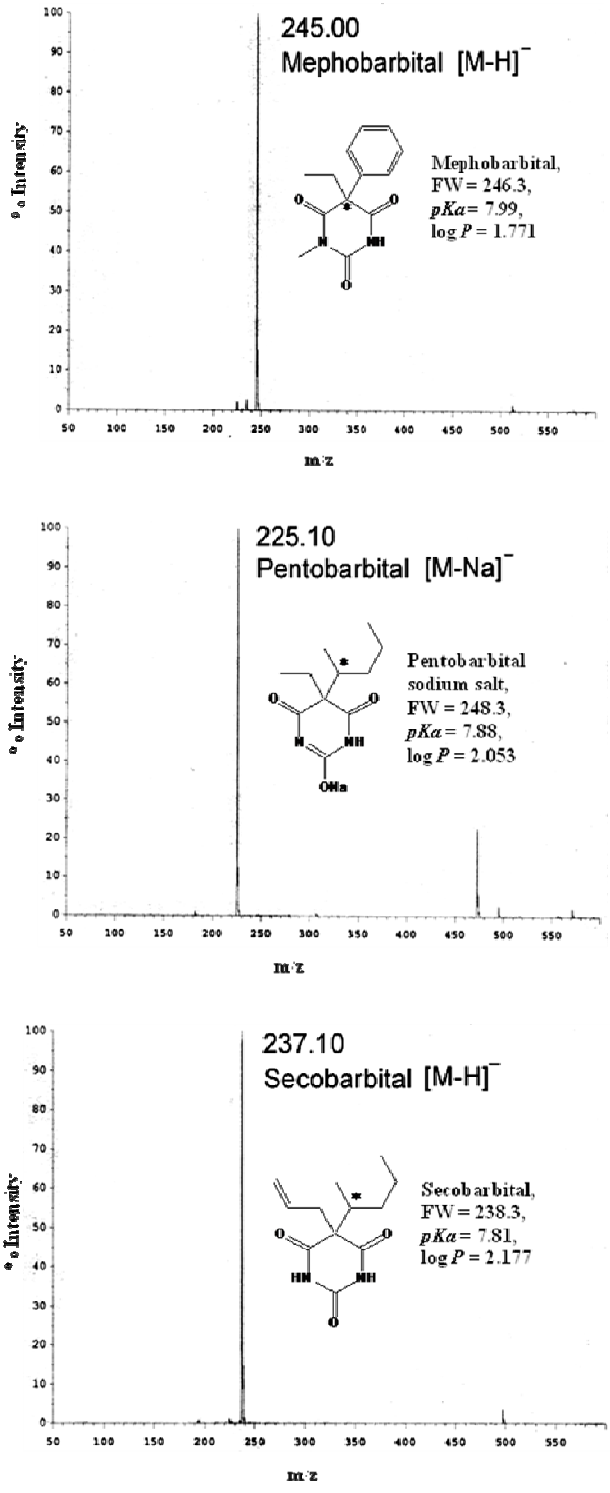

Figure 3.2 Direct infusion mass spectrums of (A) mephobarbital, (B) pentobarbital, and (C) secobarbital. The inset of each mass spectrum provides information on the physicochemical properties of barbiturates (Data from SciFinder Scholar 2008).

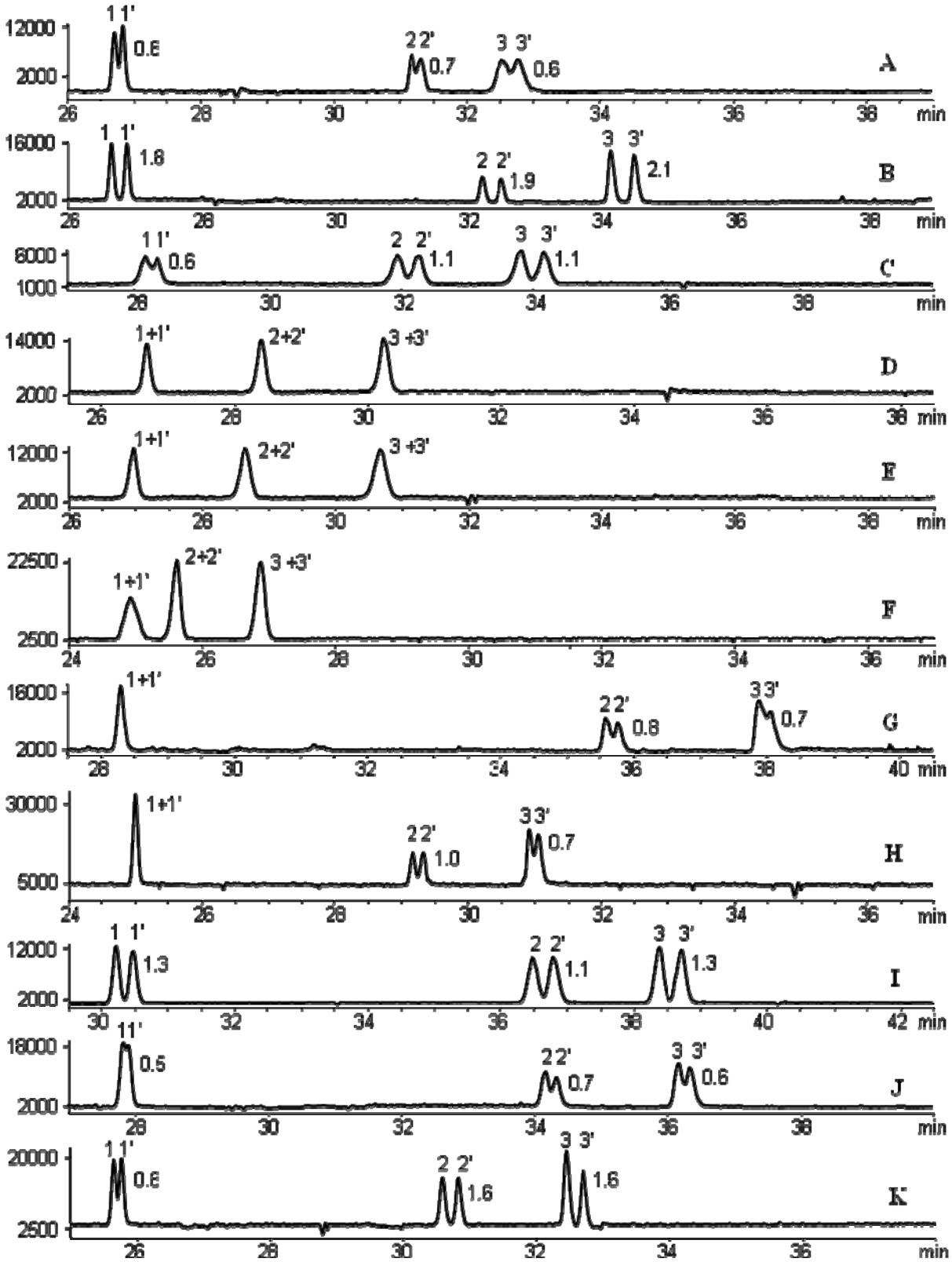
A
1 1' 0.8
2 2' 0.7
3 3' 0.6
B
1 1' 1.8
2 2' 1.9
3 3' 2.1
C'
1 1' 0.6
2 2' 1.1
3 3' 1.1
D
1+1'
2+2'
3+3'
E
1+1'
2+2'
3+3'
F
1+1'
2+2'
3+3'
G
1+1'
2 2' 0.8
3 3' 0.7
H
1+1'
2 2' 1.0
3 3' 0.7
I
1 1' 1.3
2 2' 1.1
3 3' 1.3
J
1 1' 0.5
2 2' 0.7
3 3' 0.6
K
1 1' 0.8
2 2' 1.6
3 3' 1.6
min

Figure 3.3 The on-line MEKC-MS of three chiral barbiturates mixture using various polymeric surfactants in MEKC. Capillary 125.0 cm, ID 50 µm, 20 °C, +25 kV. CE buffer: 25.00 mM NH_4OAc, pH 8.0, 50.00 mM surfactant. Barbiturates mixture: 125.0 µg/mL of each racemate in ACN:H_2O 80:20 (v:v), injection 2 mbar, 5 sec. Spray chamber: NP 3 psi, DGF 5.0 mL/min, DGT 250 °C. Sheath liquid: 5 mM NH_4OAc in MeOH:H_2O 80:20 (v:v), 5 µL/min. Pea 11': mephobarbital, 22': pentobarbital, 33': secobarbital. A: poly-L-SUCL, B: poly-L-SUCIL, C: poly-L-SUCV, D: poly-L-SUCLS, E: poly-L-SUCVS, F: poly-L-SOCL, G: poly-L-SULV, H: poly-L-SUPA, I: the mixed micelle of poly-L-SUCL and poly-L-SUCIL 1:1 (M:M), J: the mixed micelle of poly-L-SULV and poly-L-SUCIL 1:1 (M:M), K: the mixed micelle of poly-L-SUPA and poly-L-SUCIL 1:1 (M:M). The numbers on the right side of the peaks in A-C and G-K represent the resolution values.

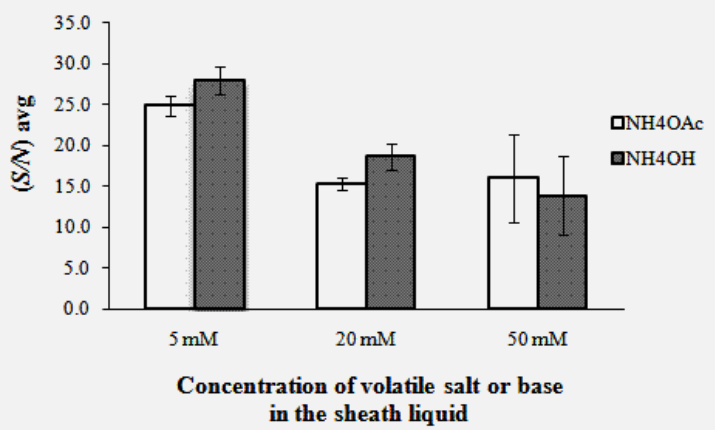

Figure 3.4 Comparison of *S/N* ratios of barbiturates using different concentrations of NH_4OAc and NH_4OH in the sheath liquids of MeOH:H_2O 80:20 (v:v). The *S/N* ratio is the average value of six peaks of barbiturates enantiomers. The error bar represents the one standard deviation of two measurements.

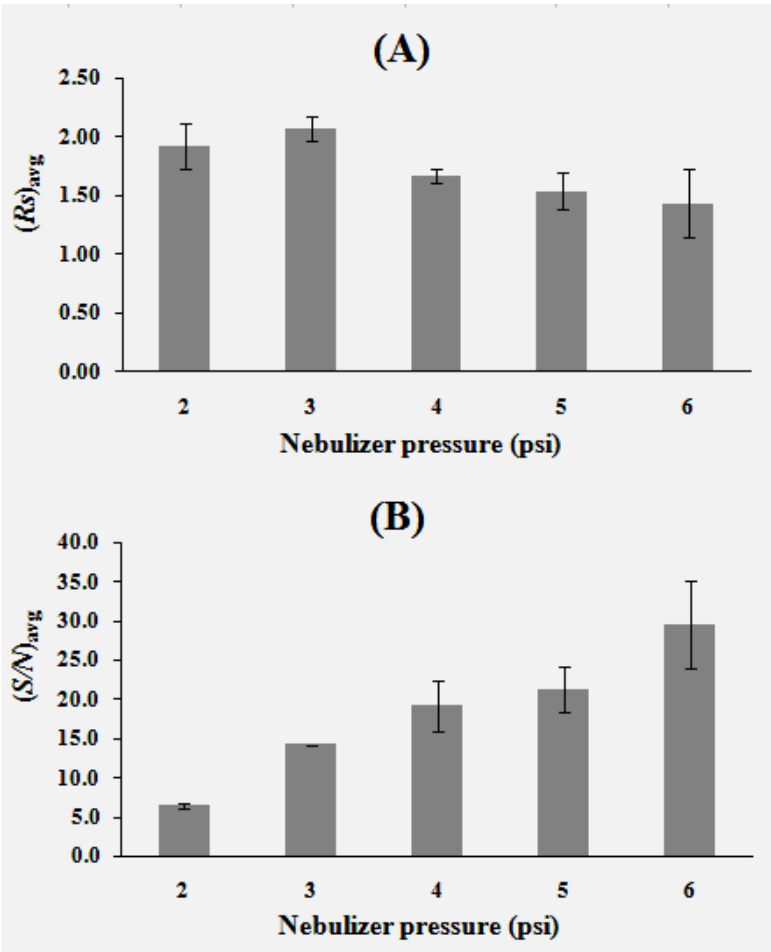

Figure 3.5 Comparison of chiral resolutions and *S/N* ratios of barbiturates as the nebulizer pressure changed from 2 psi to 6 psi. The chiral resolution value is the average value obtained for three pairs of barbiturate enantiomers. The *S/N* ratio is the average value obtained for six peaks of barbiturates enantiomers. The error bar represents the one standard deviation of two measurements.

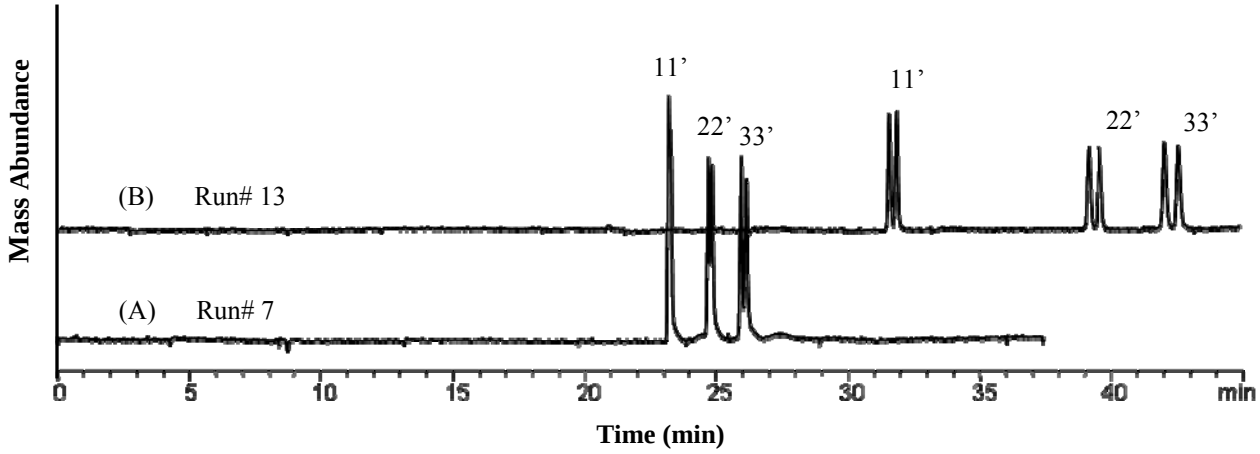

Figure 3.6 The representative MS experimental responses for the optimization of MEKC conditions. Capillary 125.0 cm, ID 50 μm, 20 °C, +25 kV. Barbiturates mixture: 125.0 μg/mL of each racemate in ACN:H_2O 80:20 (v:v), injection 2 mbar, 5 sec. Spray chamber: NP 3 psi, DGF 5.0 mL/min, DGT 250 °C. Sheath liquid: 5 mM NH_4OAc in MeOH:H_2O 80:20 (v:v), 5 μL/min. The MEKC conditions for run# 7 and run# 13 are listed in Table 3.2. Peak 11': mephobarbital, 22': pentobarbital, 33': secobarbital.

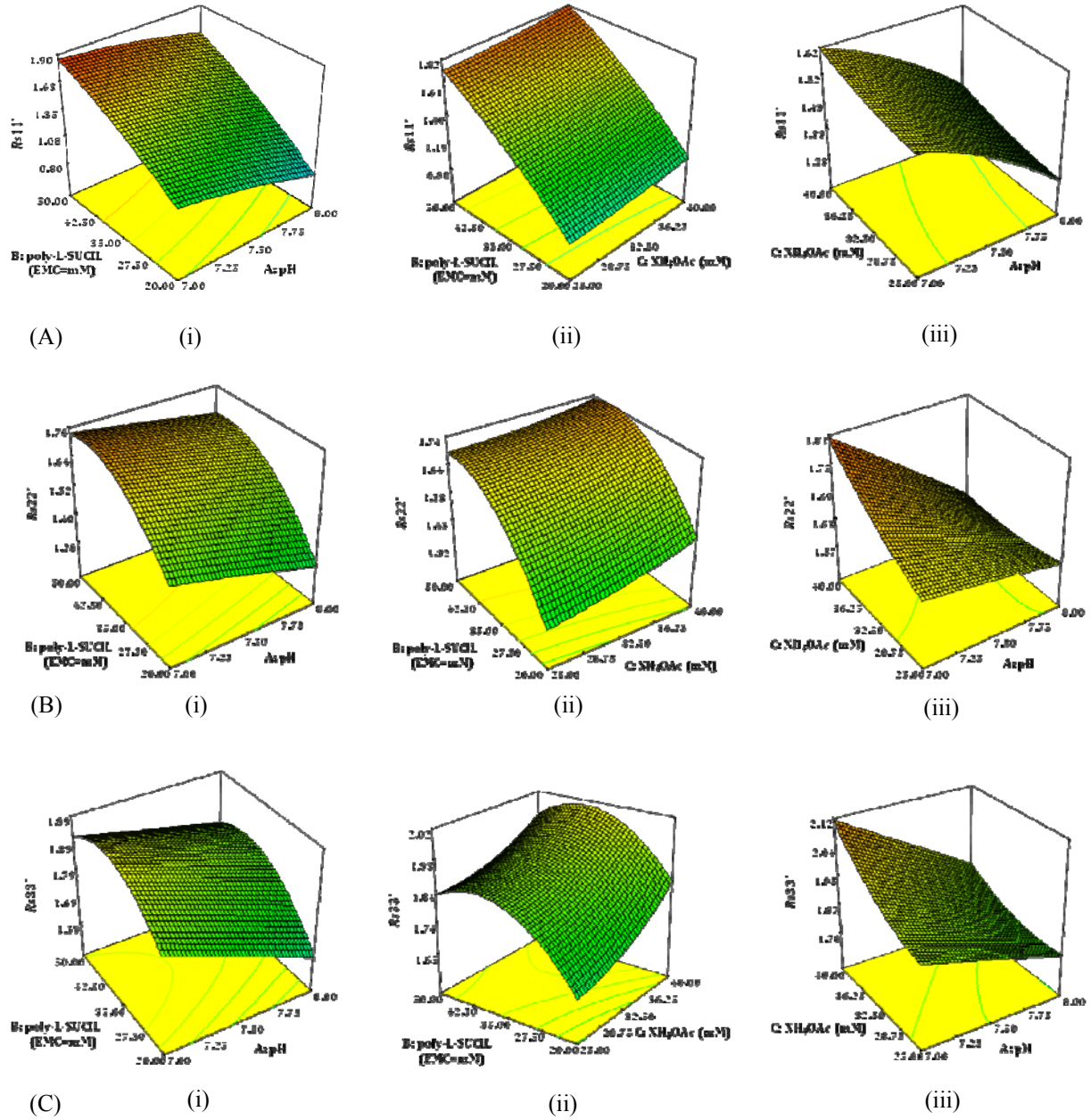

(A) (i) (ii) (iii)

(B) (i) (ii) (iii)

(C) (i) (ii) (iii)

Figure 3.7 The response surface plot for the optimization of chiral resolutions of mephobarbital (A), pentobarbital (B), and secobarbital (C) as a function of [poly-L-SUCIL] versus pH (i), [poly-L-SUCIL] versus [NH_4OAc] (ii), and [NH_4OAc] versus pH (iii). *Rs*11': chiral resolution of mephobarbital, *Rs*22': chiral resolution of pentobarbital, *Rs*33': chiral resolution of secobarbital.

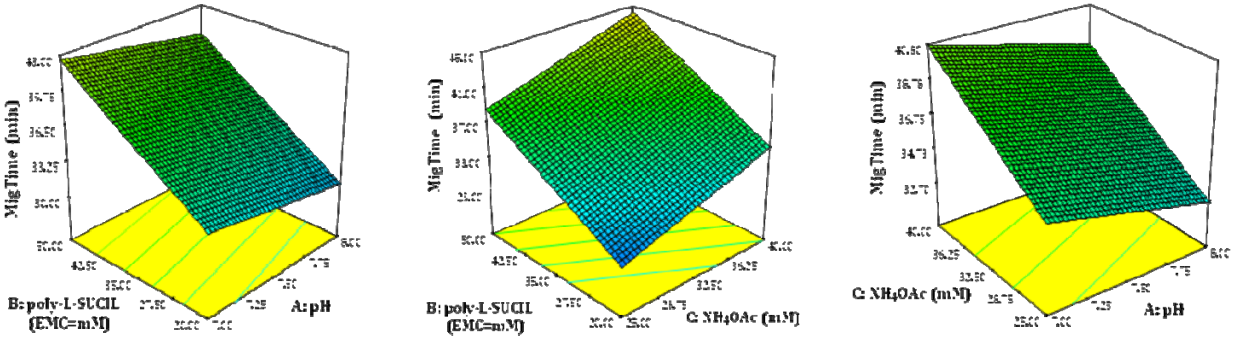

(A) (B) (C)

Figure 3.8 The response surface plots for the optimization of the migration time as a function of [poly-L-SUCIL] versus pH (A), [poly-L-SUCIL] versus [NH_4OAc] (B), and [NH_4OAc] versus pH (C). The *S/N* ratio is the average value of six peaks of barbiturates enantiomers.

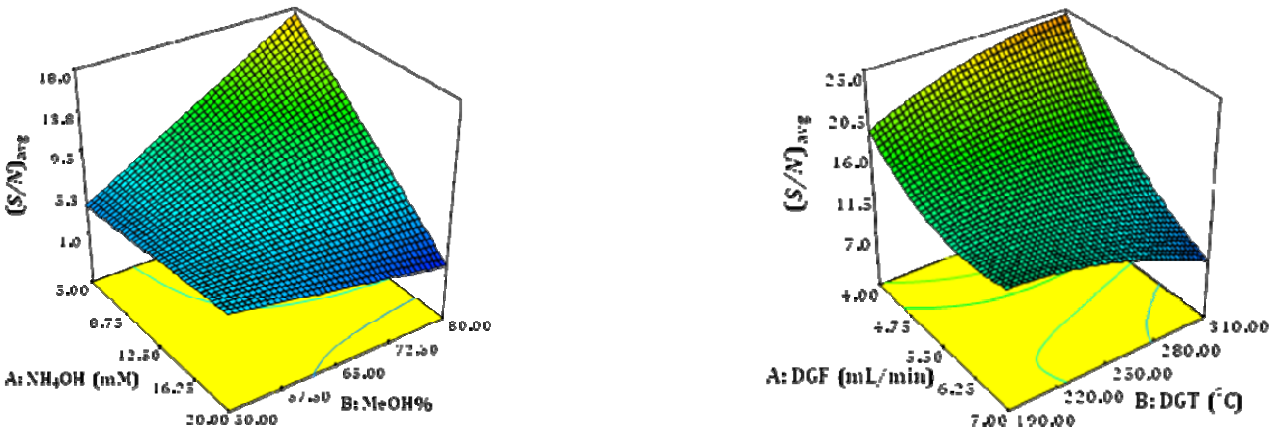

(A) (B)

Figure 3.9 The response surface plots for the optimization of sheath liquid conditions (A), and spray chamber parameters (B) for *S/N* ratio as the function of [NH_4OAc] versus %MeOH. The *S/N* ratio is the average value of six peaks of barbiturate enantiomers.

	Rs11’	Rs22’	Rs33’	MigTime (min)	$(S/N)_{avg}$
Predicted	1.6	1.7	1.9	36.6	24.5
Experimental	1.4	1.5	1.6	32.0	25.2

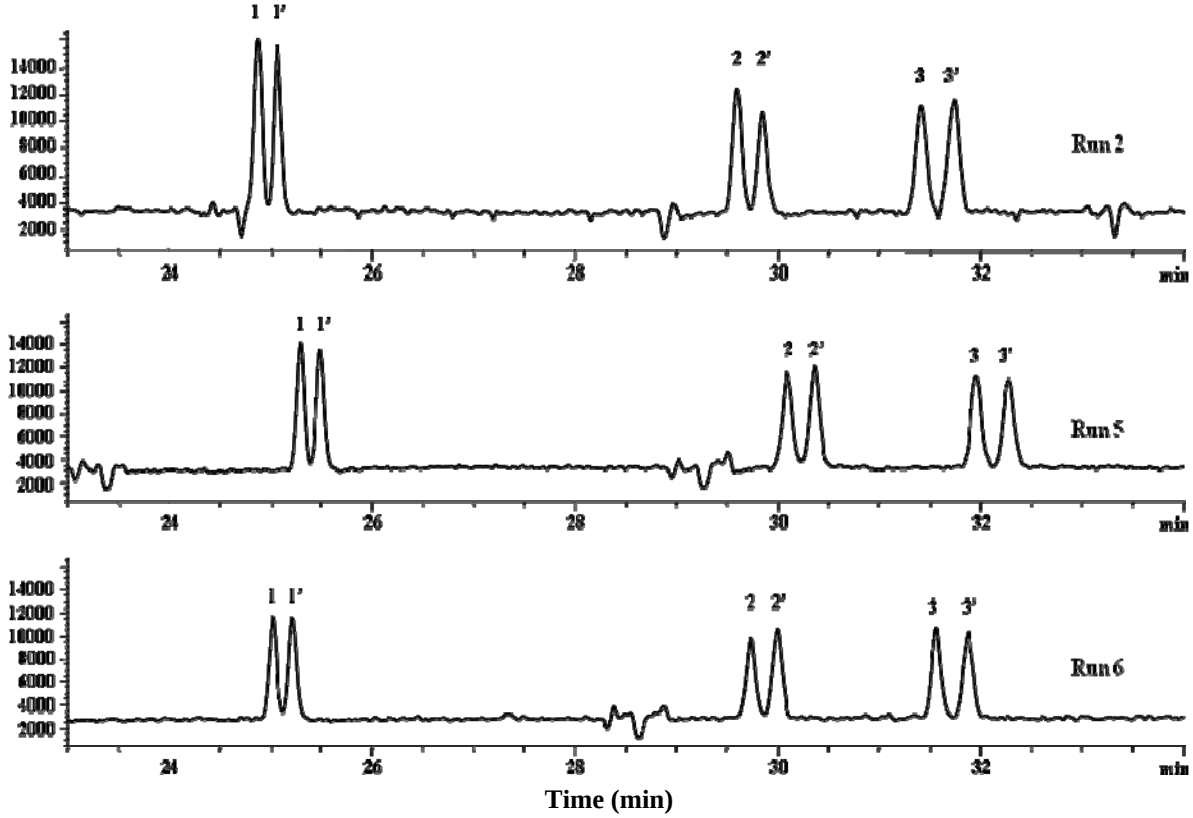

Figure 3.10 The electropherograms obtained under final optimum conditions of MEKC-ESI-MS. Capillary 125.0 cm, ID 50 μm, 20 °C, +25 kV. 25.00 mM NH_4OAc, pH 7.0, 39.69 mM poly-L-SUCIL. Barbiturates mixture: 125.0 μg/mL of each racemate in ACN:H_2O 80:20 (v:v), injection 2 mbar, 5 sec. Sheath liquid: 5 mM NH_4OAc in MeOH:H_2O 80:20 (v:v), 5 μL/min. Spray chamber: NP 5 psi, DGF 4.0 mL/min, DGT 310 °C. Peak 11’: mephobarbital, 22’: pentobarbital, 33’: secobarbital. The inset table compares the predicted values with the experimental data.

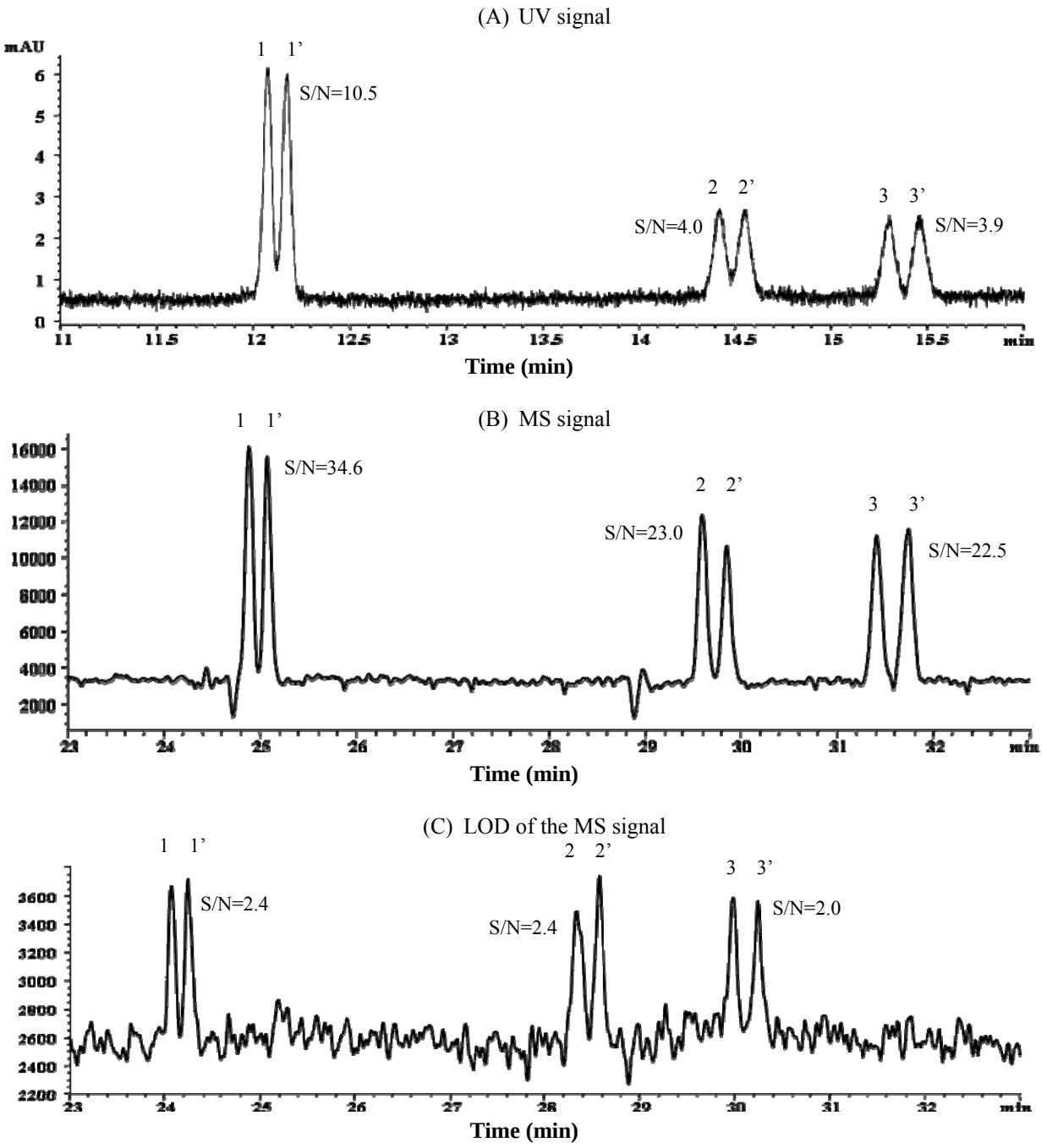

Figure 3.11 The comparison of UV signal and MS signal at optimum MEKC-ESI-MS conditions. A and B: 125 μg/mL for each racemic barbiturate; C: 7.8 μg/mL for each racemic barbiturate. All other conditions are same as described in Figure 3.10. The *S/N* ratios labeled are the average values of the two enantiomers. Peak 11': mephobarbital, 22': pentobarbital, 33': secobarbital.

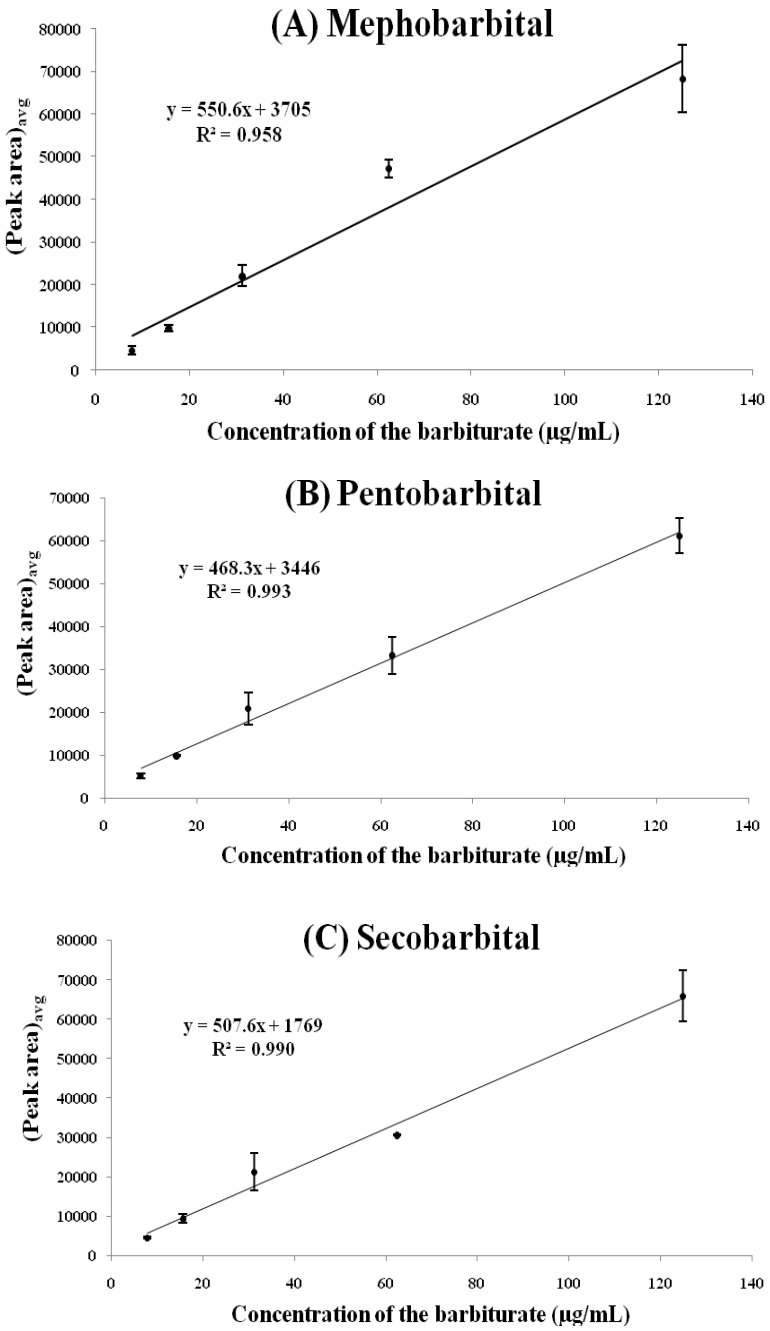

Figure 3.12 The calibration plots of barbiturates for MEKC-MS quantitation. $(\text{Peak area})_{avg}$ are the average values of the two enantiomer peaks. A: mephobarbital, B: pentobarbital, C: secobarbital. The error bar represents one standard deviation of two measurements.

FUTURE DIRECTION

The utility of IL-type surfactants and TM-β-CD as dual chiral selector has proved to be successful for enantioseparation of negatively charged species. The future direction will be focused on the enantioseparation of neutral species and even positively charged species. In addition, the structure-enantioselectivity relationship need to be investigated on details such as the effects of different head groups on the surfactant molecule, the length of the hydrocarbon chain, and the type of CD derivatives.

The MEKC-ESI-MS technique is a powerful analytical tool for simultaneous enantio-separation. The polymeric surfactants can be used to form molecular micelles or mixed molecular micelles as pseudostationary phase and chiral selector. The future step is to analyze the parent chiral drugs and their chiral metabolites in human blood or urine by this technique. On the other hand, the multivariate optimization can be used to improve the performance of other CE-MS techniques such as atmospheric pressure photoionization (APPI) coupled to MEKC-MS.

REFERENCES

[1] Vindevogel, J., Sandra, P., *Introduction to Micellar Electrokinetic Chromatography*; Heidelberg: Huthig, 1992.

[2] Iqbal, R., M.S. thesis, Georgia State University, Atlanta, GA, 2004.

[3] *Capillary Electrophoresis: Theory & Practice*, Grossman, P. D., Colburn j. C., Eds, Academic Press: San Diego, CA, 1992.

[4] Bard, A. J., Faulkner, L. R., *Electrochemical Methods: Fundamentals and Applications, 2nd ed*, John Wiley & Sons: New York, NY, 2001.

[5] Shamsi, S. A., Danielson, N. D., *J. Sep. Sci.* 2007, *30*, 1729-1750.

[6] Rizvi, S. A. A., Shamsi, S. A., *Anal. Chem.* 2006, *78*, 7061-7069.

[7] Rundlett, K. L., Armstrong, D. W., *J. Chromatogr. A* 1996, *721*, 173-186.

[8] Copeland, R. A., *Enzymes: a practical introduction to structure, mechanism, and data analysis, 2nd ed*, Wiley-VCH: New York, 2000.

[9] Smith, H. J., Simons, C., *Enzymes and their inhibition: drug development,* CRC press: Boca Raton, 2005.

[10] *Affinity capillary electrophoresis in pharmaceutics and biopharmaceutics*, Neubert, R. H. H., Ruttinger, H., Eds, Marcel Dekker, New York, 2003.

[11] François, Y et al., *J. Sep. Sci.* 2007, 30, 751-760.

[12] Bowser, M. T., Chen, D. D. Y., *J. Phys. Chem.* 1998, 102, 8063-8071.

[13] Bowser, M. T., Chen, D. D. Y., *J. Phys. Chem.* 1999, 103, 197-202.

[14] Rundlett, K. L., Armstrong, D. W., *Electrophoresis* 1997, 18, 2194-2202.

[15] Rundlett, K. L., Armstrong, D. W., *Electrophoresis* 2001, 22, 1419-1427.

APPENDIX A: THE CALCULATION PROCEDURE OF EFFECTIVE MOBILITIES TO OBTAIN LINEAR AND NON-LINEAR PLOTS FOR THE ESTIMATION OF K_1 AND K_2

The calculation procedure involves calculating the effective mobility of L-UCLB from the migration time of neutral marker and L-UCLB. Next, the viscosity correction factor is calculated and used in the calculation of the x-axis and y-axis values for x-reciprocal plot, y-reciprocal plot, double-reciprocal plot, and isotherm plot. Other parameters such as total length of capillary (L) and effective length of capillary (l) were measured experimentally for each capillary used in CE instrument, and the voltage applied was 20000 V. Therefore, the effective mobility is calculated by the equation of $\mu_{ep}=L\times l\times(1/t(i)-1/t(m))/V$. The detailed data treatment for K_1 is shown in Appendix B.

Similarly, the effective mobility of fenoprofen is calculated from the migration time of neutral marker and *R*-/*S*-fenoprofen. Then the x-axis and y-axis values for double-reciprocal plots are calculated with the viscosity correction factors to estimate K_2 at different concentration of L-UCLB from 0.0 mM to 1.0 mM. Other parameters such as total length of capillary (L) and effective length of capillary (l) were measured experimentally for each capillary used in CE instrument, and the voltage applied was 10000 V. Therefore, the effective mobility is calculated by the equation of $\mu_{ep}=L\times l\times(1/t(i)-1/t(m))/V$. The detailed data treatment for K_2 can be found in Appendix C.

APPENDIX B: THE DETAILED DATA TREATMENT TO CALCULATE THE X-AXIS AND Y-AXIS VALUES OF LINEAR AND NON-LINEAR PLOTS FOR THE ESTIMATION OF K_1

L=64.5 cm, l=56.0 cm.

[TM-β-CD] (mM)	1/[TM-β-CD] (M^{-1})	t(i) (min)	1/t(i) (s^{-1})	t(m) (min)	1/t(m) (s^{-1})	1/t(i)-1/t(m) ($s^{-1}\times10^{-3}$)
0.00	N/A	7.598	0.0021936	12.215	0.0013644	0.0008291
		7.682	0.0021696	12.596	0.0013232	0.0008464
		7.663	0.0021750	12.635	0.0013191	0.0008559
2.50	400	8.163	0.0020417	11.459	0.0014545	0.0005873
		7.933	0.0021009	11.099	0.0015016	0.0005993
		7.717	0.0021597	10.712	0.0015559	0.0006038
3.00	333	7.502	0.0022216	10.261	0.0016243	0.0005974
		7.601	0.0021927	10.496	0.0015879	0.0006048
		7.831	0.0021283	10.877	0.0015323	0.0005960
3.50	286	7.521	0.0022160	10.254	0.0016254	0.0005906
		8.095	0.0020589	11.348	0.0014687	0.0005902
		8.128	0.0020505	11.476	0.0014523	0.0005982
4.00	250	8.040	0.0020730	11.297	0.0014753	0.0005977
		9.063	0.0018390	13.393	0.0012444	0.0005945
		9.613	0.0017338	14.619	0.0011401	0.0005937
4.50	222	9.223	0.0018071	13.613	0.0012243	0.0005828
		8.706	0.0019144	12.610	0.0013217	0.0005927
		9.630	0.0017307	14.487	0.0011505	0.0005802
5.00	200	9.154	0.0018207	13.323	0.0012510	0.0005697
		9.028	0.0018461	12.993	0.0012827	0.0005634
		9.094	0.0018327	13.330	0.0012503	0.0005824
5.50	182	10.000	0.0016667	15.174	0.0010984	0.0005683
		10.573	0.0015763	16.421	0.0010150	0.0005614
		9.414	0.0017704	14.020	0.0011888	0.0005816
6.00	167	8.629	0.0019315	12.198	0.0013663	0.0005651
		8.183	0.0020367	11.411	0.0014606	0.0005762
		8.526	0.0019548	11.926	0.0013975	0.0005573
7.00	143	8.303	0.0020073	11.427	0.0014585	0.0005488
		8.508	0.0019589	11.923	0.0013979	0.0005611
		8.587	0.0019409	12.048	0.0013834	0.0005576
8.00	125	9.041	0.0018435	12.863	0.0012957	0.0005477
		8.533	0.0019532	11.871	0.0014040	0.0005492
		9.138	0.0018239	13.074	0.0012748	0.0005491
9.00	111	9.018	0.0018482	12.852	0.0012968	0.0005513
		8.921	0.0018683	12.624	0.0013202	0.0005480
		9.121	0.0018273	12.938	0.0012882	0.0005391
10.00	100	9.041	0.0018435	12.735	0.0013087	0.0005347
		9.498	0.0017548	13.885	0.0012003	0.0005544
		10.050	0.0016584	14.936	0.0011159	0.0005425

μ_{ep} ($cm^2 \times V^{-1} \times s^{-1} \times 10^{-3}$)	Average ($cm^2 \times V^{-1} \times s^{-1} \times 10^{-3}$)	STD ($cm^2 \times V^{-1} \times s^{-1} \times 10^{-3}$)	t (min)	t average (min)	ν=t/t0
0.1497385			15.455		
0.1528603	0.1524	0.0024	15.904	15.929	1.000
0.1545694			16.427		
0.1060614			16.394		
0.1082321	0.1078	0.0015	16.825	16.747	1.051
0.1090547			17.023		
0.1078826			16.230		
0.1092246	0.1082	0.0009	16.220	16.150	1.014
0.1076391			16.001		
0.1066688			16.020		
0.1065895	0.1071	0.0008	16.258	16.075	1.009
0.1080383			15.948		
0.1079357			15.928		
0.1073753	0.1075	0.0004	15.934	15.958	1.002
0.1072212			16.013		
0.1052458			15.893		
0.1070391	0.1057	0.0012	15.956	15.936	1.000
0.1047924			15.959		
0.1028929			16.005		
0.1017440	0.1033	0.0017	16.025	16.042	1.007
0.1051810			16.097		
0.1026344			16.103		
0.1013855	0.1030	0.0019	16.103	16.103	1.011
0.1050433			16.103		
0.1020620			16.137		
0.1040552	0.1023	0.0017	16.166	16.157	1.014
0.1006480			16.169		
0.0991084			16.237		
0.1013314	0.1004	0.0011	16.389	16.572	1.040
0.1006959			17.089		
0.0989233			16.421		
0.0991891	0.0991	0.0001	16.848	16.735	1.051
0.0991658			16.935		
0.0995721			16.824		
0.0989714	0.0986	0.0011	16.604	16.628	1.044
0.0973597			16.456		
0.0965713			16.381		
0.1001281	0.0982	0.0018	16.363	16.396	1.029
0.0979760			16.443		

ν×μ(i)-μ(f) ($cm^2 \times V^{-1} \times s^{-1} \times 10^{-3}$)	Average ($cm^2 \times V^{-1} \times s^{-1} \times 10^{-3}$)	STD ($cm^2 \times V^{-1} \times s^{-1} \times 10^{-3}$)	95% CI ($cm^2 \times V^{-1} \times s^{-1} \times 10^{-3}$)
-0.00266 0.00046 0.00217	-0.00001	0.00245	0.00277
-0.04093 -0.03865 -0.03778	-0.03912	0.00163	0.00184
-0.04302 -0.04166 -0.04326	-0.04264	0.00087	0.00098
-0.04475 -0.04483 -0.04337	-0.04432	0.00082	0.00093
-0.04426 -0.04482 -0.04498	-0.04469	0.00038	0.00043
-0.04711 -0.04531 -0.04756	-0.04666	0.00119	0.00135
-0.04877 -0.04993 -0.04647	-0.04839	0.00176	0.00199
-0.04864 -0.04990 -0.04621	-0.04825	0.00188	0.00213
-0.04887 -0.04685 -0.05031	-0.04868	0.00174	0.00196
-0.04929 -0.04698 -0.04764	-0.04797	0.00119	0.00135
-0.04847 -0.04819 -0.04822	-0.04829	0.00015	0.00018
-0.04846 -0.04908 -0.05077	-0.04944	0.00119	0.00135
-0.05300 -0.04934 -0.05155	-0.05130	0.00184	0.00209

$1/(v\times\mu(i)-\mu(f))$ ($V\times s\times cm^{-2}$)	Average ($V\times s\times cm^{-2}$)	STD ($V\times s\times cm^{-2}$)	95% CI ($V\times s\times cm^{-2}$)
N/A	N/A	N/A	N/A
-24432 -25875 -26467	-25591	1046	1184
-23247 -24006 -23114	-23456	481	545
-22347 -22307 -23059	-22571	423	479
-22592 -22309 -22233	-22378	189	214
-21229 -22069 -21026	-21442	553	626
-20503 -20028 -21520	-20684	762	862
-20558 -20038 -21642	-20746	818	926
-20461 -21344 -19878	-20561	738	835
-20288 -21287 -20991	-20855	513	581
-20631 -20750 -20740	-20707	66	75
-20637 -20374 -19698	-20236	484	548
-18869 -20269 -19398	-19512	707	800

$(\nu \times \mu(i) - \mu(f))/[TM\text{-}\beta\text{-}CD]$ $(cm^2 \times V^{-1} \times s^{-1} \times M^{-1})$	Average $(cm^2 \times V^{-1} \times s^{-1} \times M^{-1})$	STD $(cm^2 \times V^{-1} \times s^{-1} \times M^{-1})$	95% CI $(cm^2 \times V^{-1} \times s^{-1} \times M^{-1})$
N/A	N/A	N/A	N/A
-0.01637 -0.01546 -0.01511	-0.01565	0.00065	0.00074
-0.01434 -0.01389 -0.01442	-0.01421	0.00029	0.00033
-0.01279 -0.01281 -0.01239	-0.01266	0.00023	0.00027
-0.01107 -0.01121 -0.01124	-0.01117	0.00009	0.00011
-0.01047 -0.01007 -0.01057	-0.01037	0.00026	0.00030
-0.00975 -0.00999 -0.00929	-0.00968	0.00035	0.00040
-0.00884 -0.00907 -0.00840	-0.00877	0.00034	0.00039
-0.00815 -0.00781 -0.00838	-0.00811	0.00029	0.00033
-0.00704 -0.00671 -0.00681	-0.00685	0.00017	0.00019
-0.00606 -0.00602 -0.00603	-0.00604	0.00002	0.00002
-0.00538 -0.00545 -0.00564	-0.00549	0.00013	0.00015
-0.00530 -0.00493 -0.00516	-0.00513	0.00018	0.00021

[TM-β-CD]/(v×μ(i)-μ(f)) ($V \times s \times M \times cm^{-2}$)	Average ($V \times s \times M \times cm^{-2}$)	STD ($V \times s \times M \times cm^{-2}$)	95% CI ($V \times s \times M \times cm^{-2}$)
N/A	N/A	N/A	N/A
-61.08 -64.69 -66.17	-63.98	2.62	2.96
-69.74 -72.02 -69.34	-70.37	1.44	1.63
-78.21 -78.07 -80.71	-79.00	1.48	1.68
-90.37 -89.24 -88.93	-89.51	0.76	0.86
-95.53 -99.31 -94.62	-96.49	2.49	2.82
-102.52 -100.14 -107.60	-103.42	3.81	4.31
-113.07 -110.21 -119.03	-114.10	4.50	5.09
-122.77 -128.07 -119.27	-123.37	4.43	5.01
-142.01 -149.01 -146.94	-145.99	3.59	4.06
-165.05 -166.00 -165.92	-165.66	0.53	0.60
-185.73 -183.36 -177.28	-182.13	4.36	4.93
-188.69 -202.69 -193.98	-195.12	7.07	8.00

APPENDIX C: THE DETAILED DATA TREATMENT TO CALCULATE THE X-AXIS AND Y-AXIS VALUES OF DOUBLE-RECIPROCAL PLOTS FOR THE ESTIMATION OF K_2

1. *R*-fenoprofen, 0.0 mM TM-β-CD. L=64.6 cm, l=56.0 cm.

[TM-β-CD] (mM)	1/[TM-β-CD] (M^{-1})	v=t/t0	t(i) (min)	1/t(i) ($s^{-1}\times10^{-3}$)	t(m) (min)	1/t(m) ($s^{-1}\times10^{-3}$)	1/t(i)-1/t(m) ($s^{-1}\times10^{-3}$)
0.00	N/A	1.000	31.82	0.5238	17.41	0.9573	-0.4335
			35.34	0.4716	18.87	0.8832	-0.4116
			47.62	0.3500	21.77	0.7656	-0.4156
1.00	1000	0.9880	47.99	0.3473	26.06	0.6395	-0.2923
			45.52	0.3661	25.44	0.6551	-0.2890
			47.23	0.3529	25.80	0.6460	-0.2931
2.00	500	0.9909	41.50	0.4016	25.89	0.6437	-0.2421
			40.29	0.4137	25.47	0.6544	-0.2407
			40.04	0.4163	25.33	0.6580	-0.2417
3.00	333	0.9830	37.01	0.4503	25.36	0.6572	-0.2069
			36.06	0.4622	24.94	0.6683	-0.2061
			34.45	0.4838	24.18	0.6893	-0.2055
4.00	250	0.9997	40.09	0.4157	27.13	0.6143	-0.1986
			44.70	0.3729	29.75	0.5602	-0.1874
			49.44	0.3371	31.99	0.5210	-0.1839
5.00	200	1.0057	48.03	0.3470	32.55	0.5120	-0.1650
			48.53	0.3434	32.71	0.5095	-0.1661
			47.11	0.3538	31.99	0.5210	-0.1672
6.00	167	0.9905	57.38	0.2905	37.86	0.4402	-0.1498
			55.74	0.2990	37.17	0.4484	-0.1494
			54.24	0.3073	36.29	0.4593	-0.1520
8.00	125	1.0253	52.32	0.3186	36.77	0.4533	-0.1347
			50.54	0.3298	35.89	0.4644	-0.1346
			49.02	0.3400	35.08	0.4751	-0.1351
10.00	100	1.0156	N/A	N/A	N/A	N/A	N/A
			42.96	0.3880	32.68	0.5100	-0.1220
			43.71	0.3813	33.11	0.5034	-0.1221
15.00	67	1.0222	44.71	0.3728	35.03	0.4758	-0.1030
			49.97	0.3335	38.49	0.4330	-0.0995
			50.45	0.3304	38.68	0.4309	-0.1005
35.00	29	1.1838	N/A	N/A	N/A	N/A	N/A
			N/A	N/A	N/A	N/A	N/A
			51.20	0.3255	43.04	0.3872	-0.0617
50.00	20	1.2846	N/A	N/A	N/A	N/A	N/A
			51.52	0.3235	44.63	0.3734	-0.0499
			48.17	0.3460	41.91	0.3977	-0.0517

μ_{ep} ($cm^2 \times V^{-1} \times s^{-1} \times 10^{-3}$)	$\nu \times \mu(i) - \mu(f)$ ($cm^2 \times V^{-1} \times s^{-1} \times 10^{-3}$)	$1/(\nu \times \mu(i) - \mu(f))$ ($V \times s \times cm^{-2}$)	Average ($V \times s \times cm^{-2}$)	STD ($V \times s \times cm^{-2}$)	95% CI ($V \times s \times cm^{-2}$)
-0.1568 -0.1489 -0.1504	N/A, $\mu(f)$=0.1520	N/A	N/A	N/A	N/A
-0.1057 -0.1046 -0.1060	0.0475 0.0487 0.0472	21039 20536 21175	20917	337	381
-0.0876 -0.0871 -0.0875	0.0652 0.0657 0.0653	15340 15219 15305	15288	62	71
-0.0748 -0.0746 -0.0743	0.0784 0.0787 0.0789	12751 12705 12671	12709	40	45
-0.0719 -0.0678 -0.0665	0.0802 0.0842 0.0855	12474 11872 11697	12014	407	461
-0.0597 -0.0601 -0.0605	0.0920 0.0916 0.0912	10875 10921 10970	10922	47	54
-0.0542 -0.0540 -0.0550	0.0983 0.0985 0.0975	10170 10156 10253	10193	53	59
-0.0487 -0.0487 -0.0489	0.1020 0.1021 0.1019	9801 9798 9815	9805	9	11
N/A -0.0442 -0.0442	N/A 0.1072 0.1071	N/A 9332 9333	9333	1	1
-0.0373 -0.0360 -0.0364	0.1139 0.1152 0.1148	8779 8680 8709	8723	51	58
N/A N/A -0.0223	N/A N/A 0.1256	N/A N/A 7964	7964	N/A	N/A
N/A -0.0181 -0.0187	N/A 0.1288 0.1280	N/A 7765 7814	7789	35	48

2. *R*-fenoprofen, 0.2 mM TM-β-CD. L=64.6 cm, l=56.0 cm.

[TM-β-CD] (mM)	1/[TM-β-CD] (M^{-1})	ν=t/t0	t(i) (min)	1/t(i) ($s^{-1}\times10^{-3}$)	t(m) (min)	1/t(m) ($s^{-1}\times10^{-3}$)	1/t(i)-1/t(m) ($s^{-1}\times10^{-3}$)
0.00	N/A	1.000	N/A 70.80 51.35	N/A 0.2354 0.3246	N/A 26.71 22.97	N/A 0.6240 0.7256	N/A -0.3886 -0.4010
1.00	1000	0.9880	33.89 41.45 42.16	0.4918 0.4021 0.3953	21.38 23.98 24.37	0.7795 0.6950 0.6839	-0.2878 -0.2929 -0.2886
2.00	500	0.9909	36.89 36.90 37.52	0.4518 0.4517 0.4442	24.06 24.09 24.01	0.6927 0.6919 0.6942	-0.2409 -0.2402 -0.2499
3.00	333	0.9830	34.15 35.05 33.04	0.4880 0.4755 0.5044	23.96 24.39 23.39	0.6956 0.6833 0.7126	-0.2076 -0.2078 -0.2081
4.00	250	0.9997	36.64 36.23 37.91	0.4549 0.4600 0.4396	25.98 26.09 27.04	0.6415 0.6388 0.6164	-0.1866 -0.1788 -0.1767
5.00	200	1.0057	38.39 39.16 42.34	0.4341 0.4256 0.3936	27.88 28.25 30.47	0.5978 0.5900 0.5470	-0.1637 -0.1644 -0.1533
6.00	167	0.9905	40.93 41.60 45.62	0.4072 0.4006 0.3653	30.15 30.35 32.33	0.5528 0.5491 0.5155	-0.1456 -0.1485 -0.1502
8.00	125	1.0253	43.42 42.56 41.93	0.3838 0.3916 0.3975	32.01 31.52 31.48	0.5207 0.5288 0.5294	-0.1368 -0.1372 -0.1319
10.00	100	1.0156	38.89 38.16 37.16	0.4286 0.4368 0.4485	30.45 29.99 29.33	0.5473 0.5557 0.5682	-0.1188 -0.1190 -0.1197
15.00	67	1.0222	36.09 35.42 34.72	0.4618 0.4705 0.4800	29.81 29.39 28.88	0.5591 0.5671 0.5771	-0.0973 -0.0965 -0.0971
35.00	29	1.1838	N/A 44.81 44.82	N/A 0.3719 0.3719	N/A 38.12 38.12	N/A 0.4372 0.4372	N/A -0.0653 -0.0654
50.00	20	1.2846	47.22 47.59 47.00	0.3530 0.3502 0.3546	40.16 41.61 41.06	0.4150 0.4005 0.4059	-0.0620 -0.0503 -0.0513

μ_{ep} ($cm^2 \times V^{-1} \times s^{-1} \times 10^{-3}$)	$\nu \times \mu(i) - \mu(f)$ ($cm^2 \times V^{-1} \times s^{-1} \times 10^{-3}$)	$1/(\nu \times \mu(i) - \mu(f))$ ($V \times s \times cm^{-2}$)	Average ($V \times s \times cm^{-2}$)	STD ($V \times s \times cm^{-2}$)	95% CI ($V \times s \times cm^{-2}$)
N/A -0.14059 -0.14509	N/A, $\mu(f)$=-0.1428	N/A	N/A	N/A	N/A
-0.10411 -0.10598 -0.10441	0.0399 0.0381 0.0396	25038 26254 25224	25506	655	741
-0.08716 -0.08690 -0.09043	0.0564 0.0567 0.0532	17721 17639 18800	18053	648	733
-0.07510 -0.07519 -0.07530	0.0690 0.0689 0.0688	14497 14517 14538	14517	21	24
-0.06753 -0.06469 -0.06394	0.0753 0.0781 0.0789	13281 12799 12678	12919	319	361
-0.05921 -0.05947 -0.05548	0.0833 0.0830 0.0870	12012 12049 11494	11852	310	351
-0.05268 -0.05373 -0.05434	0.0906 0.0896 0.0890	11034 11163 11238	11145	103	117
-0.04950 -0.04962 -0.04774	0.0920 0.0919 0.0939	10864 10879 10655	10799	125	142
-0.04298 -0.04305 -0.04332	0.0992 0.0991 0.0988	10085 10093 10121	10100	19	21
-0.03520 -0.03493 -0.03512	0.1068 0.1071 0.1069	9362 9337 9354	9351	12	14
N/A -0.02362 -0.02365	N/A 0.1148 0.1148	N/A 8708 8710	8709	2	3
-0.02245 -0.01821 -0.01856	0.1140 0.1194 0.1190	8775 8375 8406	8519	222	252

3. *R*-fenoprofen, 0.5 mM TM-β-CD. L=64.4 cm, l=55.8 cm.

[TM-β-CD] (mM)	1/[TM-β-CD] (M^{-1})	v=t/t0	t(i) (min)	1/t(i) ($s^{-1}\times10^{-3}$)	t(m) (min)	1/t(m) ($s^{-1}\times10^{-3}$)	1/t(i)-1/t(m) ($s^{-1}\times10^{-3}$)
0.00	N/A	1.000	93.53	0.1782	29.01	0.5745	-0.3963
			78.31	0.2128	27.50	0.6061	-0.3932
			N/A	N/A	N/A	N/A	N/A
1.00	1000	0.9880	47.06	0.3542	25.29	0.6590	-0.3049
			52.03	0.3203	26.94	0.6187	-0.2983
			58.09	0.2869	28.17	0.5916	-0.3047
2.00	500	0.9909	N/A	N/A	N/A	N/A	N/A
			77.84	0.2141	35.91	0.4641	-0.2500
			68.75	0.2424	34.09	0.4889	-0.2465
3.00	333	0.9830	58.50	0.2849	33.76	0.4937	-0.2088
			56.86	0.2931	32.87	0.5070	-0.2139
			54.00	0.3086	31.95	0.5216	-0.2130
4.00	250	0.9997	49.61	0.3360	31.67	0.5263	-0.1903
			49.40	0.3374	31.56	0.5281	-0.1907
			54.00	0.3086	33.48	0.4978	-0.1892
5.00	200	1.0057	N/A	N/A	N/A	N/A	N/A
			50.36	0.3310	32.82	0.5078	-0.1769
			54.39	0.3064	35.03	0.4758	-0.1694
6.00	167	0.9905	57.73	0.2887	37.53	0.4441	-0.1554
			N/A	N/A	N/A	N/A	N/A
			52.88	0.3152	35.43	0.4704	-0.1552
8.00	125	1.0253	48.58	0.3431	34.73	0.4799	-0.1368
			49.22	0.3386	35.14	0.4743	-0.1357
			48.25	0.3454	34.39	0.4846	-0.1392
10.00	100	1.0156	45.70	0.3647	33.95	0.4909	-0.1262
			43.34	0.3846	32.82	0.5078	-0.1233
			42.69	0.3904	32.38	0.5147	-0.1243
15.00	67	1.0222	42.87	0.3888	34.21	0.4872	-0.0984
			43.73	0.3811	34.81	0.4788	-0.0977
			47.23	0.3529	37.08	0.4495	-0.0966
35.00	29	1.1838	50.24	0.3317	42.18	0.3951	-0.0634
			53.36	0.3123	44.57	0.3739	-0.0616
			55.6	0.2998	46.05	0.3619	-0.0622
50.00	20	1.2846	58.61	0.2844	50.03	0.3331	-0.0488
			55.78	0.2988	47.81	0.3486	-0.0498
			54.67	0.3049	46.89	0.3554	-0.0506

μ_{ep} ($cm^2 \times V^{-1} \times s^{-1} \times 10^{-3}$)	$\nu \times \mu(i) - \mu(f)$ ($cm^2 \times V^{-1} \times s^{-1} \times 10^{-3}$)	$1/(\nu \times \mu(i) - \mu(f))$ ($V \times s \times cm^{-2}$)	Average ($V \times s \times cm^{-2}$)	STD ($V \times s \times cm^{-2}$)	95% CI ($V \times s \times cm^{-2}$)
-0.1424 -0.1413 N/A	N/A, $\mu(f)$=-0.1419	N/A	N/A	N/A	N/A
-0.1096 -0.1072 -0.1095	0.0336 0.0360 0.0337	29721 27804 29680	29068	1095	1239
N/A -0.0898 -0.0886	N/A 0.0529 0.0541	N/A 18913 18477	18695	309	350
-0.0750 -0.0769 -0.0766	0.0681 0.0663 0.0666	14676 15078 15004	14919	214	243
-0.0684 -0.0685 -0.0680	0.0735 0.0734 0.0739	13601 13628 13526	13585	53	60
N/A -0.0636 -0.0609	N/A 0.0780 0.0807	N/A 12825 12394	12609	305	346
-0.0558 N/A -0.0558	0.0866 N/A 0.0866	11550 N/A 11542	11546	5	6
-0.0492 -0.0488 -0.0500	0.0915 0.0919 0.0906	10931 10881 11037	10950	80	90
-0.0454 -0.0443 -0.0447	0.0958 0.0969 0.0965	10435 10319 10360	10371	59	67
-0.0354 -0.0351 -0.0347	0.1057 0.1060 0.1064	9457 9432 9397	9429	30	34
-0.0228 -0.0221 -0.0223	0.1149 0.1157 0.1155	8701 8644 8662	8669	29	41
-0.0175 -0.0179 -0.0182	0.1194 0.1189 0.1185	8376 8410 8435	8407	30	34

4. *R*-fenoprofen, 0.8 mM TM-β-CD. L=64.6 cm, l=56.0 cm.

[TM-β-CD] (mM)	1/[TM-β-CD] (M^{-1})	v=t/t0	t(i) (min)	1/t(i) ($s^{-1}\times10^{-3}$)	t(m) (min)	1/t(m) ($s^{-1}\times10^{-3}$)	1/t(i)-1/t(m) ($s^{-1}\times10^{-3}$)
0.00	N/A	1.000	N/A	N/A	N/A	N/A	N/A
			132.33	0.1259	37.05	0.4498	-0.3239
			123.83	0.1346	31.08	0.5363	-0.4017
1.00	1000	0.9835	74.19	0.2246	31.11	0.5357	-0.3111
			77.13	0.2161	31.67	0.5263	-0.3102
			82.37	0.2023	33.17	0.5025	-0.3001
2.00	500	0.9911	60.69	0.2746	32.06	0.5199	-0.2452
			N/A	N/A	N/A	N/A	N/A
			65.83	0.2532	34.46	0.4837	-0.2305
3.00	333	0.9848	N/A	N/A	N/A	N/A	N/A
			66.42	0.2509	36.24	0.4599	-0.2090
			59.97	0.2779	34.05	0.4895	-0.2116
4.00	250	0.9956	54.29	0.3070	33.04	0.5044	-0.1974
			52.65	0.3166	32.37	0.5149	-0.1983
			N/A	N/A	N/A	N/A	N/A
5.00	200	1.006	58.58	0.2845	40.85	0.4080	-0.1235
			55.01	0.3030	36.32	0.4589	-0.1559
			50.39	0.3308	33.96	0.4908	-0.1600
6.00	167	0.9873	51.46	0.3239	35.37	0.4712	-0.1473
			55.81	0.2986	37.37	0.4460	-0.1474
			56.66	0.2942	37.75	0.4415	-0.1473
8.00	125	1.031	55.90	0.2982	39.17	0.4255	-0.1273
			46.22	0.3606	34.29	0.4861	-0.1255
			48.02	0.3471	35.16	0.4740	-0.1269
10.00	100	1.016	47.74	0.3491	35.89	0.4644	-0.1153
			54.12	0.3080	39.50	0.4219	-0.1140
			55.23	0.3018	40.43	0.4122	-0.1105
15.00	67	1.022	54.63	0.3051	41.49	0.4017	-0.0966
			54.16	0.3077	41.67	0.4000	-0.0922
			54.85	0.3039	42.18	0.3951	-0.0913
35.00	29	1.184	63.82	0.2612	51.66	0.3226	-0.0615
			64.94	0.2566	52.64	0.3166	-0.0600
			65.05	0.2562	53.40	0.3121	-0.0559
50.00	20	1.284	N/A	N/A	N/A	N/A	N/A
			69.73	0.2390	57.78	0.2885	-0.0494
			64.58	0.2581	54.58	0.3054	-0.0473

μ_{ep} ($cm^2 \times V^{-1} \times s^{-1} \times 10^{-3}$)	$\nu \times \mu(i) - \mu(f)$ ($cm^2 \times V^{-1} \times s^{-1} \times 10^{-3}$)	$1/(\nu \times \mu(i) - \mu(f))$ ($V \times s \times cm^{-2}$)	Average ($V \times s \times cm^{-2}$)	STD ($V \times s \times cm^{-2}$)	95% CI ($V \times s \times cm^{-2}$)
N/A -0.1172 -0.1453	N/A, $\mu(f)$=-0.1313	N/A	N/A	N/A	N/A
-0.1126 -0.1122 -0.1086	0.0206 0.0209 0.0245	48528 47778 40804	45703	4259	4820
-0.0887 N/A -0.0834	0.0434 N/A 0.0487	23062 N/A 20552	21807	1774	2459
N/A -0.0756 -0.0765	N/A 0.0568 0.0559	N/A 17592 17882	17737	205	285
-0.0714 -0.0718 N/A	0.0602 0.0599 N/A	16617 16705 N/A	16661	62	86
-0.0447 -0.0564 -0.0579	0.0864 0.0746 0.0731	11580 13413 13688	12894	1146	1297
-0.0533 -0.0533 -0.0533	0.0787 0.0787 0.0787	12711 12712 12712	12712	1	1
-0.0461 -0.0454 -0.0459	0.0838 0.0845 0.0839	11933 11834 11912	11893	52	59
-0.0417 -0.0412 -0.0400	0.0889 0.0894 0.0907	11245 11186 11026	11152	113	128
-0.0350 -0.0334 -0.0330	0.0956 0.0972 0.0976	10463 10289 10251	10334	113	128
-0.0222 -0.0217 -0.0202	0.1050 0.1056 0.1074	9527 9469 9315	9437	110	124
N/A -0.0179 -0.0171	N/A 0.1083 0.1093	N/A 9231 9146	9188	60	83

5. *R*-fenoprofen, 1.0 mM TM-β-CD. L=64.6 cm, l=56.0 cm.

[TM-β-CD] (mM)	1/[TM-β-CD] (M^{-1})	ν=t/t0	t(i) (min)	1/t(i) ($s^{-1}\times10^{-3}$)	t(m) (min)	1/t(m) ($s^{-1}\times10^{-3}$)	1/t(i)-1/t(m) ($s^{-1}\times10^{-3}$)
0.00	N/A	1.000	119.16	0.1399	34.43	0.4841	-0.3442
			112.88	0.1476	32.47	0.5133	-0.3656
			110.73	0.1505	36.85	0.4523	-0.3018
1.00	1000	0.9835	127.89	0.1303	40.34	0.4132	-0.2828
			91.89	0.1814	36.21	0.4603	-0.2789
			80.21	0.2078	33.64	0.4954	-0.2877
2.00	500	0.9911	113.15	0.1473	45.37	0.3673	-0.2201
			100.91	0.1652	42.46	0.3925	-0.2274
			96.82	0.1721	41.72	0.3995	-0.2273
3.00	333	0.9848	81.31	0.2050	41.72	0.3995	-0.1945
			96.12	0.1734	46.36	0.3595	-0.1861
			92.05	0.1811	46.06	0.3618	-0.1808
4.00	250	0.9956	89.30	0.1866	47.51	0.3508	-0.1642
			76.38	0.2182	43.41	0.3839	-0.1657
			69.19	0.2409	41.15	0.4050	-0.1641
5.00	200	1.006	70.89	0.2351	42.73	0.3900	-0.1549
			78.31	0.2128	45.50	0.3663	-0.1535
			85.15	0.1957	47.75	0.3490	-0.1533
6.00	167	0.9873	65.16	0.2558	42.24	0.3946	-0.1388
			61.99	0.2689	40.56	0.4109	-0.1421
			66.54	0.2505	42.59	0.3913	-0.1409
8.00	125	1.031	64.46	0.2586	43.69	0.3815	-0.1229
			82.47	0.2021	51.80	0.3218	-0.1197
			66.43	0.2509	44.67	0.3731	-0.1222
10.00	100	1.016	65.22	0.2555	45.61	0.3654	-0.1099
			62.65	0.2660	44.27	0.3765	-0.1104
			61.53	0.2709	43.66	0.3817	-0.1109
15.00	67	1.022	57.92	0.2878	44.12	0.3778	-0.0900
			57.00	0.2924	43.65	0.3818	-0.0894
			54.20	0.3075	41.96	0.3972	-0.0897
35.00	29	1.184	54.97	0.3032	46.24	0.3604	-0.0572
			54.08	0.3082	45.65	0.3651	-0.0569
			N/A	N/A	N/A	N/A	N/A
50.00	20	1.284	76.69	0.2173	63.64	0.2619	-0.0446
			83.65	0.1992	69.90	0.2384	-0.0392
			86.29	0.1931	70.28	0.2371	-0.0440

μ_{ep} ($cm^2 \times V^{-1} \times s^{-1} \times 10^{-3}$)	$\nu \times \mu(i) - \mu(f)$ ($cm^2 \times V^{-1} \times s^{-1} \times 10^{-3}$)	$1/(\nu \times \mu(i) - \mu(f))$ ($V \times s \times cm^{-2}$)	Average ($V \times s \times cm^{-2}$)	STD ($V \times s \times cm^{-2}$)	95% CI ($V \times s \times cm^{-2}$)
-0.1245 -0.1323 -0.1092	N/A, $\mu(f)$=-0.1220	N/A	N/A	N/A	N/A
-0.1023 -0.1009 -0.1041	0.0214 0.0228 0.0196	46819 43940 50906	47222	3501	3961
-0.0796 -0.0823 -0.0823	0.0431 0.0405 0.0405	23205 24708 24705	24206	867	981
-0.0704 -0.0673 -0.0654	0.0527 0.0557 0.0576	18977 17957 17365	18100	815	923
-0.0594 -0.0600 -0.0594	0.0629 0.0623 0.0629	15907 16051 15904	15954	84	95
-0.0561 -0.0555 -0.0555	0.0656 0.0661 0.0662	15242 15119 15106	15156	75	85
-0.0502 -0.0514 -0.0510	0.0724 0.0713 0.0717	13808 14034 13950	13930	114	129
-0.0445 -0.0433 -0.0442	0.0761 0.0774 0.0764	13132 12926 13087	13048	109	123
-0.0398 -0.0400 -0.0401	0.0816 0.0814 0.0812	12253 12285 12308	12282	28	31
-0.0326 -0.0324 -0.0325	0.0887 0.0889 0.0888	11271 11244 11257	11258	14	15
-0.0207 -0.0206 N/A	0.0975 0.0976 N/A	10259 10244 N/A	10251	11	15
-0.0161 -0.0142 -0.0159	0.1013 0.1038 0.1016	9872 9635 9846	9784	130	147

6. *S*-fenoprofen, 0.0 mM TM-β-CD. L=64.6 cm, l=56.0 cm.

[TM-β-CD] (mM)	1/[TM-β-CD] (M^{-1})	v=t/t0	t(i) (min)	1/t(i) ($s^{-1}\times10^{-3}$)	t(m) (min)	1/t(m) ($s^{-1}\times10^{-3}$)	1/t(i)-1/t(m) ($s^{-1}\times10^{-3}$)
0.00	N/A	1.000	31.82	0.5238	17.41	0.9573	-0.4335
			35.34	0.4716	18.87	0.8832	-0.4116
			47.62	0.3500	21.77	0.7656	-0.4156
1.00	1000	0.9880	47.99	0.3473	26.06	0.6395	-0.2923
			45.52	0.3661	25.44	0.6551	-0.2890
			47.23	0.3529	25.80	0.6460	-0.2931
2.00	500	0.9909	41.50	0.4016	25.89	0.6437	-0.2421
			40.29	0.4137	25.47	0.6544	-0.2407
			40.04	0.4163	25.33	0.6580	-0.2417
3.00	333	0.9830	37.01	0.4503	25.36	0.6572	-0.2069
			36.06	0.4622	24.94	0.6683	-0.2061
			34.45	0.4838	24.18	0.6893	-0.2055
4.00	250	0.9997	40.09	0.4157	27.13	0.6143	-0.1986
			44.70	0.3729	29.75	0.5602	-0.1874
			49.44	0.3371	31.99	0.5210	-0.1839
5.00	200	1.0057	48.03	0.3470	32.55	0.5120	-0.1650
			48.53	0.3434	32.71	0.5095	-0.1661
			47.11	0.3538	31.99	0.5210	-0.1672
6.00	167	0.9905	57.95	0.2876	37.86	0.4402	-0.1526
			56.26	0.2962	37.17	0.4484	-0.1521
			54.80	0.3041	36.29	0.4593	-0.1551
8.00	125	1.0253	53.03	0.3143	36.77	0.4533	-0.1390
			51.22	0.3254	35.89	0.4644	-0.1390
			49.66	0.3356	35.08	0.4751	-0.1395
10.00	100	1.0156	N/A	N/A	N/A	N/A	N/A
			43.53	0.3829	32.68	0.5100	-0.1271
			44.30	0.3762	33.11	0.5034	-0.1271
15.00	67	1.0222	45.56	0.3658	35.03	0.4758	-0.1100
			51.01	0.3267	38.49	0.4330	-0.1063
			51.43	0.3241	38.68	0.4309	-0.1068
35.00	29	1.1838	N/A	N/A	N/A	N/A	N/A
			N/A	N/A	N/A	N/A	N/A
			52.92	0.3149	43.04	0.3872	-0.0723
50.00	20	1.2846	N/A	N/A	N/A	N/A	N/A
			53.42	0.3120	44.63	0.3734	-0.0614
			49.74	0.3351	41.91	0.3977	-0.0626

μ_{ep} ($cm^2 \times V^{-1} \times s^{-1} \times 10^{-3}$)	$\nu \times \mu(i) - \mu(f)$ ($cm^2 \times V^{-1} \times s^{-1} \times 10^{-3}$)	$1/(\nu \times \mu(i) - \mu(f))$ ($V \times s \times cm^{-2}$)	Average ($V \times s \times cm^{-2}$)	STD ($V \times s \times cm^{-2}$)	95% CI ($V \times s \times cm^{-2}$)
-0.1568 -0.1489 -0.1504	N/A, $\mu(f)$=-0.1520	N/A	N/A	N/A	N/A
-0.1057 -0.1046 -0.1060	0.0475 0.0487 0.0472	21039 20536 21175	20917	337	381
-0.0876 -0.0871 -0.0875	0.0652 0.0657 0.0653	15340 15219 15305	15288	62	71
-0.0748 -0.0746 -0.0743	0.0784 0.0787 0.0789	12751 12705 12671	12709	40	45
-0.0719 -0.0678 -0.0665	0.0802 0.0842 0.0855	12474 11872 11697	12014	407	461
-0.0597 -0.0601 -0.0605	0.0920 0.0916 0.0912	10875 10921 10970	10922	47	54
-0.0552 -0.0550 -0.0561	0.0973 0.0975 0.0964	10277 10259 10373	10303	61	69
-0.0503 -0.0503 -0.0505	0.1004 0.1004 0.1003	9956 9956 9974	9962	11	12
N/A -0.0460 -0.0460	N/A 0.1053 0.1053	N/A 9497 9499	9498	1	1
-0.0398 -0.0385 -0.0386	0.1113 0.1127 0.1125	8982 8874 8889	8915	59	66
N/A N/A -0.0262	N/A N/A 0.1210	N/A N/A 8262	7964	N/A	N/A
N/A -0.0222 -0.0226	N/A 0.1234 0.1229	N/A 8101 8136	8119	25	35

7. *S*-fenoprofen, 0.2 mM TM-β-CD. L=64.6 cm, l=56.0 cm.

[TM-β-CD] (mM)	1/[TM-β-CD] (M^{-1})	v=t/t0	t(i) (min)	1/t(i) ($s^{-1}\times10^{-3}$)	t(m) (min)	1/t(m) ($s^{-1}\times10^{-3}$)	1/t(i)-1/t(m) ($s^{-1}\times10^{-3}$)
0.00	N/A	1.000	N/A	N/A	N/A	N/A	N/A
			70.80	0.2354	26.71	0.6240	-0.3886
			51.35	0.3246	22.97	0.7256	-0.4010
1.00	1000	0.9880	33.89	0.4918	21.38	0.7795	-0.2878
			41.45	0.4021	23.98	0.6950	-0.2929
			42.16	0.3953	24.37	0.6839	-0.2886
2.00	500	0.9909	36.89	0.4518	24.06	0.6927	-0.2409
			36.90	0.4517	24.09	0.6919	-0.2402
			37.52	0.4442	24.01	0.6942	-0.2499
3.00	333	0.9830	34.15	0.4880	23.96	0.6956	-0.2076
			35.05	0.4755	24.39	0.6833	-0.2078
			33.04	0.5044	23.39	0.7126	-0.2081
4.00	250	0.9997	36.64	0.4549	25.98	0.6415	-0.1866
			36.23	0.4600	26.09	0.6388	-0.1788
			37.91	0.4396	27.04	0.6164	-0.1767
5.00	200	1.0057	38.39	0.4341	27.88	0.5978	-0.1637
			39.16	0.4256	28.25	0.5900	-0.1644
			42.34	0.3936	30.47	0.5470	-0.1533
6.00	167	0.9905	41.23	0.4042	30.15	0.5528	-0.1486
			41.88	0.3980	30.35	0.5491	-0.1512
			45.94	0.3628	32.33	0.5155	-0.1527
8.00	125	1.0253	43.90	0.3797	32.01	0.5207	-0.1410
			43.04	0.3872	31.52	0.5288	-0.1415
			42.37	0.3934	31.48	0.5294	-0.1361
10.00	100	1.0156	39.36	0.4234	30.45	0.5473	-0.1239
			38.60	0.4318	29.99	0.5557	-0.1240
			37.58	0.4435	29.33	0.5682	-0.1247
15.00	67	1.0222	36.66	0.4546	29.81	0.5591	-0.1045
			35.96	0.4635	29.39	0.5671	-0.1036
			35.24	0.4729	28.88	0.5771	-0.1042
35.00	29	1.1838	N/A	N/A	N/A	N/A	N/A
			46.13	0.3613	38.12	0.4372	-0.0759
			46.15	0.3611	38.12	0.4372	-0.0761
50.00	20	1.2846	47.22	0.3530	40.16	0.4150	-0.0620
			49.18	0.3389	41.61	0.4005	-0.0617
			48.61	0.3429	41.06	0.4059	-0.0630

μ_{ep} ($cm^2 \times V^{-1} \times s^{-1} \times 10^{-3}$)	$\nu \times \mu(i) - \mu(f)$ ($cm^2 \times V^{-1} \times s^{-1} \times 10^{-3}$)	$1/(\nu \times \mu(i) - \mu(f))$ ($V \times s \times cm^{-2}$)	Average ($V \times s \times cm^{-2}$)	STD ($V \times s \times cm^{-2}$)	95% CI ($V \times s \times cm^{-2}$)
N/A -0.1406 -0.1451	N/A, $\mu(f)$=-0.1428	N/A	N/A	N/A	N/A
-0.1041 -0.1060 -0.1044	0.0399 0.0381 0.0396	25038 26254 25224	25506	655	741
-0.0872 -0.0869 -0.0904	0.0564 0.0567 0.0532	17721 17639 18800	18053	648	733
-0.0751 -0.0752 -0.0753	0.0690 0.0689 0.0688	14497 14517 14538	14517	21	24
-0.0675 -0.0647 -0.0639	0.0753 0.0781 0.0789	13281 12799 12678	12919	319	361
-0.0592 -0.0595 -0.0555	0.0833 0.0830 0.0870	12012 12049 11494	11852	310	351
-0.0537 -0.0547 -0.0553	0.0896 0.0886 0.0881	11165 11284 11355	11268	96	108
-0.0510 -0.0512 -0.0492	0.0905 0.0903 0.0923	11051 11074 10832	10986	134	152
-0.0448 -0.0448 -0.0451	0.0973 0.0973 0.0970	10280 10283 10313	10292	18	21
-0.0378 -0.0375 -0.0377	0.1042 0.1045 0.1043	9600 9571 9589	9587	15	17
N/A -0.0275 -0.0275	N/A 0.1103 0.1102	N/A 9067 9073	9070	4	5
-0.0224 -0.0223 -0.0228	0.1140 0.1141 0.1135	8775 8761 8811	8782	26	29

8. *S*-fenoprofen, 0.5 mM TM-β-CD. L=64.4 cm, l=55.8 cm.

[TM-β-CD] (mM)	1/[TM-β-CD] (M^{-1})	ν=t/t0	t(i) (min)	1/t(i) ($s^{-1}\times10^{-3}$)	t(m) (min)	1/t(m) ($s^{-1}\times10^{-3}$)	1/t(i)-1/t(m) ($s^{-1}\times10^{-3}$)
0.00	N/A	1.000	93.53	0.1782	29.01	0.5745	-0.3963
			78.31	0.2128	27.50	0.6061	-0.3932
			N/A	N/A	N/A	N/A	N/A
1.00	1000	0.9880	47.06	0.3542	25.29	0.6590	-0.3049
			52.03	0.3203	26.94	0.6187	-0.2983
			58.09	0.2869	28.17	0.5916	-0.3047
2.00	500	0.9909	N/A	N/A	N/A	N/A	N/A
			77.84	0.2141	35.91	0.4641	-0.2500
			68.75	0.2424	34.09	0.4889	-0.2465
3.00	333	0.9830	58.50	0.2849	33.76	0.4937	-0.2088
			56.86	0.2931	32.87	0.5070	-0.2139
			54.00	0.3086	31.95	0.5216	-0.2130
4.00	250	0.9997	49.61	0.3360	31.67	0.5263	-0.1903
			49.40	0.3374	31.56	0.5281	-0.1907
			54.00	0.3086	33.48	0.4978	-0.1892
5.00	200	1.0057	N/A	N/A	N/A	N/A	N/A
			50.54	0.3298	32.82	0.5078	-0.1780
			54.74	0.3045	35.03	0.4758	-0.1713
6.00	167	0.9905	58.31	0.2858	37.53	0.4441	-0.1583
			N/A	N/A	N/A	N/A	N/A
			53.35	0.3124	35.43	0.4704	-0.1580
8.00	125	1.0253	49.24	0.3385	34.73	0.4799	-0.1414
			49.87	0.3342	35.14	0.4743	-0.1401
			48.88	0.3410	34.39	0.4846	-0.1437
10.00	100	1.0156	46.40	0.3592	33.95	0.4909	-0.1317
			43.95	0.3792	32.82	0.5078	-0.1286
			43.28	0.3851	32.38	0.5147	-0.1296
15.00	67	1.0222	43.67	0.3817	34.21	0.4872	-0.1055
			44.48	0.3747	34.81	0.4788	-0.1041
			48.16	0.3461	37.08	0.4495	-0.1034
35.00	29	1.1838	51.87	0.3213	42.18	0.3951	-0.0738
			55.19	0.3020	44.57	0.3739	-0.0720
			57.58	0.2895	46.05	0.3619	-0.0725
50.00	20	1.2846	60.96	0.2734	50.03	0.3331	-0.0597
			57.97	0.2875	47.81	0.3486	-0.0611
			56.82	0.2933	46.89	0.3554	-0.0621

μ_{ep} ($cm^2 \times V^{-1} \times s^{-1} \times 10^{-3}$)	$\nu \times \mu(i) - \mu(f)$ ($cm^2 \times V^{-1} \times s^{-1} \times 10^{-3}$)	$1/(\nu \times \mu(i) - \mu(f))$ ($V \times s \times cm^{-2}$)	Average ($V \times s \times cm^{-2}$)	STD ($V \times s \times cm^{-2}$)	95% CI ($V \times s \times cm^{-2}$)
-0.1424 -0.1413 N/A	N/A, $\mu(f)$=-0.1419	N/A	N/A	N/A	N/A
-0.1096 -0.1072 -0.1095	0.0336 0.0360 0.0337	29721 27804 29680	29068	1095	1239
N/A -0.0898 -0.0886	N/A 0.0529 0.0541	N/A 18913 18477	18695	309	350
-0.0750 -0.0769 -0.0766	0.0681 0.0663 0.0666	14676 15078 15004	14919	214	243
-0.0684 -0.0685 -0.0680	0.0735 0.0734 0.0739	13601 13628 13526	13585	53	60
N/A -0.0640 -0.0616	N/A 0.0775 0.0800	N/A 12896 12503	12700	278	314
-0.0569 N/A -0.0568	0.0856 N/A 0.0857	11687 N/A 11675	11681	9	10
-0.0508 -0.0503 -0.0516	0.0898 0.0903 0.0890	11137 11077 11241	11152	83	94
-0.0473 -0.0462 -0.0466	0.0938 0.0950 0.0946	10659 10531 10573	10587	65	74
-0.0379 -0.0374 -0.0372	0.1031 0.1037 0.1039	9697 9647 9624	9656	37	42
-0.0265 -0.0259 -0.0260	0.1105 0.1113 0.1111	9050 8986 9004	9013	33	46
-0.0215 -0.0220 -0.0223	0.1143 0.1137 0.1132	8747 8796 8832	8792	43	48

9. *S*-fenoprofen, 0.8 mM TM-β-CD. L=64.6 cm, l=56.0 cm.

[TM-β-CD] (mM)	1/[TM-β-CD] (M^{-1})	ν=t/t0	t(i) (min)	1/t(i) ($s^{-1}\times10^{-3}$)	t(m) (min)	1/t(m) ($s^{-1}\times10^{-3}$)	1/t(i)-1/t(m) ($s^{-1}\times10^{-3}$)
0.00	N/A	1.000	N/A	N/A	N/A	N/A	N/A
			132.33	0.1259	37.05	0.4498	-0.3239
			123.83	0.1346	31.08	0.5363	-0.4017
1.00	1000	0.9835	74.19	0.2246	31.11	0.5357	-0.3111
			77.13	0.2161	31.67	0.5263	-0.3102
			82.37	0.2023	33.17	0.5025	-0.3001
2.00	500	0.9911	60.69	0.2746	32.06	0.5199	-0.2452
			N/A	N/A	N/A	N/A	N/A
			65.83	0.2532	34.46	0.4837	-0.2305
3.00	333	0.9848	N/A	N/A	N/A	N/A	N/A
			66.42	0.2509	36.24	0.4599	-0.2090
			59.97	0.2779	34.05	0.4895	-0.2116
4.00	250	0.9956	54.29	0.3070	33.04	0.5044	-0.1974
			52.65	0.3166	32.37	0.5149	-0.1983
			N/A	N/A	N/A	N/A	N/A
5.00	200	1.006	58.63	0.2843	40.85	0.4080	-0.1237
			55.33	0.3012	36.32	0.4589	-0.1577
			50.07	0.3329	33.96	0.4908	-0.1579
6.00	167	0.9873	51.96	0.3208	35.37	0.4712	-0.1504
			56.41	0.2955	37.37	0.4460	-0.1505
			57.31	0.2908	37.75	0.4415	-0.1507
8.00	125	1.031	56.76	0.2936	39.17	0.4255	-0.1319
			46.80	0.3561	34.29	0.4861	-0.1299
			48.62	0.3428	35.16	0.4740	-0.1312
10.00	100	1.016	48.46	0.3439	35.89	0.4644	-0.1205
			55.02	0.3029	39.50	0.4219	-0.1190
			56.10	0.2971	40.43	0.4122	-0.1151
15.00	67	1.022	55.89	0.2982	41.49	0.4017	-0.1035
			55.34	0.3012	41.67	0.4000	-0.0988
			56.08	0.2972	42.18	0.3951	-0.0979
35.00	29	1.184	66.53	0.2505	51.66	0.3226	-0.0721
			67.77	0.2459	52.64	0.3166	-0.0707
			67.64	0.2464	53.40	0.3121	-0.0657
50.00	20	1.284	N/A	N/A	N/A	N/A	N/A
			N/A	N/A	N/A	N/A	N/A
			67.47	0.2470	54.58	0.3054	-0.0583

μ_{ep} ($cm^2 \times V^{-1} \times s^{-1} \times 10^{-3}$)	$v \times \mu(i) - \mu(f)$ ($cm^2 \times V^{-1} \times s^{-1} \times 10^{-3}$)	$1/(v \times \mu(i) - \mu(f))$ ($V \times s \times cm^{-2}$)	Average ($V \times s \times cm^{-2}$)	STD ($V \times s \times cm^{-2}$)	95% CI ($V \times s \times cm^{-2}$)
N/A -0.11719 -0.14532	N/A, $\mu(f)$=-0.1313	N/A	N/A	N/A	N/A
-0.11255 -0.11222 -0.10858	0.0206 0.0209 0.0245	48528 47778 40804	45703	4259	4820
-0.08873 N/A -0.08339	0.0434 N/A 0.0487	23062 N/A 20552	21807	1774	2459
N/A -0.07560 -0.07654	N/A 0.0568 0.0559	N/A 17592 17882	17737	205	285
-0.07144 -0.07175 N/A	0.0602 0.0599 N/A	16617 16705 N/A	16661	62	86
-0.04476 -0.05704 -0.05713	0.0863 0.0739 0.0738	11592 13529 13545	12889	1123	1271
-0.05443 -0.05446 -0.05452	0.0776 0.0775 0.0775	12893 12899 12907	12900	7	8
-0.04771 -0.04701 -0.04748	0.0821 0.0828 0.0823	12178 12072 12143	12131	54	61
-0.04358 -0.04306 -0.04166	0.0870 0.0875 0.0890	11491 11422 11239	11384	130	147
-0.03745 -0.03575 -0.03543	0.0930 0.0948 0.0951	10749 10552 10517	10606	125	142
-0.02609 -0.02557 -0.02377	0.1004 0.1010 0.1032	9959 9899 9694	9851	139	157
N/A N/A -0.02111	N/A N/A 0.1042	N/A N/A 9597	9597	N/A	N/A

10. *S*-fenoprofen, 1.0 mM TM-β-CD. L=64.6 cm, l=56.0 cm.

[TM-β-CD] (mM)	1/[TM-β-CD] (M^{-1})	ν=t/t0	t(i) (min)	1/t(i) ($s^{-1}\times10^{-3}$)	t(m) (min)	1/t(m) ($s^{-1}\times10^{-3}$)	1/t(i)-1/t(m) ($s^{-1}\times10^{-3}$)
0.00	N/A	1.000	119.16	0.1399	34.43	0.4841	-0.3442
			112.88	0.1476	32.47	0.5133	-0.3656
			110.73	0.1505	36.85	0.4523	-0.3018
1.00	1000	0.9835	127.89	0.1303	40.34	0.4132	-0.2828
			91.89	0.1814	36.21	0.4603	-0.2789
			80.21	0.2078	33.64	0.4954	-0.2877
2.00	500	0.9911	113.15	0.1473	45.37	0.3673	-0.2201
			100.91	0.1652	42.46	0.3925	-0.2274
			96.82	0.1721	41.72	0.3995	-0.2273
3.00	333	0.9848	81.31	0.2050	41.72	0.3995	-0.1945
			96.12	0.1734	46.36	0.3595	-0.1861
			92.05	0.1811	46.06	0.3618	-0.1808
4.00	250	0.9956	89.30	0.1866	47.51	0.3508	-0.1642
			76.38	0.2182	43.41	0.3839	-0.1657
			69.19	0.2409	41.15	0.4050	-0.1641
5.00	200	1.006	71.42	0.2334	42.73	0.3900	-0.1567
			79.20	0.2104	45.50	0.3663	-0.1559
			86.02	0.1938	47.75	0.3490	-0.1553
6.00	167	0.9873	65.94	0.2528	42.24	0.3946	-0.1418
			62.72	0.2657	40.56	0.4109	-0.1452
			67.38	0.2474	42.59	0.3913	-0.1440
8.00	125	1.031	65.51	0.2544	43.69	0.3815	-0.1271
			84.13	0.1981	51.80	0.3218	-0.1236
			67.57	0.2467	44.67	0.3731	-0.1264
10.00	100	1.016	66.49	0.2507	45.61	0.3654	-0.1148
			63.83	0.2611	44.27	0.3765	-0.1154
			62.68	0.2659	43.66	0.3817	-0.1158
15.00	67	1.022	59.25	0.2813	44.12	0.3778	-0.0965
			58.28	0.2860	43.65	0.3818	-0.0958
			55.37	0.3010	41.96	0.3972	-0.0962
35.00	29	1.184	56.79	0.2935	46.24	0.3604	-0.0670
			55.84	0.2985	45.65	0.3651	-0.0666
			N/A	N/A	N/A	N/A	N/A
50.00	20	1.284	80.55	0.2069	63.64	0.2619	-0.0550
			87.72	0.1900	69.90	0.2384	-0.0484
			91.24	0.1827	70.28	0.2371	-0.0545

μ_{ep} ($cm^2 \times V^{-1} \times s^{-1} \times 10^{-3}$)	$\nu \times \mu(i) - \mu(f)$ ($cm^2 \times V^{-1} \times s^{-1} \times 10^{-3}$)	$1/(\nu \times \mu(i) - \mu(f))$ ($V \times s \times cm^{-2}$)	Average ($V \times s \times cm^{-2}$)	STD ($V \times s \times cm^{-2}$)	95% CI ($V \times s \times cm^{-2}$)
-0.1245 -0.1323 -0.1092	N/A, $\mu(f)$=-0.1220	N/A	N/A	N/A	N/A
-0.1023 -0.1009 -0.1041	0.0214 0.0228 0.0196	46819 43940 50906	47222	3501	3961
-0.0796 -0.0823 -0.0823	0.0431 0.0405 0.0405	23205 24708 24705	24206	867	981
-0.0704 -0.0673 -0.0654	0.0527 0.0557 0.0576	18977 17957 17365	18100	815	923
-0.0594 -0.0600 -0.0594	0.0629 0.0623 0.0629	15907 16051 15904	15954	84	95
-0.0567 -0.0564 -0.0562	0.0650 0.0653 0.0655	15391 15321 15272	15328	60	68
-0.0513 -0.0525 -0.0521	0.0713 0.0701 0.0706	14017 14257 14170	14148	122	138
-0.0460 -0.0447 -0.0457	0.0746 0.0759 0.0748	13404 13179 13363	13315	120	136
-0.0415 -0.0417 -0.0419	0.0798 0.0796 0.0794	12528 12564 12591	12561	32	36
-0.0349 -0.0347 -0.0348	0.0863 0.0866 0.0864	11583 11553 11570	11569	15	17
-0.0242 -0.0241 N/A	0.0933 0.0935 N/A	10716 10700 N/A	10708	12	16
-0.0199 -0.0175 -0.0197	0.0965 0.0995 0.0967	10367 10050 10342	10253	176	199